HIDRAULICA

HYDRAULICS-PNEUMATICS-TRIBOLOGY-ECOLOGY-SENSORICS-MECHATRONICS

2025

March

No. 1

ISSN 1453 - 7303
ISSN-L 1453 - 7303

https://hidraulica.fluidas.ro

CONTENTS

BOARD

Published by:
Hydraulics and Pneumatics Research Institute, Bucharest-Romania
Address: 14 Cuţitul de Argint, district 4, Bucharest, 040558, Romania
Phone: +40 21 336 39 91; Fax: +40 21 337 30 40; e-Mail: ihp@fluidas.ro; Web: www.ihp.ro
with support from:
National Professional Association of Hydraulics and Pneumatics in Romania - FLUIDAS
e-Mail: fluidas@fluidas.ro; Web: www.fluidas.ro

HIDRAULICA Magazine is indexed by international databases

ISSN 1453 – 7303; ISSN – L 1453 – 7303

EDITORIAL

Inovație sub presiune: Acționările hidraulice și pneumatice în era schimbărilor climatice

Dr. Ing. Gabriela Matache
REDACTOR ȘEF

Schimbările climatice nu mai pot fi ignorate. Dincolo de efectele lor vizibile – temperaturi extreme, fenomene meteo neobișnuite, stres hidric – ele impun o regândire profundă a modului în care industria funcționează. În acest context, domeniul acționărilor hidraulice și pneumatice este provocat să se reinventeze, iar cercetarea aplicată devine motorul acestei transformări.

Tehnologiile tradiționale, robuste și eficiente, nu mai sunt suficiente atunci când mediul înconjurător devine impredictibil. În industria agricolă, de exemplu, sistemele de irigații inteligente cu acționări pneumatice, controlate prin senzori de umiditate și automatizate pe bază de date climatice în timp real, devin esențiale. Aceste sisteme reduc consumul de apă și energie, contribuind la o agricultură sustenabilă.

În domeniul energiei regenerabile, acționările hidraulice sunt folosite în sistemele de urmărire solară (solar tracking), pentru a optimiza unghiul panourilor fotovoltaice. Cercetările recente se concentrează pe dezvoltarea de servomecanisme hidraulice cu consum redus de ulei, compatibile cu fluide ecologice sau biodegradabile – o direcție clară de adaptare tehnologică la cerințele mediului.

Mai mult, în industria transporturilor, acționările pneumatice utilizate în sistemele de frânare sau suspensii inteligente sunt reconfigurate pentru a face față condițiilor climatice variabile: fluctuații de temperatură, umiditate crescută, sau schimbări bruște de presiune atmosferică.

Toate aceste direcții arată că nu doar ce producem contează, ci cum integrăm inovația în funcție de noile realități climatice. Cercetarea aplicată devine puntea dintre inginerie și sustenabilitate, iar acționările hidraulice și pneumatice – cândva percepute ca tehnologii convenționale – se dovedesc a fi instrumente-cheie în această tranziție.

În prezent, cercetarea avansată explorează soluții concrete precum utilizarea fluidelor hidraulice biodegradabile, acționări hibride cu consum optimizat, integrarea senzorilor și a algoritmilor de control predictiv în sisteme autonome, dar și digitalizarea completă a sistemelor prin platforme IoT. Astfel, acționările devin nu doar mai eficiente, ci și mai inteligente și mai puțin dăunătoare mediului. Este clar: viitorul nu aparține doar tehnologiei brute, ci tehnologiei adaptabile și conștiente de contextul climatic în care funcționează.

Inovația nu mai poate fi separată de contextul global. Astăzi, un sistem performant este și unul adaptat, eficient, sustenabil. Sub presiunea schimbărilor climatice, hidraulica nu dispare – se transformă.

EDITORIAL

Innovation under Pressure: Hydraulic and Pneumatic Drives in the Era of Climate Change

Ph.D.Eng. Gabriela Matache
EDITOR-IN-CHIEF

Climate change can no longer be ignored. Beyond its visible effects – extreme temperatures, unusual weather phenomena, water stress – it demands a profound rethinking of how industry operates. In this context, the field of hydraulic and pneumatic actuation is challenged to reinvent itself, and applied research becomes the driving force of this transformation.

Traditional technologies, once valued for their robustness and efficiency, are no longer sufficient when the environment becomes unpredictable. In agriculture, for example, smart irrigation systems powered by pneumatic actuators, controlled by soil moisture sensors and real-time climate data, have become essential. These systems reduce water and energy consumption, contributing to sustainable farming.

In the field of renewable energy, hydraulic actuators are used in solar tracking systems to optimize the angle of photovoltaic panels. Recent research focuses on developing low-consumption hydraulic servomechanisms compatible with eco-friendly or biodegradable fluids – a clear direction for adapting technology to environmental demands.

Furthermore, in the transportation industry, pneumatic actuators used in braking systems or intelligent suspensions are being reconfigured to cope with changing climate conditions: temperature fluctuations, increased humidity, or sudden atmospheric pressure shifts.

All these developments show that it is not only what we produce that matters, but how we integrate innovation in response to new climate realities. Applied research becomes the bridge between engineering and sustainability, and hydraulic and pneumatic systems – once seen as conventional – are proving to be key tools in this transition.

Current advanced research explores practical solutions such as the use of biodegradable hydraulic fluids, hybrid actuators with optimized energy consumption, integration of sensors and predictive control algorithms in autonomous systems, as well as full system digitalization through IoT platforms. Thus, actuators become not only more efficient but also smarter and less harmful to the environment. One thing is clear: the future does not belong to brute force technology alone, but to intelligent and climate-aware systems.

Innovation can no longer be separated from the global context. Today, a high-performance system must also be adaptive, efficient, and sustainable. Under the pressure of climate change, hydraulics does not disappear – it transforms itself.

Braking Energy Recovery Hydraulic System for Heavy-Duty Machine Tools. Mathematical Modeling and Simulation

Prof. PhD Eng. **Anca BUCUREȘTEANU**[1,*]

[1] University POLITEHNICA of Bucharest

* ancabucuresteanu@gmail.com

Abstract: *This paper examines the opportunity to recover the kinetic energy accumulated by the main kinematic chains of the heavy-duty machine-tools in downtime phase. The proposed unit can shorten the stopping time of the main spindle, with or without a blank, and would allow the recovery and storage of the accumulated kinetic energy in order to use it in a new start. The paper presents a basic diagram, and also the results of the first simulations.*

Keywords: *Heavy-duty machine-tools, kinetic energy recovery, increase of efficiency*

1. Introduction

In the case of some heavy-duty machine-tools, the main spindle, with or without a blank, is a large inertial load during the acceleration and braking phases [1, 2]. Large masses, distributed on radii that can reach values of 4, 6 or 8 - 10 m, are accelerated and braked within the specific main kinematic chains. The mechanical energy accumulated by these ones can be transformed into hydraulic energy [1].
Figure 1 shows the table of a vertical lathe with the diameter of 4300 mm. Working pieces up to 60 t can be machined on this table, with a speed range of 1 ÷ 100 rpm [2, 3].

Fig. 1. Main spindle of a heavy-duty vertical lathe

The main spindle of a heavy-duty normal lathe, able to machine parts of more than 100 t, with maximum length of 20 m, is presented in Figure 2.
In both cases, the power of the main kinematic chain drive motor [2, 3] is of the order of 100 KW. In the phases of clamping and centering the blank, repeated starts and stops are required, which entails peak charges of the electric motor caused by the high value of the acceleration or braking torque.
The braking energy recovery system presented below is especially recommended for such machines.

Fig. 2. Main spindle of a normal heavy-duty lathe

2. Hydraulic system for energy recovery and storage

In the case of normal braking, the kinetic energy, accumulated by the distributed mass during the rotational motion, is transformed into heat due to the friction from bearings, gears or even from mechanical braking systems [2]. Once transformed into heat, this energy is lost, which results in the diminution of the machine efficiency.
The energy recovery hydraulic system would allow the recovery and storage of the energy in order to be used again in the subsequent acceleration phases. The basic hydraulic diagram is shown in Figure 3.

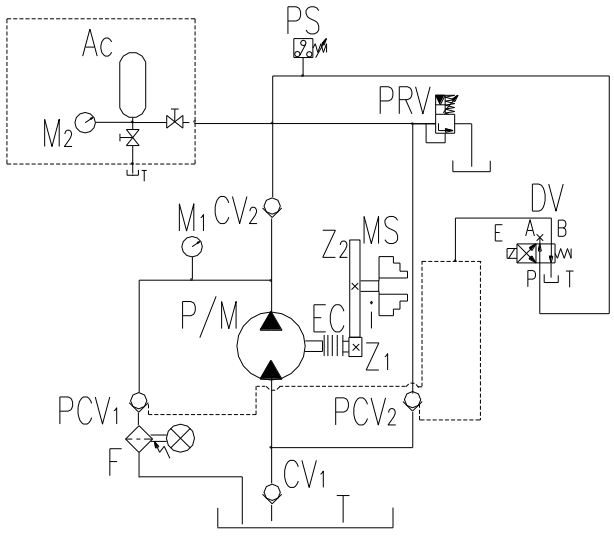

Fig. 3. Hydraulic diagram for energy recovery and storage

The following denotations are used in Figure 3: CV_1, CV_2 - check valves; PCV_1, PCV_2 - pilot operated check valves; F - filter; MS - main spindle; EC - electrical coupling; M_1, M2 - manometers; DV - directional valve; E - electromagnet; PRV - pressure relief valve; Ac - accumulator; PS - pressure switch; P/M – pump/motor reversible hydraulic machine; T - tank; Z_1, Z_2 - gear number of teeth; i - transfer ratio.
During the operation of the main kinematic chain, the electrical coupling EC is not actuated. This coupling will be actuated if the main spindle MS must be braked. The P/M reversible machine (a unit with axial pistons is recommended) will operate in PUMP mode, sucking oil through the check valve CV_1 from the tank T. The oil is sent to the accumulator (or the battery of accumulators) Ac through the check valve CV_2. The pressures are displayed on the manometers M_1 and M_2 and

electrically confirmed by the pressure switch PS. In this phase, the directional valve DV is not actuated, as the electromagnet E is not under power. When the main spindle MS is completely stopped, the coupling EC must be disengaged. The entire unit is protected against overpressure by the pressure relief valve PRV. The accumulator Ac is bladder type and is charged with nitrogen at the appropriate pressure [4, 5, 6, 7]. Depending on the machine size, batteries of accumulators can be used [3, 4, 7].
For restarting the machine, the coupling EC and the electromagnet E of the directional valve DV will be actuated. The P/M reversible machine will operate in hydraulic MOTOR. The pressure existing in the accumulator will drive, on the P - B path of the directional valve DV, the two pilot operated check valves PCV_1 and PCV_2, allowing the supply of the motor through PCV_2 and its discharge through PCV_1. In this phase, the hydraulic motor together with the motor of the main kinematic chain will start the main spindle.
Figure 3 shows a basic diagram; in reality there are also other mechanical and electronic systems for synchronization and protection. After reaching the intended rotational speed, the EC couplingis deactivated.

3. Calculation of the braking system

For the beginning, the following elements are considered as known: E_C – kinetic energy accumulated by the mobile assembly that is to be recovered; n_T – number of revolutions accepted at the level of the spindle of the P/M reversible hydraulic machine. The following notations will be also used: V_0 - total volume of the accumulator; p_0 – nitrogen pre-charge pressure [4, 8, 9]; γ - nitrogen adiabatic coefficient; ΔV – volume of oil circulated between the P/M hydraulic machine and the accumulator in the braking and acceleration phases; p_1 - nitrogen maximum pressure in accumulator; p_2 - nitrogen minimum pressure in accumulator; p_{PRV} – pressure set at the pressure valve. It is assumed that between all these pressures there is a relation as follows:

$$p_0 < p_2 < p_1 < p_{PRV} \tag{1}$$

If the mechanical losses by friction are neglected, it can be considered that the energy transfer is made according to the relation:

$$E_C = \frac{p_1+p_2}{2} \times \frac{p_0 \times V_0}{p_1} \times \left[\left(\frac{p_1}{p_2}\right)^{\frac{1}{\gamma}} - 1\right] \tag{2}$$

In relation (2) it was considered that the discharge of the accumulator is made adiabatically [4, 5, 8] and that the pressure throughout this entire phase is the average of the minimum and maximum pressures.
The volume circulated, in the absence of flow losses, will have the value:

$$\Delta V = q_{P/M} \times n_1 \tag{3}$$

$$\Delta V = \frac{p_0 \times V_0}{p_1} \times \left[\left(\frac{p_1}{p_2}\right)^{\frac{1}{\gamma}} - 1\right] \tag{4}$$

In the above relation, the number of revolutions performed till the stop of the main spindle is noted by n_1. The main spindle in turn will perform a number of revolutions n_2, according to the relations:

$$n_2 = i \times n_1 \tag{5}$$

$$i = \frac{Z_1}{Z_2} = \frac{n_2}{n_1} < 1 \tag{6}$$

The analysis of the relation (2) highlights a limitation of the energy that can be stored, according to the relation:

$$E_C < p_0 \times V_0 \tag{7}$$

At the present moment, the most commonly used accumulators operate at pressures of 320 bar at the most. According to relation (2), it is observed that under these conditions, depending on the field of application, one or several accumulators will be chosen. It should be noted once again that the very large machines may require a big number of accumulators, which can lead to excessive price increases.
For example, consider the following situation: p_0 = 180 bar, p_1 = 280 bar, p_2 = 200 bar, p_{PRV} = 300 bar. It is assumed that two accumulators with the total volume of V_0 = 50 l will be selected. In these conditions, the maximum accumulated energy, in conformity with the relation (2), is E_C = 100285 J.
If one considers that a machine with axial pistons is used, having $q_{P/M}$ = 150 cm^3, according to the relations (3) it will make a number of ~60 revolutions until it stops. If one considers that i = 1/20, the main spindle will perform ~20 revolutions until stopping.
If it is intended to use smaller hydro-pneumatic accumulators, they could be associated with accumulators exclusively used for gas.
Given these conditions, the volume V_0, distributed as in Figure 4, could be considered:

$$V_0 = V_{O/G} + V_G \tag{8}$$

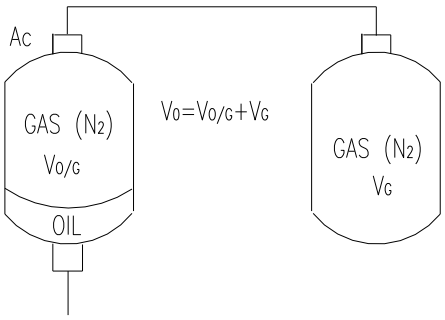

Fig. 4. Gas-oil distribution when using supplementary accumulators

The minimum recommended volume for the hydro-pneumatic accumulator (gas and oil) is:

$$V_{O/GMin} = \frac{V_0}{0.9} \times \left(1 - \frac{0.9 \times p_2}{p_1}\right) \tag{9}$$

The system will be loaded with gas taking into account the following recommendations:
If:

$$\frac{V_0}{3} \ll V_{O/G} \ll \frac{V_0}{2} \tag{10}$$

It is recommended to make the loading at the value:

$$p_0' = 0.95 \times p_0 \tag{11}$$

If the value of $V_{O/G}$ verifies the condition:

$$\frac{V_0}{4} \ll V_{O/G} \ll \frac{V_0}{3} \tag{11}$$

It is considered that the pre-load pressure must be:

$$p_0' = 0.97 \times p_0 \tag{12}$$

Subsequent research will examine the extent to which the use of additional accumulators, only with gas, can have positive influences.

4. Simulation of the operation of the hydraulic system for braking energy recovery [9, 10]

In addition to the above data, it will be considered that the value of the starting resistance moment is T = 500 Nm, at the level of the rotary spindle.
Following the simulation, the dynamic characteristics for the system pressure and the rotational speed of the hydraulic machine with axial pistons were obtained.
In the accumulator charging stage, which corresponds to the main spindle braking, the pressure in accumulator evolves as in Figure 5.

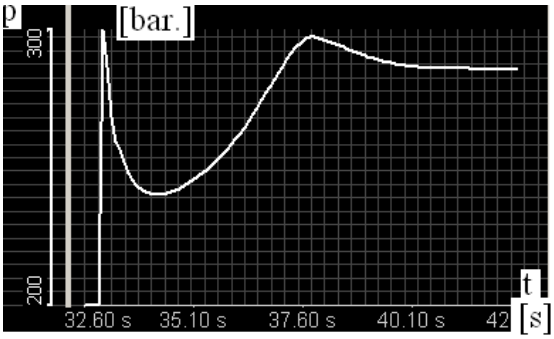

Fig. 5. Evolution of the pressure in accumulator when braking the main spindle

In a first phase, when the P/M motor is coupled, the pressure decreases due to its filling; afterwards the pressure increases up to the maximum value of 300 bar, value when the pressure valve opens and the pressure stabilizes at the value p_1.
When the main spindle is restarted, the accumulator will discharge and the pressure inside will evolve as shown in Figure 6.

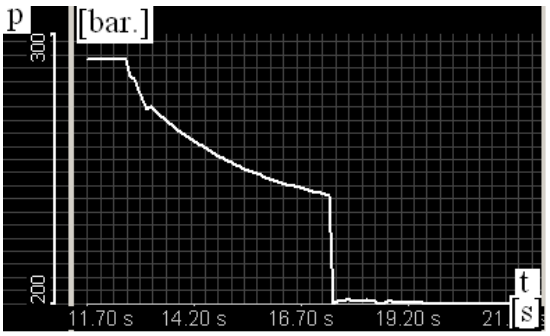

Fig. 6. Evolution of the pressure in accumulator when starting the main spindle

The pressure decreases from value p_1 = 280 bar to value p_2 = 200 bar. The system will be charged at the next braking. In this phase, depending also on the torque value, the speed of the rotary hydraulic machine, working as a motor, evolves as in Figure 7.

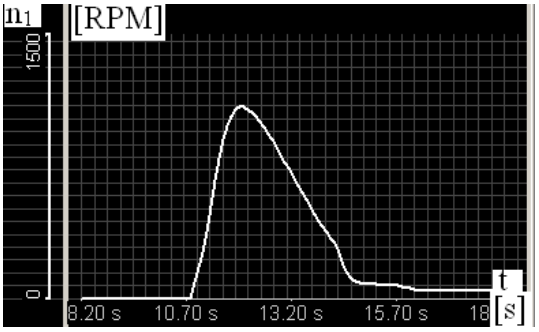

Fig. 7. Evolution of the rotary hydraulic motor in the braking phase of the main spindle

The P/M rotary hydraulic motor takes over part of the drive motor load of the main kinematic chain. The electromagnetic clutch will be deactivated after starting.

5. Conclusions

A thorough analysis of both technical and financial capacities shows that the recovery of the kinetic energy of the main kinematic chains by hydraulic way can represent an acceptable solution. Thus, the acceptable working pressures for the usual equipment do not exceed 320 bar, and the prices of the accumulators increase considerably when the accumulator volume increases.
As for the heavy or very heavy machines, the accumulators volume can exceed values of the order of hundreds of liters. This fact can also lead to considerable increases of the unit overall size, in addition to a very high price.
In further research, the aim is to develop calculation programs and methods which will allow to take also into consideration other specific parameters such as the frictions in gears and bearings and their thermal effects. It will be also studied the opportunity to use accumulators for gas only, besides the oil/gas type accumulators.

References

[1] Cristescu, Corneliu. *Recovery of Kinetic Energy in Motor Vehicles Braking/Recuperarea energiei cinetice la frânarea autovehiculelor.* Bucharest, AGIR Publishing House, 2008.
[2] Prodan, Dan. *Heavy-duty machine tools. Manufacturing, re-manufacturing/Maşini–unelte grele. Fabricare-Refabricare.* Bucharest, Printech Publishing House, 2008.
[3] ***. Catalogues and leaflets PIETRO CRANAGHI, HYDAC, BOSCH REXROTH.
[4] Guibert, Ph. *Applied Industriel Hydraulics/Hydraulique industrielle appliquee*, Université de Metz, 1991.
[5] Prodan, Dan. *Hydraulics of Production Systems /Hidraulica sistemelor de productie*. Bucharest, Printech Publishing House, 2011.
[6] Portelli, Michel. *Industrial Hydraulic Technology/Technologie d'hydraulique industrielle*. Paris, Editions Casteilla, 1995.
[7] Prodan, Dan, Mircea Duca, Anca Bucureşteanu, and Tiberiu Dobrescu. *Hydrostatic Drives - Machine Parts/Acţionări hidrostatice – Organologie*. Bucharest, AGIR Publishing House, 2005.
[8] Bucureşteanu, Anca. *Hydro-Pneumatic Accumulators. Use and Modeling/Acumulatoare pneumohidraulice. Utilizare si modelare*. Bucharest, Printech Publishing House, 2001.
[9] Prodan, Dan. *Machine Tools. Modeling and Simulation of Hydrostatic Elements and Systems/Maşini-Unelte. Modelarea şi Simularea Elementelor şi Sistemelor Hidrostatice*. Bucharest, Printech Publishing House, 2006.
[10] ***. AUTOMATION STUDIO Software package.

Signal Processing Techniques and Mathematical Modeling for Analyzing and Diagnosing Cavitation in Centrifugal Pumps

Assoc. Prof. PhD. Eng. **Ştefan ŢĂLU**

Technical University of Cluj-Napoca, The Directorate of Research, Development and Innovation Management (DMCDI), Constantin Daicoviciu St., no. 15, Cluj-Napoca, 400020, Cluj county, Romania

* stefan_ta@yahoo.com; stefan.talu@auto.utcluj.ro

Abstract: *Cavitation remains a critical issue in centrifugal pump operation, leading to performance degradation, structural damage, and increased maintenance costs. Effective cavitation detection and modeling are essential for improving pump reliability and efficiency. This review integrates two key aspects of cavitation research: signal-based fault detection methods and mathematical modeling approaches. First, we review various cavitation detection techniques based on vibration, acoustic emission, noise, and pressure pulsation signals. Each method's advantages and limitations are discussed, focusing on their effectiveness in early-stage detection, robustness, and implementation feasibility. Next, we compare different mathematical models used to simulate cavitating flows, highlighting their assumptions, strengths, and limitations in accurately predicting cavitation behavior. By bridging experimental detection techniques with computational modeling, this review provides a perspective on cavitation analysis, offering insights into future research directions that combine advanced sensing, intelligent algorithms, and improved multiphase flow simulations.*

Keywords: *Cavitation detection, Centrifugal pump, Intelligent algorithms, Fault diagnosis, Mathematical modeling, Multiphase flow, Signal processing*

1. Introduction

Hydraulic systems are indispensable in various industries, enabling the efficient and controlled transmission of power through fluid movement, which provides precise control over machinery and equipment. This allows for the execution of critical tasks such as lifting, pressing, and driving complex systems with high efficiency and reliability [1-3]. The design and study of hydraulic systems [4, 5], along with mathematical modeling and simulation of their operation [6], further enhance the understanding and optimization of these systems, allowing for accurate prediction of performance, energy consumption, and system behavior under varying operational conditions [7].
Pumps, as integral components of hydraulic systems, play a fundamental role in various industrial, agricultural, and domestic applications by ensuring efficient fluid circulation, pressure regulation, and energy conversion [8-10]. Despite their widespread utilization, pump systems are inherently susceptible to various operational inefficiencies and mechanical failures [8]. Recent developments in intelligent diagnostic methods for hydraulic piston pumps have provided valuable insights into detecting and mitigating such faults, enhancing pump systems' overall reliability [11, 12].
Centrifugal pumps are extensively used in industries including manufacturing, agriculture, oil and chemicals, and aerospace. Pump systems are inherently vulnerable to various problems, with cavitation being one of the most damaging [13, 14]. Cavitation, a complex multiphase flow phenomenon, arises when local static pressure drops below the vapor pressure of the working fluid, leading to the formation of vapor bubbles. As these bubbles travel into regions of higher pressure, they undergo rapid implosion, generating high-intensity pressure waves that result in severe material erosion, flow disturbances, noise, and excessive vibration. Over time, the persistence of cavitation leads to significant degradation in pump performance, reduced energy efficiency, and increased maintenance costs, making it a critical subject of investigation in hydraulic machinery [15]. The transient and highly nonlinear nature of cavitation poses significant challenges in both its detection and predictive modeling. The collapse of vapor cavities introduces unsteady flow characteristics that complicate conventional diagnostic approaches. Additionally, the unpredictability of cavitation initiation and development due to factors such as flow velocity, system pressure, temperature variations, and pump geometry further complicates its analysis. Traditional detection methods rely on physical inspection and performance monitoring; however, these

techniques often fail to provide early warnings or quantify the severity of cavitation in real time. In response to these limitations, modern signal processing techniques have emerged as powerful tools for cavitation diagnosis. By leveraging acoustic emission, vibration analysis, noise monitoring, and pressure pulsation measurements, researchers have developed advanced methodologies to characterize cavitation-induced fluctuations and identify early warning indicators [15, 16]. The integration of artificial intelligence (AI), machine learning (ML), and deep learning (DL) algorithms further enhances the capability of these techniques by enabling automated feature extraction, pattern recognition, and state classification with improved accuracy and robustness [17-21].

In parallel, mathematical modeling has played a crucial role in understanding the fundamental mechanisms governing cavitating flows [22]. Theoretical frameworks based on fluid dynamics, such as the Bernoulli equation and Navier-Stokes formulations, provide a foundation for simulating cavitation dynamics under varying operational conditions. Computational Fluid Dynamics (CFD) models have been extensively developed to predict cavitation inception, bubble dynamics, and flow field variations [23-25]. These models incorporate multiphase flow representations, including homogeneous and heterogeneous cavitation models, to capture the phase transition phenomena with greater fidelity. Despite significant advancements, challenges remain in achieving computational efficiency, model validation, and adaptability to real-world pump systems.

This review explores cavitation detection methods utilizing signal processing techniques, providing a comparative analysis of existing mathematical models for cavitation simulation. The discussion encompasses the principles, methodologies, and recent developments in vibration-based, acoustic, noise, and pressure pulsation detection approaches. Furthermore, a critical evaluation of different cavitation models is provided, highlighting their applicability, accuracy, and computational constraints. By integrating experimental and theoretical perspectives, this review aims to bridge the gap between empirical diagnostics and predictive modeling, offering insights into future research directions in cavitation analysis of centrifugal pumps.

2. Research methodology

A comprehensive survey was conducted to evaluate the increasing research focus on signal processing techniques and mathematical modeling for centrifugal pump cavitation analysis and diagnosis. Recognizing the practical significance of this domain, the investigation covers studies published between 2011 and 2024. This review examines a range of journal articles exploring key concepts and their applications in cavitation detection and modelling for centrifugal pumps.

2.1 The common mathematical formulations for cavitation modelling

Cavitation modeling plays a crucial role in understanding and predicting the behavior of multiphase flows, particularly in hydraulic systems and turbomachinery. Cavitation can lead to three distinct and unfavorable consequences: (1) a reduction in head-capacity and efficiency performance, (2) impeller deterioration due to pitting and erosion, and (3) structural vibrations accompanied by increased noise levels. Due to the complex nature of cavitation, various mathematical models have been developed to simulate its dynamics with varying levels of fidelity.

1) Multiphase flow modeling

Multiphase flow modeling describes the behavior of two or more coexisting phases within a fluid system. The classification of multiphase flows includes:

• Gas–liquid and liquid–liquid flows, which encompass cavitation phenomena where vapor bubbles form and collapse within a liquid medium.
• Gas–solid flows, involving dispersed solid particles in a gaseous carrier fluid.
• Liquid–solid flows, where solid particles interact with a surrounding liquid phase.

Cavitation is a subset of gas–liquid multiphase flows, specifically categorized as bubbly flow, in which discrete gaseous bubbles are suspended in a continuous liquid phase. The accurate modeling of cavitation requires capturing phase interactions, bubble dynamics, and mass transfer mechanisms. Cavitation models are typically categorized into two-fluid and one-fluid models, each with its own advantages and limitations [22]. Additionally, cavitation modeling approaches can be broadly classified into two primary categories: direct models and averaged models [26].

2) Two–fluid models

Two-fluid models are employed to separately resolve the conservation equations governing both the discrete and continuous phases in cavitating flows. These models provide a detailed representation of phase interactions, enabling a more accurate prediction of cavitation dynamics. The solution of these conservation equations can be achieved using one of the following approaches:

• Euler approach: This method involves solving the conservation equations for each phase by considering the flow properties at a fixed spatial location while monitoring the transport of individual phases. This approach is particularly useful when treating both phases as interpenetrating continua, where phase interaction terms, such as momentum and mass exchange, must be carefully modeled.

• Lagrange approach: In this method, the conservation equations for the continuous phase are solved using the Eulerian framework, whereas the discrete phase (e.g., cavitation bubbles) is tracked along individual trajectories using a Lagrangian formulation. This allows for a more detailed representation of bubble dynamics, including coalescence, breakup, and transport, but requires substantial computational resources due to the necessity of tracking numerous discrete elements.

While these methods offer high accuracy in modeling cavitating flows, they become computationally expensive when the vapor volume fraction exceeds a critical threshold. In practical simulations, alternative modeling approaches may be preferred to reduce computational costs while maintaining acceptable accuracy.

3) One–fluid models

One-fluid models provide a simplified yet effective approach to modeling cavitating flows by assuming that the conservation equations govern a homogeneous mixture of liquid and vapor phases. Unlike two-fluid models, where the individual phases are treated separately, the one-fluid framework integrates the two phases into a single continuum with averaged properties. Given that cavitating flows are typically assumed to be isothermal, only the mass and momentum conservation equations are considered, while energy conservation equations are often omitted.

$$\rho = \alpha\rho_v + (1-\alpha)\rho_l \tag{1}$$

$$(\rho u) = \alpha(\rho u)_v + (1-\alpha)(\rho u)_l \tag{2}$$

where: ρ, ρ_v, ρ_l represent the densities of the mixture, vapor phase, and liquid phase, respectively [$kg \cdot m^{-3}$]; (ρu), $(\rho u)_v$, $(\rho u)_l$ denote the momentum of the mixture, vapor phase, and liquid phase, respectively [$kg \cdot m^{-2} \cdot s^{-1}$]; u is the velocity of the mixture [$m \cdot s^{-1}$]; α is the vapor volume fraction, a dimensionless parameter ranging from 0 (pure liquid) to 1 (pure vapor).

Several variations of one-fluid models exist, each differing in their assumptions regarding phase interactions and the additional equations required to close the system:

• Zero-equation models

Zero-equation models take an even more simplified approach by solving only the mixture conservation equations without introducing any additional transport equations. Instead of explicitly modeling phase interactions, these models rely on a barotropic state law, which defines the relationship between density and pressure. The density of the mixture is directly computed as a function of pressure, eliminating the need for additional conservation equations.

• One-equation models

One-equation models assume that there is no slip between the phases, meaning that both the liquid and vapor phases move with the same velocity. Instead of solving separate conservation equations for the individual phases, these models introduce a single additional equation governing the conservation of vapor mass, expressed as:

$$\frac{\partial \alpha\rho_v}{\partial t} + \nabla(\alpha\rho_v u) = R_e - R_c \tag{3}$$

where: R_e and R_c represent the source terms corresponding to vapor generation (evaporation) and condensation, respectively [$kg \cdot m^{-3} \cdot s^{-1}$]. The primary distinction among different one-equation models lies in the formulation of these source terms, which govern the rate of phase transition between liquid and vapor.

Several one-equation models have been developed to describe cavitation phenomena, primarily based on transport equations for vapor volume fraction. These models incorporate phase change

dynamics using source terms derived from bubble dynamics equations, such as the Rayleigh-Plesset equation.
- Kunz model. The Kunz model is a one-equation cavitation model where the vapor volume fraction is governed by a transport equation. The source terms, R_e and R_c, represent the mass transfer between liquid and vapor and are determined empirically. This model is widely used due to its simplicity and computational efficiency. However, its reliance on empirical coefficients makes it less adaptable to complex cavitation phenomena.
- Singhal model. The Singhal model incorporates the Rayleigh–Plesset equation, providing a more physics-based approach to cavitation modeling. It includes corrections for turbulent pressure fluctuations, making it suitable for a wide range of flow conditions. However, the model requires additional parameters such as the turbulent kinetic energy (k), which can increase computational cost.
- Zwart–Gerber–Belamri (ZGB) model. The ZGB model also relies on the Rayleigh–Plesset equation but introduces nucleation site volume fraction (α_{nuc}) to model cavitation inception. This model is particularly useful for industrial applications due to its balance between accuracy and computational efficiency. However, it requires careful calibration of the nucleation site volume fraction and bubble radius.
- Schnerr and Sauer model. The Schnerr and Sauer model uses a bubble dynamics-based approach, where the number of bubbles per unit volume is a key parameter. This model is highly effective in simulating cavitation in high-speed flows and turbine applications. However, it can be computationally expensive due to its detailed bubble tracking mechanism.
A comparative analysis of one-equation cavitation models are shown in Tables 1 and 2.

Table 1: A comparative analysis of one-equation cavitation models

Model	Governing equation	Advantages	Limitations
Kunz Model	One-equation transport model	- Computationally efficient - Simple implementation	- Empirical nature limits accuracy in complex flows - Less physics-based
Singhal Model	Rayleigh–Plesset equation with turbulence correction	- More physics-based than Kunz - Accounts for turbulent fluctuations	- Requires additional turbulence parameters - Higher computational cost
ZGB Model	Rayleigh–Plesset equation with nucleation site correction	- Balances accuracy and computational efficiency - Suitable for industrial applications	- Requires calibration of nucleation site parameters
Schnerr and Sauer Model	Bubble dynamics-based approach	- Detailed cavitation representation - Suitable for high-speed flows	- Computationally intensive due to bubble tracking

Table 2: Comparison of one-equation cavitation models in terms of computational efficiency, stability, accuracy, and applications

Model	Computational efficiency	Numerical stability	Accuracy in predicting cavitation	Applications
Kunz Model	High (fastest)	High	Moderate	Fast simulations with moderate accuracy
Singhal Model	Moderate	Moderate	High	Turbulent cavitating flows
ZGB Model	Moderate to High	Moderate to High	High	Industrial applications
Schnerr and Sauer Model	Low (most expensive)	Moderate to Low	Very High	High-speed, detailed cavitation studies

• Two-equation models
Two-equation models account for slip between the liquid and vapor phases, meaning that each phase can move at different velocities. In addition to the conservation equations of the mixture, two additional equations are introduced to govern the conservation of either the liquid or vapor phase. These models allow for a more accurate representation of phase interactions, but at the cost of increased computational complexity.

Advantages and limitations of one-fluid models
One-fluid models offer computational efficiency and simplicity compared to two-fluid models, making them attractive for simulating cavitating flows in engineering applications such as hydrofoils, pumps, and nozzles. However, their reliance on averaged properties and simplified phase interaction assumptions may lead to inaccuracies in highly dynamic cavitating flows where phase separation, slip velocity, and bubble dynamics play a significant role. The choice between different one-fluid modeling approaches depends on the required accuracy and computational resources available for the simulation.

2.2 Principles and approaches in cavitation detection

Several methods are employed to detect cavitation of pumps based on different physical principles such as vibration, acoustic emission, noise, and pressure pulsation (Table 3). These methods are distinguished by their ability to monitor different parameters, which help identify cavitation onset, progression, and severity. Each method has its own strengths and weaknesses depending on the specific pump system, operating conditions, and desired level of sensitivity. Combining multiple techniques can enhance the reliability and accuracy of cavitation detection [15].

Table 3: Overview of common detection cavitation methods

Method	Parameters monitored	Detection principle	Advantages	Limitations
Vibration method	Vibration acceleration, frequency, RMS, variance	Vibration signals detected by accelerometers	- High sensitivity - Suitable for real-time detection	- Requires placement of sensors - May not detect early cavitation
Acoustic emission	Signal energy, amplitude, rise time, duration	Microjet or shockwave induced acoustic signals	- Sensitive to high-frequency cavitation signals - Non-invasive	- Requires high-quality sensors - Signal attenuation in air
Noise method	Noise intensity, frequency spectrum	Noise generated by cavitation bubble formation and collapse	- Useful for early detection - Simple and cost-effective	- Difficult to distinguish from other types of noise - Limited to detectable noise frequency range
Pressure pulsation	Pressure fluctuations, frequency spectrum	Pressure pulsations caused by cavitation-induced flow field disturbances	- Effective in varying pump flow conditions - High signal-to-noise ratio	- Complex data interpretation - Requires high precision sensors

a) Vibration signal processing methods
Vibration signal processing techniques employed for cavitation detection and analysis primarily fall into three broad categories: time-domain analysis, frequency-domain analysis, and time–frequency domain analysis. These methodologies play a crucial role in extracting meaningful information from vibration signals, enabling the identification and characterization of cavitation phenomena in pumping systems. Time-domain analysis focuses on the direct examination of vibration signals over time, capturing transient characteristics and statistical parameters such as root mean square (RMS), peak values, crest factor, and kurtosis. These features provide essential insights into the severity and evolution of cavitation-induced vibrations. Frequency-domain analysis involves transforming time-domain signals into their spectral representations using techniques such as the Fast Fourier Transform (FFT) and Power Spectral Density (PSD). This approach facilitates the identification of dominant frequency components associated with cavitation, distinguishing them from other mechanical or hydraulic disturbances. Time–frequency domain analysis integrates both time and frequency characteristics, allowing for the assessment of non-stationary signals. Methods such as Wavelet Transform (WT), Short-Time Fourier Transform (STFT), and Hilbert-Huang Transform (HHT) enable the precise localization of cavitation-induced transient events across different frequency bands. These techniques are particularly advantageous in detecting early-stage cavitation, where signal characteristics dynamically evolve over time.

A comprehensive summary of the latest advancements and applications of these vibration signal processing methodologies in cavitation diagnosis is shown in Table 4.

Table 4: Comprehensive overview of vibration signal processing methods

Analytical method	Techniques used	Advantages	Limitations
Time-domain analysis (Refs. [27], [28])	Correlation analysis, amplitude range analysis, statistical feature extraction (RMS, peak values, kurtosis, crest factor)	Simple and intuitive; directly reflects cavitation-induced variations; effective for periodic signals	Limited to stationary signals; lacks frequency-related insights; susceptible to noise
Frequency-domain analysis (Ref. [28])	Fourier Transform (FT), Power Spectral Density (PSD), envelope analysis, difference frequency analysis, cepstral analysis	Provides insight into dominant frequency components related to cavitation; useful for steady-state conditions	Inability to capture transient, time-varying characteristics; requires pre-filtering for accuracy
Time–frequency domain analysis (Ref. [29], [30])	Short-Time Fourier Transform (STFT), Wavelet Transform (WT), Empirical Mode Decomposition (EMD), Wigner–Ville Distribution (WVD), Hilbert-Huang Transform (HHT)	Suitable for non-stationary signals; enables localized analysis of transient events; effective for cavitation detection and diagnosis	Computationally intensive; choice of transformation parameters affects accuracy

Figure 1 illustrates the relationship between cavitation states and their corresponding vibration characteristics in centrifugal pumps.

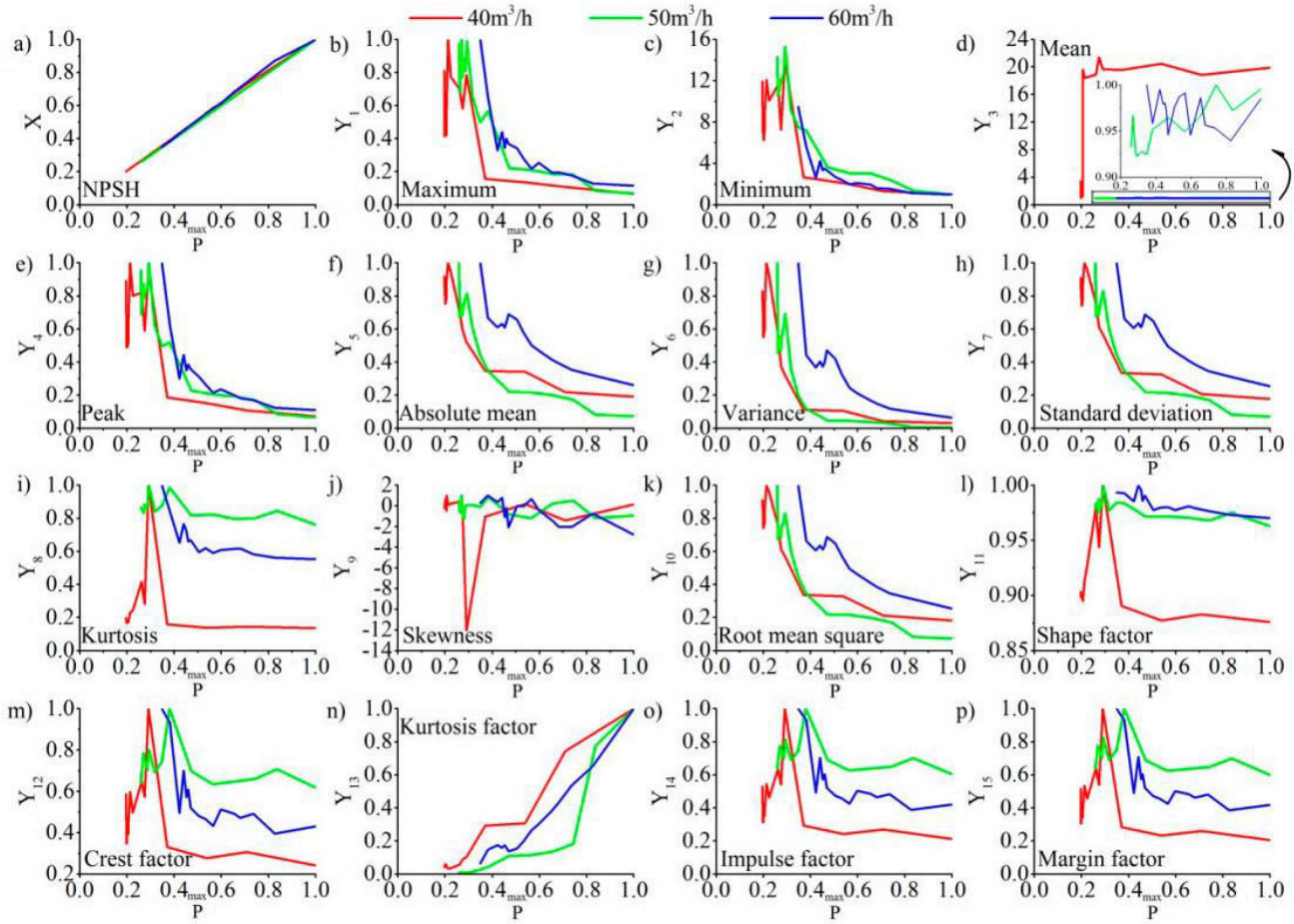

Fig. 1. Normalization value: (a) The net positive suction head (NPSH), (b) Maximum, (c) Minimum, (d) Mean, (e) Peak, (f) Absolute mean, (g) Variance, (h) Standard deviation, (i) Kurtosis, (j) Skewness, (k) Root mean square, (l) Shape factor, (m) Crest factor, (n) Kurtosis factor, (o) Impulse factor, (p) Margin factor. (Reprinted from ref. [27] with permission of MDPI AG publisher).

Figure 2 illustrates the cavitation-induced vibration signal at 40 Hz for a centrifugal pump, shown in time and frequency domains, with random high-frequency components indicating cavitation [28].

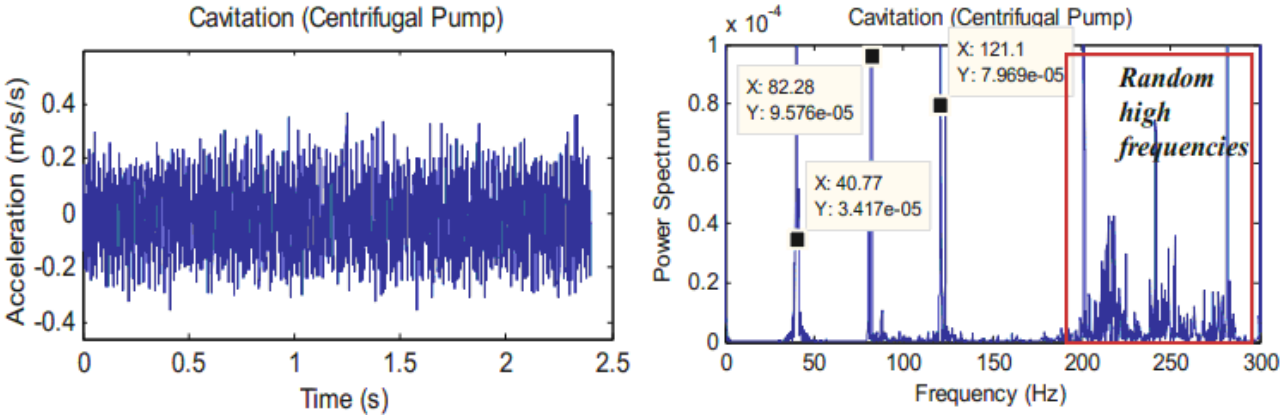

Fig. 2. Cavitation-induced vibration signal at a rotational speed of 40 Hz for a centrifugal pump. (a) Time-domain representation. (b) Frequency-domain representation, where random high-frequency components indicate cavitation. (Reprinted from ref. [28] with permission of Springer Nature Switzerland AG publisher).

Figure 3 illustrates the time-domain representation of signal x(t) and the corresponding results of three computational methods (time–frequency algorithms) for a centrifugal pump: (a) time-domain diagram of x(t), (b) time–frequency algorithm (Wigner–Ville distribution method), (c) time–frequency algorithm (short time Fourier transform method), and (d) time–frequency algorithm (United algorithm of STFT–WVD method) [29].

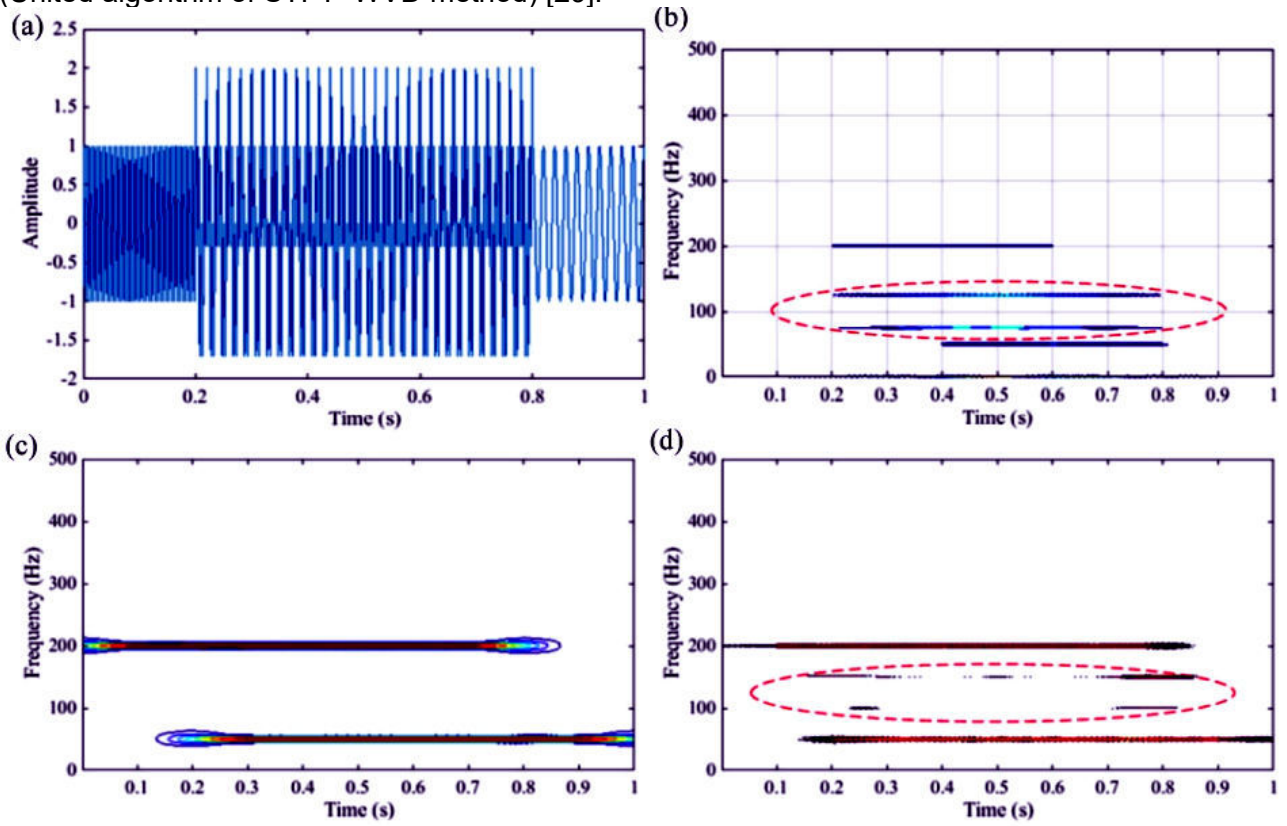

Fig. 3. Cavitation-induced vibration signal for a centrifugal pump. Time-domain representation of signal x(t) and corresponding results of three time–frequency algorithms. (a) Time-domain representation of x(t). (b) Wigner–Ville distribution (WVD) method. (c) Short-Time Fourier Transform (STFT) method. (d) Combined STFT–WVD method. (Reprinted from ref. [29] with permission of Springer Nature Switzerland AG publisher).

Table 5 provides a comparative analysis of various frequency-domain techniques used for cavitation diagnosis, highlighting the advantages such as the ability to identify dominant frequency components and the limitations like difficulty in capturing transient characteristics. Similarly, Table

6 shows a review of time-frequency domain techniques, emphasizing the strengths of adaptability to non-stationary signals and the challenges, such as the trade-offs in time-frequency resolution or issues like mode mixing in some methods.

Table 5: Comparative analysis of frequency-domain techniques for cavitation diagnosis

Method	Key Principle	Advantages	Limitations	Common Applications
Fourier Transform (FT)	Decomposes the signal into its frequency components	Simple and well-established; identifies dominant frequencies	Inability to capture transient, time-varying characteristics	Identifying steady-state cavitation frequencies
Power Spectral Density (PSD)	Measures the power distribution of the signal across frequencies	Provides a clear representation of frequency components	Requires steady-state conditions; cannot handle transient events	Monitoring dominant frequencies in cavitating pumps
Envelope Analysis	Analyzes the modulation of the signal amplitude	Effective for detecting low-frequency cavitation signatures	Can miss high-frequency cavitation details	Detecting cavitation-induced vibration signatures
Difference Frequency Analysis	Analyzes the difference between peak frequencies in the signal	Highlights cavitation-induced low-frequency variations	Sensitivity to signal noise can reduce accuracy	Detecting cavitation by evaluating frequency shifts
Cepstral Analysis	Uses the inverse Fourier transform of the log-spectral representation	Helps separate periodic components from a signal's noise	Less effective for non-stationary signals	Identifying cavitation by examining harmonic components

Table 6: Comparative analysis of time–frequency domain techniques for cavitation diagnosis

Method	Key principle	Advantages	Limitations	Common applications
Short-Time Fourier Transform (STFT)	Segments the signal and applies FT to each segment	Provides a time-localized frequency representation	Fixed time-frequency resolution trade-off	Detecting cavitation onset and transient events
Wavelet Transform (WT)	Uses scalable wavelets to analyze signals at multiple resolutions	Adaptive resolution; effective for both transient and periodic signals	Requires appropriate wavelet selection for optimal performance	Identification of cavitation-induced broadband noise
Empirical Mode Decomposition (EMD)	Decomposes signals into intrinsic mode functions (IMFs) using adaptive filtering	Suitable for non-linear and non-stationary signal analysis	Mode mixing issues can affect interpretation	Feature extraction in cavitation pattern recognition
Hilbert-Huang Transform (HHT)	Combines EMD with Hilbert spectral analysis	High adaptability for analyzing complex, non-stationary signals	Computationally expensive; requires robust mode decomposition	Time-localized cavitation feature analysis
Wigner–Ville Distribution (WVD)	Provides high-resolution time-frequency representation	Superior energy concentration; precise localization of transients	Prone to cross-term interference	High-resolution cavitation impact signal analysis

The frequency distribution of cavitation-induced vibrations spans a broad spectrum, predominantly concentrated in high-frequency bands, with distinct sensitivity characteristics observed across these frequency ranges [15]. Cavitation, being a dynamic and nonlinear phenomenon, interacts differently with various frequency bands, leading to variations in vibration patterns. The high-

frequency vibrations are often associated with the rapid formation and collapse of cavitation bubbles, which generates sharp, high-energy pulses. These pulses typically manifest as significant peaks in the vibration signal at frequencies ranging from several kilohertz to tens of kilohertz. However, the interaction between cavitation and low-frequency components, especially below 1 kHz, has also been of significant interest in the literature, as these frequencies are often linked to broader system responses, such as mechanical resonances and pump rotor behavior. Studies have shown varying responses of cavitation to different frequency ranges, with some researchers emphasizing high-frequency bands for fault detection, while others point to the importance of low-frequency signals in capturing early-stage cavitation and identifying subtle pump instabilities [31-36]. These findings highlight the complexity of cavitation vibration characteristics and the need for comprehensive frequency-domain analysis to fully understand its impact on pump performance.

In recent years, machine learning has emerged as a pivotal tool within artificial intelligence for extracting meaningful insights from vast and intricate datasets. Fault classification algorithms, such as Support Vector Machines (SVM), Extreme Learning Machines (ELM), and their enhanced variants, are among the prominent methodologies employed in this domain. The integration of machine learning with vibration analysis has further enhanced its efficacy, becoming a powerful approach for detecting pump cavitation faults [37-39]. Artificial neural networks (ANNs), have significantly advanced in fault detection applications. Techniques such as nonlinear autoregressive models, support vector machines, and random forests are commonly employed for cavitation detection. Among these, the extreme learning machine (ELM) has demonstrated superior accuracy compared to other methods like BP neural networks and random forests. While machine learning approaches have evolved, challenges remain, including the inability of shallow neural networks to handle complex nonlinear relationships without expert input. The advent of deep learning models, particularly deep neural networks like SAE, LSTM, and CNN, has enhanced the ability to process large datasets with high precision. CNN, in particular, has outperformed other methods in cavitation diagnosis, showing higher accuracy in analyzing vibration signals. Despite the success of deep learning, challenges such as resource limitations and the need for multi-channel sensor inputs remain. Traditional methods, however, continue to hold value in specific scenarios, and the choice of method should be tailored to the working conditions [40-43].

In cavitation detection, recent advancements have focused on improving both accuracy and speed, with various innovative methods demonstrating significant progress. Techniques such as hybrid feature selection combined with empirical modal decomposition and generalized regression neural networks (GRNN) have achieved near-perfect detection accuracy, while also enhancing speed [44]. Additionally, noise reduction methods, like time-frequency image denoising and convolutional neural networks (CNN), have proven effective in improving detection accuracy in noisy environments. Other strategies, including artificial immune algorithms, bispectral analysis with transfer learning, and the constant false alarm rate (CFAR) criterion, have demonstrated superior accuracy compared to traditional methods, particularly in the early stages of cavitation detection [45-47]. The location of vibration measurement points significantly influences the accuracy of cavitation detection, with certain areas, such as near the volute tongue, proving most effective for capturing reliable signals [30]. Research shows that sensors positioned closer to the cavitation zone yield higher detection accuracy, while optimizing sensor placement can reduce costs and improve inspection efficiency [15].

b) Acoustic emission signals processing methods

Acoustic emission (AE) refers to releasing elastic waves when particles within a material experience relative motion, thereby discharging strain energy in the form of these waves. This phenomenon provides a means of evaluating materials' internal condition or structural integrity. The application of AE technology in detecting equipment faults is closely linked to the discovery of the Kaiser effect, which demonstrated that materials have the ability to 'remember' previous stress events. In pumps, the primary sources of AE signals are associated with the following conditions [48-50]:

- Low-pressure zones: These are typically located behind the pump blade inlet, an area particularly prone to cavitation due to significant pressure drops.

- Pressure instability: Unstable conditions within the pump lead to irregular pressure fluctuations, which contribute to AE emissions.
- Shear stress: Large shear forces generated within the fluid flow also induce AE signals, particularly in turbulent regions.

When cavitation occurs, microjets and shock waves are generated by the collapse of vapor bubbles, interacting with the pump's components, such as the impeller and pipe walls. These interactions create AE signals that predominantly fall within the medium to high-frequency range, spanning from 1 kHz to 1 MHz. These signals propagate through the pump system, enabling sensitive detection of cavitation-related phenomena. AE signals are particularly effective for detecting impulsive pressure variations within the pump, which are indicative of cavitation, especially in large-scale systems. Acoustic emission sensors are strategically placed in high-risk areas, such as near the impeller, inlet, and outlet of the pump, to capture the AE signals generated during cavitation events. However, since AE signals attenuate rapidly in air, the use of couplants is essential for ensuring effective signal transmission. Several characteristics of AE signals, such as amplitude, energy, rise time, duration, and event counts, can be extracted and analyzed to assess the presence and severity of cavitation. These parameters are crucial for identifying cavitation faults and can significantly enhance diagnostic accuracy in pump monitoring systems. By leveraging AE technology, cavitation can be detected at an early stage, allowing for timely maintenance and preventing potential damage.

c) Noise processing methods

The acoustic emissions produced by a centrifugal pump are intrinsically influenced by its geometric configuration, including size and structural design, as well as the operational parameters such as rotational speed and load conditions. Additionally, hydrodynamic instabilities within the pump significantly contribute to elevated noise levels. These instabilities may arise due to phenomena such as flow separation (stall), system-wide oscillations (surge), and cavitation, each of which induces fluctuating pressure fields and turbulence, thereby amplifying acoustic disturbances [51].

It is known that cavitation-induced noise in centrifugal pumps is a type of hydrodynamic noise distinct from mechanical noise, characterized by a unique frequency differing from the blade passing frequency. This noise results from the formation and collapse of bubbles, with the collapse generating radiation noise that is transmitted through the pump body and detected by sound sensors, although the precise mathematical model of this process remains under experimental investigation [51-54]. Figure 9 illustrates the impact of cavitation on noise characteristics in a centrifugal pump, comparing noise spectra before and after cavitation inception and analyzing the relationship between noise levels, specific frequency components, and total delivery head under varying NPSH conditions.

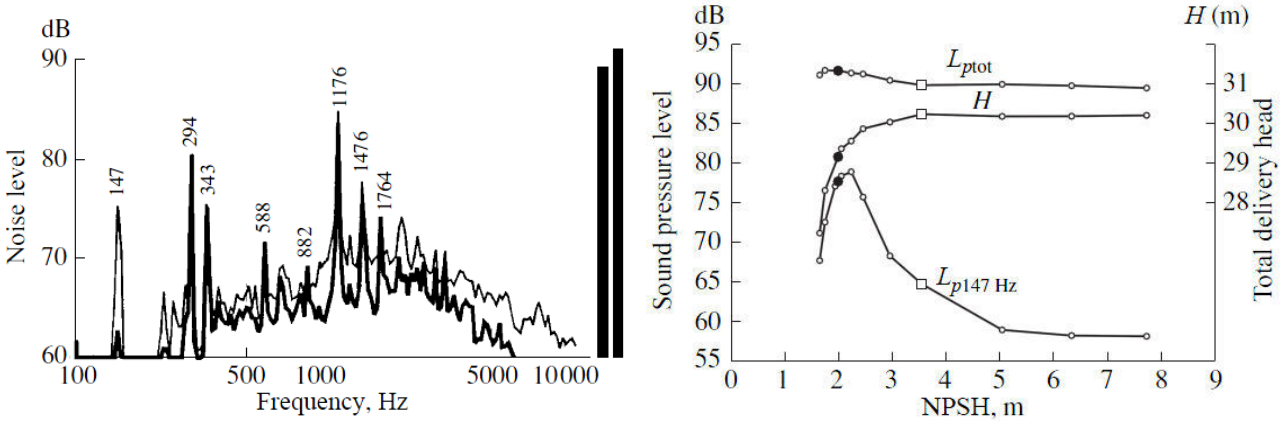

Fig. 4. (a) Noise spectra before cavitation inception (thick line) and after full development (thin line) for a centrifugal pump. (b) Comparison of total noise level (L_{ptot}), noise level at 147 Hz (L_{p147} Hz), and total delivery head (H) for different available NPSH values. (Reprinted from ref. [51] with permission of Springer Nature Switzerland AG publisher).

Noise measurements are frequently integrated with other signal analyses, particularly vibration signals, to enhance the accuracy and reliability of cavitation detection.

d) Pressure pulsation methods

Research on cavitation-induced pressure pulsation in centrifugal pumps focuses on key locations such as the inlet, outlet, volute, and impeller [15]. Studies indicate that inlet pressure pulsations are more sensitive to cavitation, with frequency components shifting from low to high as cavitation progresses [55]. At the volute tongue, cavitation leads to broadband pulsation and reduced main frequency amplitude. Severe cavitation increases high-frequency components, while pressure pulsation amplitudes vary across different pump sections. For cavitation detection, pressure pulsation signals, being nonlinear and non-stationary, require advanced signal processing techniques. Methods like wavelet analysis, singular value decomposition, and deep learning improve fault diagnosis accuracy. While pressure-based detection is less comprehensive than vibration or acoustic methods, it is cost-effective, resistant to interference, and crucial for monitoring pump faults [56-60]. Figure 5 compares pressure pulsation amplitudes at at f_{BPF} under non-cavitation and critical $NPSH_c$ conditions (a) and shows angular distributions for different cavitation numbers at the nominal flow rate (b).

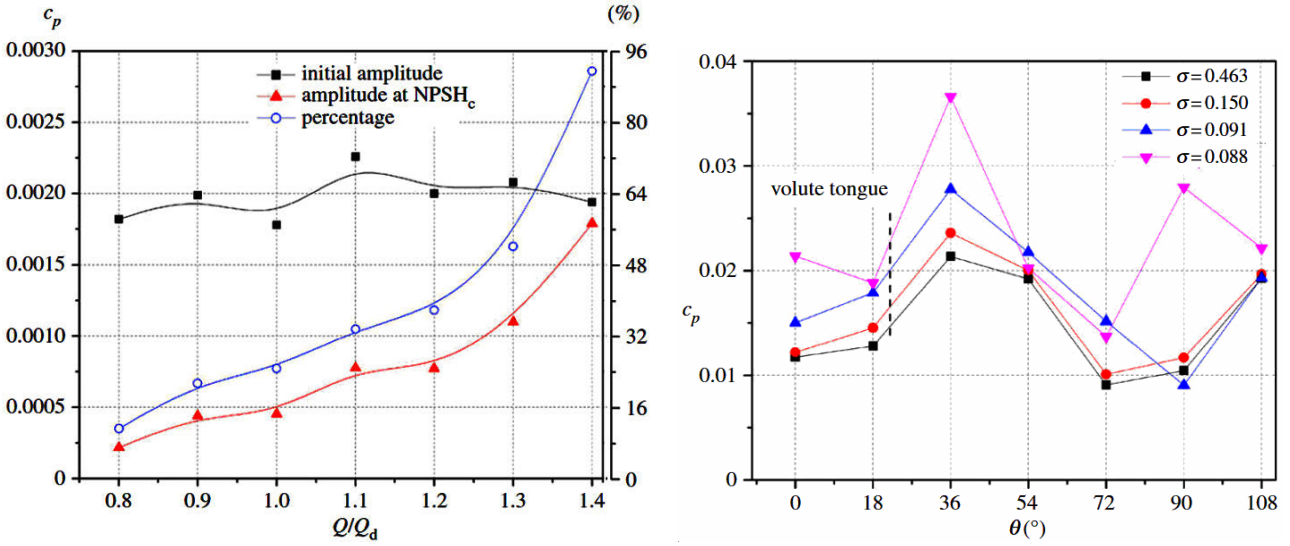

Fig. 5. a) Comparison of amplitudes at f_{BPF} for In1 under non-cavitation and critical point $NPSH_c$ conditions. b) Angular distributions of pressure amplitudes at f_{BPF} for different cavitation numbers at nominal flow rate. (Reprinted from ref. [55] with permission of Royal Society publisher).

3. Analysis, limitations, comparison of methods and future challenges

Acoustic emission and noise methods excel in early cavitation detection, particularly in non-contact settings, but are hindered by noise reduction challenges and high sensor costs. Acoustic emission is effective in complex, harsh environments but remains underexplored in industrial applications. Vibration-based detection faces signal attenuation and lower accuracy for early cavitation detection, while pressure pulsation methods are more resistant to interference but less accurate and difficult to implement in practical settings due to sensor installation complexity.

Signal-based cavitation detection methods are evolving to address challenges such as noise interference and complex signals. Key trends include:

- Advancement in signal acquisition: while pump systems complicate signal acquisition, advancements in sensing and signal processing are improving cavitation fault detection.
- Optimization of existing methods: many current methods can be refined, with ongoing research focusing on enhancing algorithms and detection accuracy.
- Integration of AI: AI and machine learning, particularly reinforcement learning, are enhancing the efficiency and precision of cavitation detection.
- Cross-field innovations: techniques from other fault detection fields are being adapted to improve cavitation detection through innovative signal processing and computational models.
- Versatility in detection systems: cavitation detection systems need to be more versatile, as current methods are often pump-specific. Future research should aim for generalized solutions applicable to various pump types.

4. Conclusions

This review examines various fault detection methods based on different signals, providing valuable insights into centrifugal pump cavitation detection. It highlights advancements in vibration, noise, acoustic emission, and pressure pulsation methods, emphasizing their contributions to improving detection accuracy and reliability. Despite progress, challenges such as sensor costs, noise reduction, and feature extraction remain, requiring further research to fully realize the potential of these methods. Additionally, the integration of advanced technologies, such as artificial intelligence, could significantly enhance the effectiveness of these detection systems. With continued development, signal-based cavitation detection methods will find substantial applications in fault detection systems, ultimately contributing to the optimization of pump performance and the prevention of costly mechanical failures.

Conflicts of Interest: The author declares no conflict of interest.
ORCID: Ştefan Ţălu, https://orcid.org/0000-0003-1311-7657.

References

[1] Yaghoubi, Majid, and Hamed Tavakoli. "Hydraulic Systems". In: *Mechanical Design of Machine Elements by Graphical Methods. Materials Forming, Machining and Tribology*. Cham, Springer, 2022. https://doi.org/10.1007/978-3-031-04329-1_23.
[2] Ţălu, Mihai, Ştefan Ţălu, and Mircea Rădulescu. *Fluid Mechanics. Volumetric and hydrodynamic machines. Theory and simulation*. Craiova, Universitaria Publishing House, 2011. ISBN 978-606-14-0035-5.
[3] Tudor-Rotilă, Bogdan Alexandru, Radu-Iulian Rădoi, Ștefan-Mihai Șefu, and Robert Blejan. "Experimental evaluation of a digital hydraulic pumping system." *Hidraulica Magazine*, no. 4 (December 2024): 69-75.
[4] Diaconu, Mihai, Tiberiu Axinte, Cătălin Frățilă, Paul Bocănete, and Remus Cojocaru. "Design and study of hydraulic systems." *Hidraulica Magazine*, no. 2 (June 2021): 49-56.
[5] Katgeri, Darshan, and Basavaraj Hubballi. "A review & progress on digital hydraulic pumps and valves." *Hidraulica Magazine*, no. 1 (March 2019): 116-123.
[6] Bucureșteanu, Anca. "Mathematical modeling and simulation of the operation of hydraulic systems with resistive adjustment." *Hidraulica Magazine*, no. 2 (June 2022): 15-22.
[7] Bucureșteanu, Anca, Adrian Motomancea, and Alina Ovanisof. "Energy loss reduction in hydraulic installations of the machine tools served by constant flow pumps." *Hidraulica Magazine*, no. 1 (March 2021): 17-23.
[8] Volk, Michael. *Pump characteristics and applications*. 3rd edition, CRC Press, Taylor & Francis Group, Boca Raton, FL, USA, 2014.
[9] Ţălu, Ştefan. "Insights on hydroponic systems: understanding consumer attitudes in the cultivation of hydroponically grown fruits and vegetables." *Hidraulica Magazine*, no. 1 (March 2024): 56-67.
[10] Dick, Erik. "Pumps". In: *Fundamentals of Turbomachines. Fluid Mechanics and Its Applications*, vol 130. Cham, Springer, 2022. https://doi.org/10.1007/978-3-030-93578-8_8.
[11] Ţălu, Ştefan. "Assessing the remaining useful life of hydraulic pumps: a review." *Hidraulica Magazine*, no. 3 (September 2024): 7-18.
[12] Ţălu, Ştefan. "New developments in intelligent diagnostic methods for hydraulic piston pumps faults." *Hidraulica Magazine*, no. 4 (December 2024): 7-16.
[13] Jablonská, Jana, and Milada Kozubková, "Physical and mathematical fundamentals of cavitation." *AIP Conf. Proc*. 1768 (2016): 020015. https://doi.org/10.1063/1.4963037.
[14] Fecser, Nikolett, Balázs Sára, and Rajmund Kuti. "Examining centrifugal pump on cavitation." *Hidraulica Magazine*, no. 4 (December 2019): 7-12.
[15] Xiaohui, Liu, Jiegang Mou, Xin Xu, Zhi Qiu, and Buyu Dong. "A review of pump cavitation fault detection methods based on different signals." *Processes* 11, no. 7 (2023): 1-21. https://doi.org/10.3390/pr11072007.
[16] Budea, Sanda. "Analysis of vibrations and noise in a centrifugal pump for predictive maintenance." *Hidraulica Magazine*, no. 3 (September 2020): 25-32.
[17] Salman, Khalid, Soo-Ho Jo, Syed Yaseen Shah, Joon Ha Jung, and Heung Soo Kim. "Artificial intelligence-driven prognostics and health management for centrifugal pumps: a comprehensive review." *Actuators* 13, no. 12 (2024): 1-31. https://doi.org/10.3390/act13120514.
[18] Dutta, Nabanita, Palanisamy Kaliannan, and Umashankar Subramaniam. "Application of machine learning algorithm for anomaly detection for industrial pumps." In: Das, S., Das, S., Dey, N., Hassanien, AE. (eds.) *Machine Learning Algorithms for Industrial Applications. Studies in Computational Intelligence*, vol. 907. Cham, Springer, 2021. https://doi.org/10.1007/978-3-030-50641-4_14.

[19] Sunal, Cem Ekin, Vladimir Dyo, and Vladan Velisavljevic. "Review of machine learning based fault detection for centrifugal pump induction motors." *IEEE Access* 10 (2022): 71344-71355. https://doi.org/10.1109/ACCESS.2022.3187718.
[20] Tan, Yangyang, Guoying Wu, Yanlin Qiu, Honggang Fan, and Jun Wan. "Fault diagnosis of a mixed-flow pump under cavitation condition based on deep learning techniques." *Front. Energy Res.* 10 (2023):1109214. https://doi.org/10.3389/fenrg.2022.1109214.
[21] Qiu, Chengcheng, Qiaogao Huang, and Guang Pan. "Prediction of Cavitation Performance over the Pump-Jet Propulsor Using Computational Fluid Dynamics and Hybrid Deep Learning Method." *Journal of Marine Science and Engineering* 10, no. 7 (2022): 918. https://doi.org/10.3390/jmse10070918.
[22] Homa, Dorota. "Comparison of different mathematical models of cavitation." *Transactions of the VŠB – Technical University of Ostrava, Mechanical Series* 60, no. 2 (2014): 7-14, article 1985.
[23] Wang, Yong, Jianing Lei, Jie Chen, Xiaolin Wang, and Ming Li. "Investigation of typical cavitation flow mode and flow field characteristics in a centrifugal pump." *Comp. Part. Mech*. (2024). https://doi.org/10.1007/s40571-024-00878-w.
[24] Ramirez, R., E. Avila, L. Lopez, A. Bula, and J. Duarte Forero. "CFD characterization and optimization of the cavitation phenomenon in dredging centrifugal pumps." *Alexandria Engineering Journal* 59, no. 1 (2020): 291-309. https://doi.org/10.1016/j.aej.2019.12.041.
[25] Gong, Jie, Luo Wan-zhen, Wu Tie-cheng, and Zhang Zhi-yuan. "Numerical analysis of vortex and cavitation dynamics of an axial-flow pump." *Engineering Applications of Computational Fluid Mechanics* 16, no. 1 (2022): 1921–1938. https://doi.org/10.1080/19942060.2022.2122570.
[26] Pouffary, B. "Numerical modelling of cavitation". In *Design and analysis of high speed pumps* (2006) (pp. 3-1 – 3-54).
[27] Cao, R., and J. Yuan. "Selection strategy of vibration feature target under centrifugal pumps cavitation." *Applied Sciences* 10, no. 22: (2020): 8190. https://doi.org/10.3390/app10228190.
[28] Altobi, M.A.S., G. Bevan, P. Wallace, D. Harrison, and K.P. Ramachandran. "Centrifugal pump condition monitoring and diagnosis using frequency domain analysis." In: Fernandez Del Rincon, A., Viadero Rueda, F., Chaari, F., Zimroz, R., Haddar, M. (eds) *Advances in condition monitoring of machinery in non-stationary operations*. CMMNO 2018. *Applied Condition Monitoring*, vol 15. Cham, Springer. https://doi.org/10.1007/978-3-030-11220-2_13.
[29] Li, Y., G. Feng, X. Li, Q. Si, and Z. Zhu. "An experimental study on the cavitation vibration characteristics of a centrifugal pump at normal flow rate." *J. Mech. Sci. Technol*. 32 (2018): 4711–4720. https://doi.org/10.1007/s12206-018-0918-x.
[30] Al-Obaidi, A. "Detection of cavitation phenomenon within a centrifugal pump based on vibration analysis technique in both time and frequency domains." *Experimental Techniques* 44 (2020): 329–347. https://doi.org/10.1007/s40799-020-00362-z.
[31] Su, Y.S., Y.S. Wang, and X.Y. Duan. "Cavitation Experimental Research on Centrifugal Pump." *Trans. Chin. Soc. Agric. Mach.* 44 (2010): 77–80.
[32] Gong, B., S.Q. Yuan, Y. Luo, Y.J. Han, and J. Dong. "Vibration signal characteristics of centrifugal pumps with cavitation erosion impellers." *J. Vib. Shock*. 39 (2020): 92–99.
[33] Zhang, N., M. Yang, B. Gao, and Z. Li. "Vibration Characteristics Induced by Cavitation in a Centrifugal Pump with Slope Volute." *Shock and Vibration*. 2015 (2015): 294980.
[34] Gao, B., P. Guo, N. Zhang, Z. Li, and M. Yang. "Experimental Investigation on Cavitating Flow Induced Vibration Characteristics of a Low Specific Speed Centrifugal Pump." *Shock and Vibration* 2017 (2017): 6568930.
[35] Sánchez, W., C. Carvajal, J. Poalacin, and E. Salazar. "Detection of cavitation in centrifugal pump for vibration analysis." 2018 4th International Conference on Control, Automation and Robotics (ICCAR), Auckland, New Zealand, 2018, pp. 460-464. doi: 10.1109/ICCAR.2018.8384720.
[36] Mostafa, M., M. Elsakka, M.S. Soliman, and M. El-Ghandour. "Condition monitoring as a pathway for sustainable operation: a case study for vibration analysis on centrifugal pumps". In: Negm, A.M., Rizk, R.Y., Abdel-Kader, R.F., Ahmed, A. (eds.) *Engineering solutions toward sustainable development*. IWBBIO 2023. Earth and Environmental Sciences Library. Cham, Springer (2024). https://doi.org/10.1007/978-3-031-46491-1_47.
[37] Dutta, N., S. Umashankar, V. K. A. Shankar, S. Padmanaban, Z. Leonowicz and P. Wheeler. "Centrifugal Pump Cavitation Detection Using Machine Learning Algorithm Technique." 2018 IEEE International Conference on Environment and Electrical Engineering and 2018 IEEE Industrial and Commercial Power Systems Europe (EEEIC / I&CPS Europe), Palermo, Italy, (2018), pp. 1-6. https://doi.org/10.1109/EEEIC.2018.8494594.
[38] Li, Gaoyang, Haiyi Sun, Jiachao He, Xuhui Ding, Wenkun Zhu, Caiyan Qin, Xuelan Zhang, Xinwu Zhou, Bin Yang, and Yuting Guo. "Deep learning, numerical, and experimental methods to reveal hydrodynamics performance and cavitation development in centrifugal pump." *Expert Systems with Applications* 237, Part C (2024): 121604. https://doi.org/10.1016/j.eswa.2023.121604.

[39] Stephen, C., V. Guguloth, K. Sivasailam, Y. Gu, R. Parmar, and C. Banerjee. "Prediction of cavitation using machine learning techniques on centrifugal pump." *J. Phys.: Conf. Ser.* 2854 (2024): 012014. https://doi.org/10.1088/1742-6596/2854/1/012014.
[40] Tiwari, R., D.J. Bordoloi, and Aakash Dewangan. "Blockage and cavitation detection in centrifugal pumps from dynamic pressure signal using deep learning algorithm." *Measurement* 173 (2021): 108676. https://doi.org/10.1016/j.measurement.2020.108676.
[41] He, Xiaoke, Yu Song, Kaipeng Wu, Asad Ali, Chunhao Shen, and Qiaorui Si. "Intelligent Identification of Cavitation State of Centrifugal Pump Based on Support Vector Machine". *Energies* 15, no. 23 (2022): 8907. https://doi.org/10.3390/en15238907.
[42] Song, H., H. Sun, and N. Chen. “Cavitation fault diagnosis of centrifugal pump based on RIME-SDAE.” *Vibroengineering Procedia* 54 (2024): 46–52. https://doi.org/10.21595/vp.2024.24039.
[43] Dai, Cui, Siyuan Hu, Yuhang Zhang, Zeyu Chen, and Liang Dong, "Cavitation state identification of centrifugal pump based on CEEMD-DRSN." *Nuclear Engineering and Technology* 55, no. 4 (2023): 1507-1517. https://doi.org/10.1016/j.net.2023.01.009.
[44] Azizi, R., B. Attaran, A. Hajnayeb, A. Ghanbarzadeh, and M. Changizian. "Improving accuracy of cavitation severity detection in centrifugal pumps using a hybrid feature selection technique." *Measurement* 108 (2017): 9–17.
[45] Matloobi, S.M., and M. Riahi. "Identification of cavitation in centrifugal pump by artificial immune network." *Proc. Inst. Mech. Eng. Part E J. Process Mech. Eng*. 235 (2021): 2271–2280.
[46] Hajnayeb, A., and Y. Qin. "Cavitation Analysis in Centrifugal Pumps Based on Vibration Bispectrum and Transfer Learning." *Shock. Vib*. 2021 (2021): 6988949.
[47] Chu, N., L. Wang, L. Yu, C. He, L. Cao, B. Huang, and D. Wu. "An Adaptive Autogram Approach Based on a CFAR Detector for Incipient Cavitation Detection." *Sensors* 20 (2020): 2303.
[48] Swelam, Mostafa, Ashraf Kotb, and A. M. Abdulaziz. "Acoustic diagnosis of cavitation for centrifugal pumps of different materials." *Engineering Research Journal* 164, no. 13 (2019): 214-228. https://doi.org/10.21608/erj.2019.131374.
[49] Mousmoulis, Georgios, Nilla Karlsen-Davies, George Aggidis, Ioannis Anagnostopoulos, and Dimitrios Papantonis. "Experimental analysis of cavitation in a centrifugal pump using acoustic emission, vibration measurements and flow visualization." *European Journal of Mechanics - B/Fluids* 75 (2019): 300-311. https://doi.org/10.1016/j.euromechflu.2018.10.015.
[50] Liang, D., Z. Yuqi, D. Cui, and Yong W. "Research on cavitation acoustic characteristics of centrifugal pump based on fluid-acoustic field coupling method." *Advances in Mechanical Engineering* 10, no. 5 (2018). https://doi.org/10.1177/1687814018773665.
[51] Chudina, M. "Noise as an indicator of cavitation in a centrifugal pump." *Acoustical Physics* 49, no. 4 (2003): 463–474.
[52] Dong-wei, W., W. Wei-dong, H. Jia-jun, Z. Wei-guo, and L. Lai. "Experimental study of cavitation noise characteristics in a centrifugal pump based on power spectral density and wavelet transform." *Flow Measurement and Instrumentation* 94 (2023): 102481. https://doi.org/10.1016/j.flowmeasinst.2023.102481.
[53] Qiaorui, Si, Ali Asad, Yuan Jianping, Fall Ibra, and Muhammad Yasin Faisal. "Flow-Induced Noises in a Centrifugal Pump: A Review." *Science of Advanced Materials* 11, no. 7 (2019): 909-924(16). https://doi.org/10.1166/sam.2019.3617.
[54] Al-Obaidi, Ahmed. "Experimental investigation of cavitation characteristics within a centrifugal pump based on acoustic analysis technique." *International Journal of Fluid Mechanics Research* 47, no. 6 (2020): 501-515. https://doi.org/10.1615/InterJFluidMechRes.2020029862.
[55] Zhang, Ning, Bo Gao, Zhong Li, and Qifeng Jiang. "Cavitating flow-induced unsteady pressure pulsations in a low specific speed centrifugal pump." *Royal Society Open Science* 5, no. 7 (2018). https://doi.org/10.1098/rsos.180408.
[56] Lu, J., Z. Luo, Q. Chen, X. Liu, and B. Zhu. "Study on pressure pulsation induced by cavitation at the tongue of the volute in a centrifugal pump." *Arab. J. Sci. Eng.* 47 (2022): 16033–16048.
[57] Wang, K.L., H. Li, and Z.H. Shen. "Pressure pulsation characteristics of down-scaled high specific speed centrifugal pump under cavitation state." *J. Drain. Irrig. Mach. Eng*. 38 (2020): 891–897.
[58] He, G., Y.L. Cao, X.C. Wang, T.F. Ming, and Y.S. Su. "Characteristic analysis of cavitation pressure fluctuation in centrifugal pump." *J. Wuhan Univ. Technol.* 41 (2017): 549–553.
[59] Wang, C., Y.X. Zhang, K.Z. Ji, C. Xu, and M. Liu. "Investigation on pressure fluctuation affected by cavitation in ultra-low specific speed centrifugal pump." *Trans. Chin. Soc. Agric. Mach.* 51 (2020): 122–129.
[60] Shi, W., C. Wang, W. Wang, and B. Pei. "Numerical calculation on cavitation pressure pulsation in centrifugal pump". *Adv. Mech. Eng.* 6 (2015): 367631.

Considerations regarding the Use of Infrared Thermography in the Maintenance of Hydraulic Drive Installations

SR1 PhD. Eng. **Teodor Costinel POPESCU[1,*]**, SRA Dipl. Eng. **Alina Iolanda POPESCU[1]**

[1] National Institute of Research & Development for Optoelectronics/INOE 2000, Subsidiary Hydraulics and Pneumatics Research Institute/IHP, Romania

* popescu.ihp@fluidas.ro

Abstract: *Infrared thermography, as a non-contact investigation technique, has proven its usefulness in preventive maintenance and in monitoring mechanical, electrical systems or production processes. Engines, pumps, couplings, hydraulic installations, rotating equipment, servomechanisms, furnaces, tanks, but also other equipment can be found in all industrial activities. Examples of the use of infrared thermography are known only at the level of hydraulic components, not hydraulic drive installations / systems. For this reason, the authors present several points of view regarding the use of this technique on a specific case of a hydraulic drive installation.* ***The installation*** *contains a high-pressure* ***pumping station,*** *consisting of a double electric pump, low-pressure equipment for flow distribution / pressure regulation, three oscillating hydraulic pressure amplifiers of the mini booster type and two* ***double-acting hydraulic cylinders****. The following are presented: the composition, technical characteristics and operation of the hydraulic drive installation; diagnostic method, through infrared thermography, of the installation in operation.*

Keywords: *Infrared thermography, hydraulic drive system, high-pressure pumping station, mini booster*

1. Introduction

The high-precision results obtained by infrared thermography lead to a reduction in the time required to detect defects and to an efficient assessment of the condition of technical equipment during operation, without the need to stop them or perform more complicated operations, such as dismantling and transporting them to a testing/diagnostic center. The infrared thermography method is currently used in multiple technical applications [1] in: the industrial field, the most targeted being energy, electrical engineering, electronics and microelectronics; the machine-building, oil, metallurgical/steel, processing industries; the construction field; the field of technological processes, such as the field of welding; the field of medicine.
If one or more problems occur in the installations/systems in these fields, production interruption is very likely, and downtime is very costly. High temperatures, as seen in thermograms obtained by scanning with a thermal imaging camera, can indicate an electrical problem, wear in a component, insufficient lubrication, or other problems that can lead to expensive repairs or even production interruptions.
Many of these types of problems are not visible to the free eye and are not noticed until the equipment physically fails. Trying to find these problems through visual inspections is a time-consuming process that cannot identify the cause of the problems.
With the help of thermal imaging, thermal anomalies that endanger the safety and reliability of technical equipment can be quickly and accurately indicated [2]. Tens or even hundreds of points can be inspected with thermal imaging, which can be analyzed in a complete report of the thermal stresses hidden in this equipment.

2. Diagnosing of hydraulic drive installations by infrared thermography

Practice has shown that the correct operation of a hydraulic system under pressure is done in a well-defined temperature range. Maintaining this temperature range ensures the operation of hydraulic drive systems within parameters, without energy losses, because the properties of the hydraulic oil do not alter in terms of viscosity, density and compressibility. Therefore, the use of infrared thermography as a method of predictive maintenance of these systems is justified. However, in the field of hydraulic drive systems / installations of fixed or mobile machines /

equipment, some applications of infrared thermography are known only at the level of components, and not of the system as a whole.

A first example is the thermographic scan of a Brueninghaus (Germany) axial piston pump with inclined block, figure 1, mounted on the functional test stand in figure 2. The thermograms obtained, figure 3 and figure 4, indicate that the pump does not show wear, since the temperature difference between the left end, where the bearings are mounted, and the right end, with the distribution plate and connections, is less than 10°C [3]. The thermogram in figure 4 indicates that the pump operates within the manufacturer's catalog parameters. It can serve as a "standard thermogram" for determining the degree of wear of all similar pumps in operation, under similar conditions, on hydraulically driven machines / equipment.

Fig. 1. Brueninghaus pump

Fig. 2. Stand for testing pump

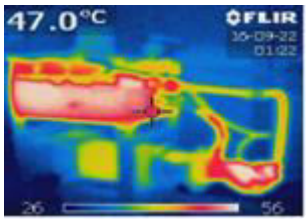

Fig. 3. Stand thermogram

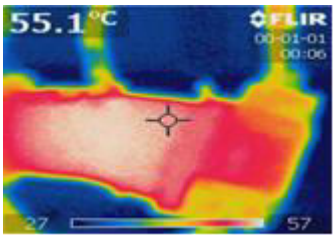

Fig. 4. Pump thermogram

Another example is the thermographic scanning of the hydraulic cylinders driving the bucket of a front-end loader, figure 5. The thermograms obtained, figure 6, indicate an equal load for the two hydraulic cylinders driving the bucket under load.

Fig. 5. Front loader with the 2 hydraulic cylinders driving the bucket

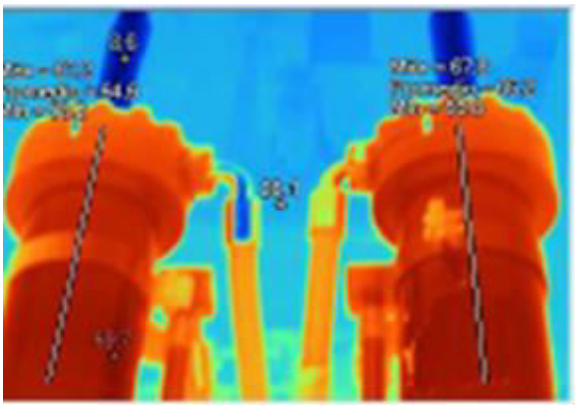

Fig. 6. Thermograms of the front loader bucket drive hydraulic cylinders

A procedure for applying infrared thermography to a real hydraulic drive installation is proposed, which consists of presenting: *the structure, technical characteristics, operating mode and main causes of installation failures; the method of predictive maintenance* of the hydraulic drive installation using infrared thermography.

2.1 Hydraulic cylinder drive system with high loads in one or both directions of travel

The installation with the hydraulic diagram in figure 7 allows the actuation, successively or simultaneously, of two double-acting hydraulic cylinders, of which the first experiences a maximum resistant load, on the advance stroke (+L) and retraction (-L) of the piston, equivalent to a pressure force of 1000 bar, and the second experiences the same resistant load only on the advance stroke (+L) of the piston. This installation is part of a range of six products in the field of high pressure generation for hydraulic drives and was developed by the authors within a research project, carried out in partnership with a private company and a higher education institute [5].

The structure of the hydraulic diagram in figure 7 is as follows: **1**= 60 l hydraulic oil tank; **2**= double low-pressure electric pump 2x8 cm3/rot, 200 bar, 1500 rot/min, 9kW; **3**= filling and venting filter; **4**= return filter; **5.1,5.2=** hydraulic blocks with four devices each, respectively: pressure regulating valve 0...200 bar; pressure gauge 250 bar; pressure filter; hydraulic directional control valve 4/3, Dn6, with electric control (electromagnets **EA** and **EB**). The blocks have four connections each: **P** (pump discharge), **T** (tank), **A** (cylinder piston chamber consumer) **B** (cylinder rod chamber consumer); **6.1, 6.2, 6.3**= **HC7** mini boosters with: amplification ratio i=5; primary connections **IN** (inlet), **R** (return); secondary connections **H1, H3** to the cylinder, **H2, H4** to *2000 bar* pressure gauges. A mini booster, figures 8 and 9, contains: two one-way valves, **SS1** and **SS2**; one unlockable one-way valve, **SSD**; a oscillating piston pumping unit, **UPO**, consisting of a two-piston assembly (**LP+HP**) and a hydraulically actuated spool valve (**BV1**), figure 9; **HC1**= double-acting hydraulic cylinder, with a maximum load of 1000 bar on both piston strokes; **HC2**= double-acting hydraulic cylinder, with a maximum load of 1000 bar only on the piston forward stroke.

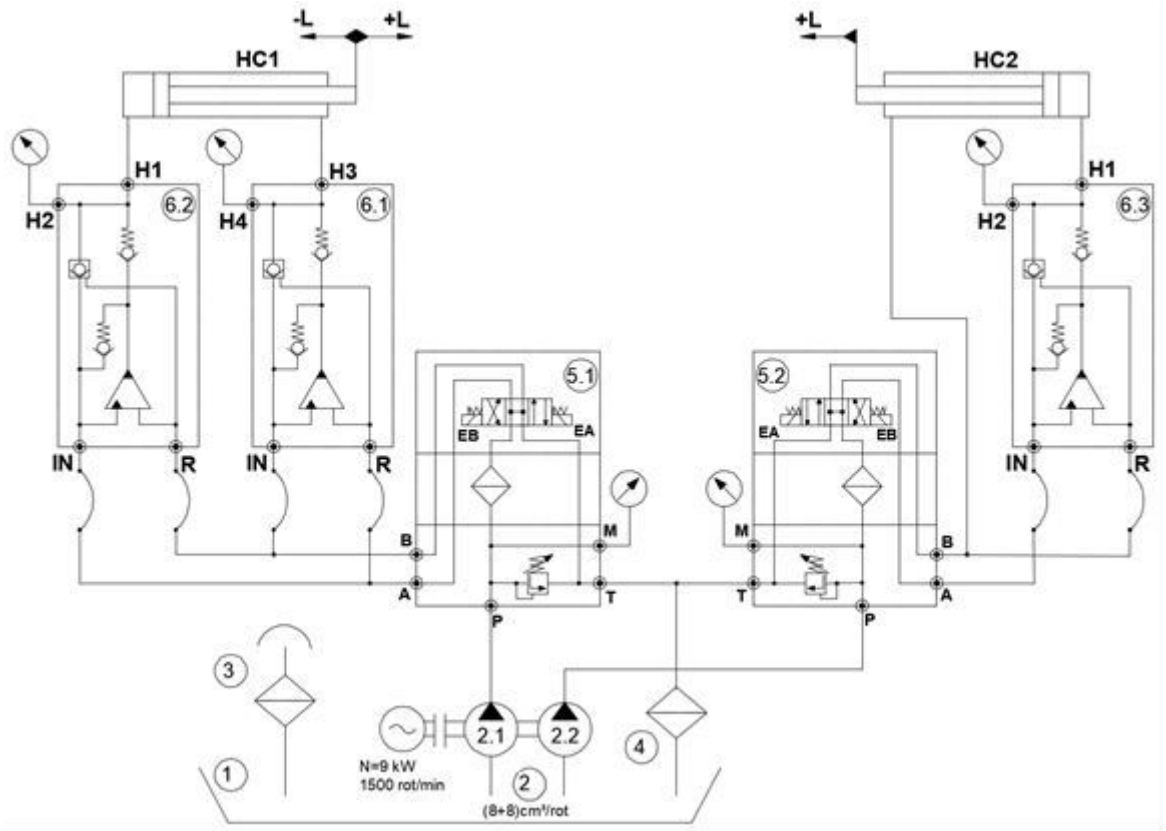

Fig. 7. Hydraulic scheme of the drive system

The **technical characteristics of** the drive system in fig.7...fig.10 are the following:
- **electric motor power** = *9 kW*; **electric motor rotational speed** = *1500 rpm*; **electric motor supply voltage** = 380V; double pump **flow rate** = *2x10.5 l/min*;
- **number** of mini boosters = *3 pcs.;* mini booster *amplification factor* = *5*; mini booster **primary pressure** = *0...200* bar; mini booster **secondary pressure** = *0...1000 bar*; **maximum primary** mini booster **flow rate** = *2x10.5 l/min*; **maximum flow rate** (at maximum pressure) secondary mini booster = *2x1.2 l/min*;
- **number** of driven hydraulic cylinders = *3 pcs.*; driven cylinder **load** = **±L**, for **HC1** and **+L**, for **HC2**; **dimensions**: Ø piston = 38.1x 10-3 m, Ø rod = 25x10-3 m, stroke length = 257x10-3 m;
- **number** of hydraulic dimensional control valves 4/3 = *2 pcs.*; **number** of pressure filters = *2 pcs.*; number of pressure valves = *2 pcs.*;
- **number** of pressure gauges 200 bar = *2 pcs.*; **number** of pressure gauges 2000 bar = 2 pcs.;
- **number** of hoses = 6 pcs.

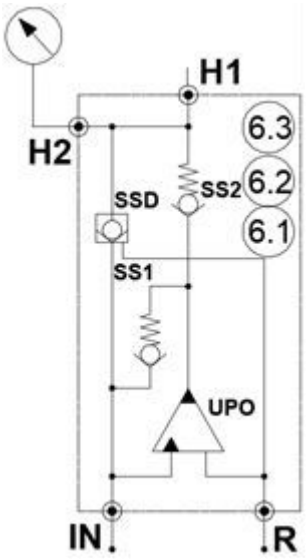

Fig. 8. Simplified mini booster hydraulic scheme

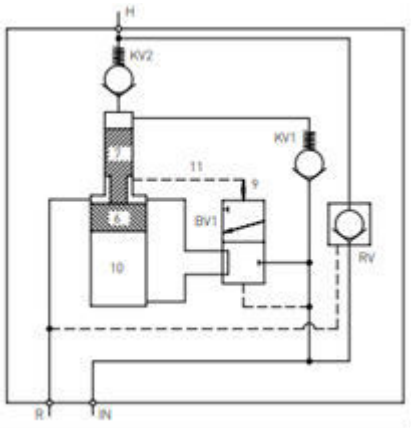

Fig. 9. Developed mini booster hydraulic scheme [4]

Fig. 10. High-pressure pumping station in the hydraulic scheme fig.7

The operating mode of the hydraulic drive system is presented in table 1. It has two phases: for low pressures on the secondary of the mini booster (0...40 bar in the primary), when the hydraulic cylinders move in idle (without load) being supplied directly by the low-pressure electric pump (the flow bypasses the **UPO** mini booster, according to fig. 8); **for high pressures** on the secondary of the mini booster (40...200 bar in the primary), when the hydraulic cylinders move in load being supplied by the **UPO** mini booster (the **LP+HP** pistons pulsate with 10...20 Hz under the hydraulic control of the **BV1** distribution spool, according to fig. 9).

Table 1: Operation of the hydraulic drive system

Controls / Adjustments / Hydraulic circuits	
Name of control/ adjustment / circuit	**Execution control/ adjustment / circuit**
HC1 cylinder piston advance	
***Actuation** of* hydraulic directional control valve block 5.1	Electromagnet status: **EA +**; **EB -**
Pressure adjustment - phase I	Pressure valve adjustment ***0...40 bar***
***Feeding circuit** of oil from chamber of HC1 cylinder piston*	pump-**tank** (2.1)-P (5.1)- pres. filter - directional control valve.-A (5.1)-IN(6.2)-SS1-SS2-SSD-H1 (6.2)- **piston chamber**
***Exhaust circuit** of oil from chamber of HC1 cylinder rod*	**rod chamber** H3 (6.1)-SSD-IN(6.1)-B (5.1)-directional control valve T (5.1)-(4)-**tank**
Pressure adjustment - phase II	Pressure valve adjustment ***40...200 bar***
***Feeding circuit** of oil from chamber of HC1 cylinder piston*	**pump-tank** (2.1)-P (5.1)- pres. filter directional control valve..-A (5.1)-IN(6.2)-UPO (6.2)-SS2-H1 (6.2)- **piston chamber**
***Exhaust circuit** of oil from chamber of HC1 cylinder rod*	**rod chamber** -H3 (6.1)-SSD-IN(6.1)-B (5.1)-directional control valve -T (5.1)-(4)-**tank**
HC1 cylinder piston stationary	
***Unactuated** of* hydraulic directional control valve block 5.1	Electromagnet status: **EA +; EB -**
***Hydraulic** circuit of pump 2.1*	**pump-tank** (2.1)-pressure valve block 5.1-4-**tanck**

HC1 cylinder piston withdrawal	
***Actuation** of hydraulic directional control valve block 5.1*	Electromagnet status: **EA -**; **EB +**
Pressure adjustment - phase I	Pressure valve adjustment 0...40 bar
***Feeding circuit** of oil from chamber of HC1 cylinder rod*	**pump-tank** (2.1)-P (5.1)- pres. filter-directional control valve B (5.1)-IN(6.1)-SS1-SS2-SSD-H3 (6.1)-**piston chamber**
***Exhaust circuit** of oil from chamber of HC1 cylinder piston*	**piston chamber**-H1 (6.2)-SSD-IN(6.2)-A (5.1)-directional control valve T (5.1)-(4)-**tank**
Pressure adjustment - phase II	Pressure valve adjustment ***40...200 bar***
***Feeding circuit** of oil from chamber of HC1 cylinder rod*	**pump-tank** (2.1)-P (5.1)- pres. filter-directional control valve-B (5.1)-IN(6.1)-SS1-SS2-SSD-H3 (6.1)-**rod chamber**
***Exhaust circuit** of oil from chamber of HC1 cylinder piston*	**piston chamber**-H1 (6.2)-SSD-IN(6.2)-A (5.1)-directional control valve-T (5.1)-(4)-**tank**
HC2 cylinder piston advance	
***Actuation** of hydraulic directional control valve block 5.2*	Electromagnet status: **EA +**; **EB -**
Pressure adjustment - phase I	Pressure valve adjustment ***0...40 bar***
***Feeding circuit** of oil from chamber of HC2 cylinder piston*	**pump -tank** (2.2)-P (5.2)-filter pres.-directional control valve -A (5.2)-IN(6.3)-SS1-SS2-SSD-H1(6.3) – **piston chamber**
***Exhaust circuit** of oil from chamber of HC2 cylinder rod*	**rod chamber**-B (5.2)- directional control valve-T (5.2)-(4)-**tank**
Pressure adjustment - phase II	Pressure valve adjustment ***40...200 bar***
***Feeding circuit** of oil from chamber of HC2 cylinder piston*	**pump-tank** (2.2)-P (5.2) pres. filter-directional control valve -A (5.2)-IN(6.3)-UPO-SS2-H1(6.3) - **piston chamber**
***Exhaust circuit** of oil from chamber of HC2 cylinder rod*	**rod chamber**-B (5.2)- directional control valve T (5.2)-(4)-**tank**
HC2 cylinder piston stationary	
***Unactuated** of* hydraulic directional control valve block 5.2	Electromagnet status: **EA -; EB -**
***Hydraulic** circuit of pump 2.2*	**pump-tank** (2.2)-pressure valve (5.2)- 4)-**tank**
HC2 cylinder piston withdrawal	
***Actuation** of hydraulic directional control valve block 5.2*	Electromagnet status: **EA -**; **EB +**
***Feeding circuit** of oil from chamber of HC2 cylinder rod*	**pump-tank** (2.2)-P (bloc 6)-) pres. filter-directional control valve -B (5.2) – **rod chamber**
***Exhaust circuit** of oil from chamber of HC2 cylinder piston*	**piston chamber**-H1(6.3)-SSD-IN (6.3)-A (5.2) - directional control valve-T (5.2)-(4)-tank.

The main causes of malfunctions of this hydraulic drive installation are:
- **vibrations, self-vibrations and shocks** caused by the pulsations of the electric pump **2**, pressure valves and hydraulic directional control valve 4/3 on blocks **5.1** and **5.2,** oscillating piston units (**UPO**) of mini boosters **6.1, 6.2, 6.3** together with nonlinearities in the dynamic regime;
- **temperature and quality of the oil** used as a working fluid;
-**selection of sealing elements** in terms of appropriate shape, material quality and its compatibility with the working fluid;
- **the quantity and size of impurities in the system** which, in addition to normal wear, cause blockages of moving parts (pistons, spools, valves), which disable the hydraulic devices to which they belong (especially the mini boosters **6.1, 6.2, 6.3,** the pressure valves and the 4/3 hydraulic directional control valves on the blocks **5.1, 5.2**) or even the entire drive system;
- **too high a temperature**, above 80°C, can cause: failures in the seals; alterations in the properties of the working fluid (especially viscosity); destruction of the lubricant film and, implicitly, of some mechanical-hydraulic components of the system. The presence of high temperatures in the hydraulic system is caused by the following factors: **the amount of hydraulic oil** in the tank **1** is below the minimum mandatory level; the **appearance of a cavity** and the production of air

bubbles in the oil; **increased drainage** of volumetric machines and hydraulic equipment which leads to an increase in the amount of fluid passing from high pressure to reservoir pressure, with heat production.
By proactively monitoring temperature increases, mainly caused by high internal losses of drive system components, which lead to premature wear, **the most important failures can be determined in advance.**

2.2 Predictive maintenance method for hydraulic drive installations using infrared thermography

Hydraulic drive systems are characterized by the combined action of thermal conduction, internal energy accumulation and mixing motion, *convection being the most important heat exchange mechanism between solid surfaces and hydraulic oil*, between which there is direct contact and relative motion.
As a result of the operation of hydraulic drive installations over time, some components wear out, more or less, having on the thermal images, respectively on the *"thermograms",* which present the "*thermal maps*", areas with different *"overheating*", compared to the "*standard thermograms*", depending on the *degree of wear*.
Figure 11 shows the block scheme of the predictive maintenance method [6] for the analyzed drive installation. It involves the use of a **CT** thermographic camera, with which all components (grouped into five classes) of the new hydraulic drive system, called the **standard system**, **IAH (e),** and all components of the same system, called the **technically revised system**, **IAH (r),** are thermographically scanned **during commissioning tests,** namely:
class 1: oil tank **1** with temperature thermostat system; filling and venting filter **3**, return filter **4**;
class 2: electric pump **2** (double pump **2.1**, **2.2** and electric drive motor);
class 3: pipes, hoses, fittings between the tank-double pump - hydraulic blocks, hydraulic directional control valves -mini boosters-hydraulic cylinders;
class 4: hydraulic equipment on blocks **5.1** and **5.2** (2 pressure filters, 2 pressure regulating valves, 2 4/3 hydraulic directional control valves) and mini boosters **6.1, 6.2, 6.3**;
class 5: linear hydraulic motors (hydraulic cylinders **HC1**, **HC2**).

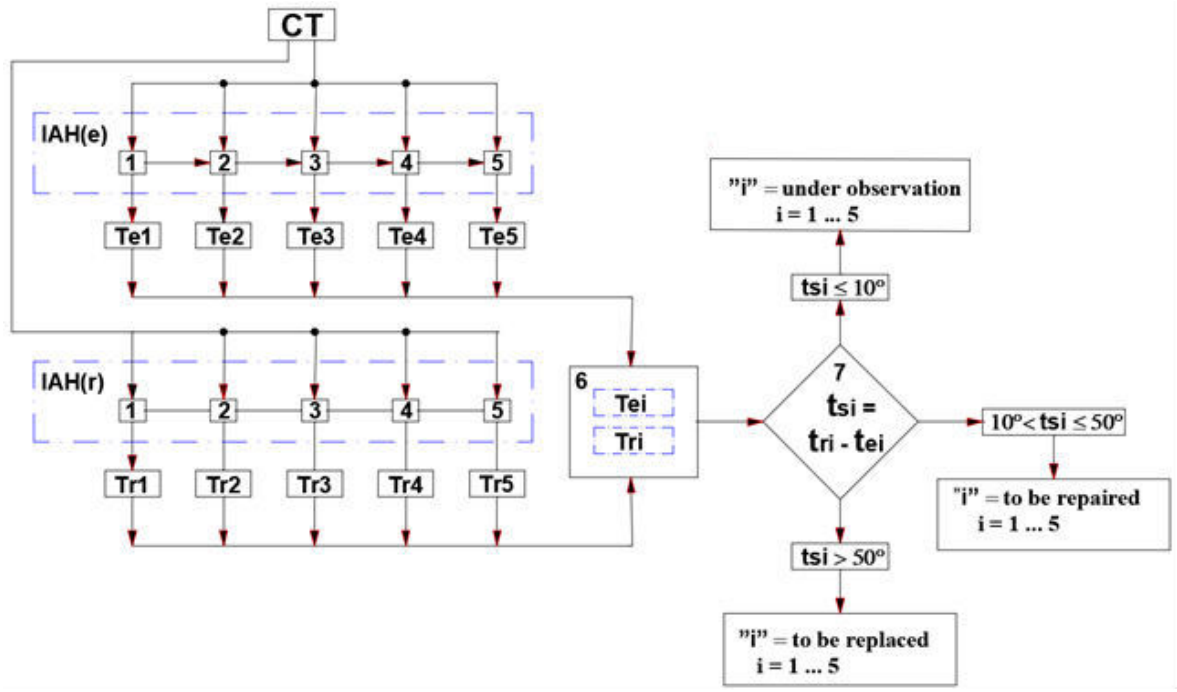

Fig. 11. Block scheme of the predictive maintenance method using infrared thermography [5]

After the first thermographic scan, a database is generated with **five sets of standard thermograms** $T_{e1}...T_{e5}$, and after **the second thermographic scan**, another database is generated with five sets of **inspection thermograms** $T_{r1}...T_{r5}$. Both databases are stored in a

module **6**, from where they are taken over by a programmable controller **7**, which, based on specialized software, compares the thermograms, calculates the overheating ***($t_{si} = t_{ri} - t_{ei}$)*** of each component of the technically inspected installation, which it then enters into one of the three files, respectively "***under observation***", "***to be repaired***", "***to be replaced***".
The "***under observation"*** file contains all the components of the installation where overheating, respectively the difference between the temperature of the standard component and the temperature of the technically inspected component, is incipient, respectively ***$t_s \leq 10^oC$***. These components ***will be thermally scanned first, at the next planned technical inspection***.
The ***"to be repaired***" file contains all the components of the installation with overheating in the range ***$10^oC < ts \leq 50^oC$***. These components have advanced overheating, are worn out and no longer perform the functional parameters, but ***can still be repaired***.
The ***"to be replaced"*** file contains all the components of the installation with overheating in the **range $t_s > 50^oC$**. These components have serious overheating, very high wear, no longer perform the functional parameters and, as a rule, can no longer be repaired.
The use of this predictive maintenance method requires that the **two thermographic scans** of the components of the hydraulic drive installation, **new** and **technically revised**, be carried out under **the same conditions of: ambient temperature**, in which the installation operates; **temperature of the working fluid**, respectively the hydraulic oil, which circulates through the installation; **nominal loads of 50%...100%,** respectively resistant forces and speeds, for the two hydraulic cylinders.
If, during the periodic inspection tests of the hydraulic drive installation, the nominal loads are achieved in a percentage lower than 50% of the nominal values, then a correction must be applied to the temperature values, calculated as overheating of the components.

3. Conclusions

The proposed investigation method, based on infrared thermography, supports the corrective, predictive and preventive maintenance of hydraulic drive installations, characterized by a high degree of complexity and a large number of components. The non-contact and early detection of worn components within a hydraulic drive installation, in operation, reduces the costs of its maintenance system.
As a rule, to detect a component, which shows faults or wear, in a hydraulic drive installation, all components are dismantled from the installation and tested individually, on specialized stands.
The proposed method has the advantage of removing this impediment, by locating the faults and non-contact detection of worn components; only these will be dismantled from the installation, for testing on the stand before and after repair or for replacement.

Acknowledgments

This work was carried out through the Core Program within the National Research Development and Innovation Plan 2022-2027, carried out with the support of MCID, project no. PN 23 05.

References

[1] https://www.virtual.identicom4.ro/wp-content/uploads/2020/09/Termografia_in_industrie.pdf.pdf.
[2] Alexandru, Costel. "Thermal imaging of mechanical equipment / Termoviziune echipamente mecanice". ALC Electrical Testing, 2017. https://www.termoviziune-termografie.ro/echipamente-mecanice.
[3 Marinescu, Alexandru-Daniel, Carmen-Anca Safta and Teodor Costinel Popescu. "Advantages, errors and limitations of infrared thermography used in the maintenance of hydraulic drive systems." Paper presented at International-multidisciplinary conference "Professor Dorin Pavel - the founder of Romanian hydropower", Sebeș, Romania, June 2-3, 2017.
[4] KVT_miniBOOSTER_DE_07-2018_web-catalog.pdf.
[5] "Digital mechatronic systems for generating 1000 bar pressure using hydraulic pressure amplifiers / Sisteme mecatronice digitale de generare a presiunii de 1000 bar, utilizand amplificatoare hidraulice de presiune." Financial agreement no. 272/24.06.2020. https://smgp.ihp.ro/.
[6] Popescu Teodor Costinel, Alexandru Daniel Marinescu, and Alina Iolanda Popescu. "Metodă și sistem de diagnosticare a instalațiilor funcționale de acționare hidraulică, utilizând termografia în infraroșu / Method and system for diagnosing functional hydraulic drive installations using infrared thermography". Patent No. RO133206(B1)-30.07.2024, OSIM.

Performance and Efficiency Aspects for Hydraulic System with LS Valve

PhD. Eng. **Fănel ȘCHEAUA**[1,*]

[1] "Dunarea de Jos" University of Galati, MECMET Research Center

* fanel.scheaua@ugal.ro

Abstract: *Hydraulic volumetric units are critical hydro-dynamical components in fluid transport systems across various industries and advancements in their performance and efficiency have become a key focus for energy conservation and operational optimization. Recent trends emphasize variable speed control, allowing pumps to adjust their speed dynamically through variable frequency drives (VFD) to match system demands, thereby reducing energy waste. Additionally, the integration of LS valve within the system, smart monitoring and predictive maintenance is enhancing real-time operation efficiency and failure prevention.*
Numerical simulations and experimental research are playing a pivotal role in optimizing hydraulic efficiency, leading to lower frictional losses and improved performance across diverse operating conditions. Furthermore, energy recovery systems, such as regenerative pumps and pressure exchanger technology, are being increasingly implemented to minimize energy consumption in industrial and water distribution applications.
Material innovations, including advanced coatings and wear-resistant materials, are also reducing cavitation and extending pump lifespan. The push towards sustainable pumping solutions, such as solar-powered and hybrid energy-driven pumps, is gaining momentum in response to environmental concerns. As industries shift towards AI-driven system optimization, real-time adaptive control mechanisms are expected to further enhance units efficiency, reduce downtime and lower costs. These trends indicate a future where hydraulic systems are more intelligent, adaptive energy-efficient, aligning with global efforts for sustainable industrial operations.

Keywords: *Hydraulic actuation, volumetric unit, LS valve, efficiency, numerical analysis*

1. Introduction

Pump performance and efficiency represents crucial aspects in hydraulic machines, as optimizing pump performance can lead to significant energy savings, improved reliability and longer equipment life.
Traditional pump units operation is achieved at constant velocity, even when the system doesn't require full capacity. This situation can be resolved using variable frequency drives (VFD) in order to control pump momentum velocity based on system demands, while this option is drastically improving efficiency values in operation.
The use of VFD combined with real-time monitoring and predictive algorithms to adjust pump velocity, pressure and flow rate values to the specific needs of the system represents a recent trend solution in the field.
Energy efficiency trends in pumping systems are directed toward to improvements in pumps efficiency by designing systems able to minimize energy losses, while this includes using more efficient pump impeller designs, improving motor efficiency and reducing friction losses in pipes.
The recent research activities and studies are showing the raising use of more aerodynamic impellers, optimized geometries and materials that can improve energy consumption, while additionally integrating energy recovery systems can help to reduce the need for external power.
Pump efficiency curves are used to identify the performance of pumps under various operating conditions. Knowing how to read and interpret these maps allows operators to select the most efficient pumps for their system.
New algorithms and software for dynamic pump performance mapping are allowing for real-time analysis and adjustments based on live data from sensors. Some systems now even use AI-based predictions to adjust pump operation for maximum efficiency.
Hydraulic losses (due to friction, turbulence, etc.) and mechanical losses (bearing friction and seal drag) can significantly reduce efficiency, while understanding and mitigating methods for these losses through improved designs and materials is a growing focus.

The use of advanced coatings, low-friction materials and design optimization (such as better shaft designs) is improving mechanical efficiency and further, based on advancements in CFD (computational fluid dynamics), better understanding and reduction of hydraulic losses are allowed.
Pump systems often consist of multiple pumps working together in a larger circuit network and the overall system efficiency depends not just on the pumps themselves but also on how they interact with each other and the surrounding infrastructure.
The Load Sensing valve brings significant advantages in hydraulic systems, particularly in terms of efficiency, cost savings, and system longevity. By dynamically adjusting the system's pressure and flow rate values in order to match the load demand, the LS valve reduces energy consumption, improves fuel efficiency, minimizes heat generation and wears on components, provides precise load control and enhances system performance and responsiveness.
These benefits make the LS valve a crucial component in modern hydraulic systems, particularly in mobile equipment, manufacturing, and industrial machinery, while it optimizes system performance at the same time as reducing operational costs and environmental impact.

2. Parametric models for volumetric unit's performance and efficiency

Volumetric units, such as positive displacement pumps, compressors or hydraulic actuators, play a critical role in fluid power and energy conversion systems. Unlike dynamic pumps, volumetric machines operate by displacing a fixed amount of fluid per cycle, making their performance highly dependent on parameters such as displacement volume, rotational velocity, leakage losses and mechanical friction. Parametric modeling provides a systematic approach to analyze and optimize the efficiency and performance of these machines by correlating key design and operational variables.
The parametric model defines the relationship between input variables such as pressure, flow rate, rotational speed and temperature) and output performance metrics related to efficiency, power consumption and volumetric losses [1-3].
For hydraulic pumps, the flow rate and pressure are the composing parameters of the dynamic model and the approach is based on a model that accounts for the system's response to changing input conditions [1-7]:

$$\frac{dp(t)}{dt} = \frac{Q(t) \cdot R}{V_f} \tag{1}$$

where:
$\frac{dp(t)}{dt}$ - the pressure rate of change in the pump chamber;
Q(t) - the flow rate into the pump;
R - the system resistance (dependent on factors like pipe size, friction and valve settings);
V_f - the fluid volume inside the pump.
For hydraulic rotary motors, the output torque and rotational velocity are influenced by the pressure applied to the motor and the flow rate:

$$T(t) = k \cdot p(t) \cdot V_d \tag{2}$$

where:
k - a constant that accounts for motor efficiency and other losses;
p(t) - the pressure applied to the engine;
V_d - the motor displacement (fluid volume displaced per revolution).

$$N(t) = \frac{Q(t)}{V_d} \tag{3}$$

$$\frac{dN(t)}{dt} = \frac{T(t) - T_l}{J} \tag{4}$$

$$\frac{dN(t)}{dt} = \frac{k \cdot p(t) \cdot V_d - T_l}{J} \tag{5}$$

$\frac{dN(t)}{dt}$ - the angular acceleration of the motor;
T(t) - is the torque applied by the fluid pressure;
T_l - the external load torque;
J - the moment of inertia of the motor (a constant depending on the motor's design).
The efficiency model reflects how well the motor converts hydraulic power (input power) into mechanical power (output power), being defined as [5-9]:

$$\eta(t) = \frac{P_o(t)}{P_i(t)} = \frac{T(t) \cdot N(t)}{P(t) \cdot Q(t)} \tag{6}$$

The fluid flow rate *Q(t)* is related to the motor velocity *N(t)* by:

$$Q(t) = V_d \cdot N(t) \tag{7}$$

The energy model is the integral of power over time. The total energy supplied or consumed by the motor can be calculated as:

$$E = \int_{t_1}^{t_2} P_m(t)\,dt \tag{8}$$

where:

E - total energy;
P_m - instantaneous power supplied or consumed by the motor.
A LS valve mounted at the working circuit adjusts the system pressure based on the load. The pressure setting for the LS valve is typically a function of the load demand and is calculated as [10-13]:

$$p_{LS} = p + \Delta p \tag{9}$$

where:

p_{LS} - pressure set by the LS valve;
p - current load pressure demand;
Δp - low differential pressure to account for system losses and ensure operation at the optimal pressure.
The LS valve ensures the pump's output correlation with the load's pressure demand without producing excessive pressure, which would waste energy.
The LS valve also helps regulate the flow rate to match the load, often through proportional control or using a flow divider. The flow adjustment equation can be represented as [10-13]:

$$Q_{LS} = Q_d \tag{10}$$

where:

Q_{LS} - flow rate adjusted by the LS valve;
Q_d - flow rate required by the load.
In this way, the LS valve modulates the flow rate based on the load's requirements, ensuring the pump does not produce more flow than needed, which would otherwise lead to energy wastage.
The equation for instantaneous power is derived from the relationship between pressure, flow rate, and motor efficiency. The LS valve helps adjust these parameters to ensure that the system operates more efficiently minimizing wasted energy and reducing the power requirements during periods of low load [7-14].

3. Efficiency system results with parameter modification depending on the output requirements

Considering the basic parameters for a hydraulic system model, the operating situation in the configuration with and without the LS system is analyzed in order to highlight the performance results achieved and to be able to describe the efficiency of the system.
The parameters of the initial and final states that are taken into account are presented in table 1.

Table 1: Parameters for hydraulic volumetric units components

Parameter	Initial Stage (No LS Valve)	Final Stage (With LS Valve)	Unit	Description
Pump pressure (P_max)	130 Constant value	90-130 Variable, adjusted based on load	bar	Pressure provided by the pump
Pump Pressure (P_min)	50 Constant, fixed at minimum	50-90 Variable, adjusted based on load	bar	Minimum pump pressure
Pump Flow Rate (Q_max)	34 Constant, fixed flow	Variable, adjusts to match motor demand	l/min	Flow rate provided by the pump
Motor Pressure	90 Constant, set pressure	Matches pump output as controlled by LS valve	bar	Pressure required by the motor; varies with LS valve operation
Motor Flow Rate	34 Constant, set flow	Matches pump output as controlled by LS valve	l/min	Flow rate required by the motor; varies with LS valve operation
Pump Efficiency (η_pump)	85	85	%	Pump efficiency
Motor Efficiency (η_motor)	90	90	%	Motor efficiency
Friction Losses	5% of pump input Fixed, based on constant high pressure	Reduced due to lower pressures and variable flow rates	W	Friction losses reduced with LS valve optimization
Leakage Losses	3% of pump input Fixed, based on constant high pressure	Reduced due to lower pressures and variable flow rates	W	Leakage losses; reduced with LS valve optimization
Energy Losses	Higher, due to constant high pressure and fixed flow rate	Reduced, thanks to dynamic pressure and flow optimization	W	Total energy losses decreased with LS valve optimization
System Efficiency	Lower, 40-50% inefficient operation due to fixed high pressure	Higher, 70-80% optimized operation with LS valve	%	System efficiency significantly improved with LS valve
Motor Power Output	Dependent on the fixed pressure and flow	Optimized to match pump output based on load demand	W	Power delivered to the motor optimized with LS valve
Pump Power Input	Constant, fixed power consumption based on max pressure	Reduced power consumption, adjusted by LS valve based on load	W	Power input to the pump reduced with LS valve optimization

The characteristics between the working operation conditions are presented, while the advantages of introducing the LS solution are evident as highlighted in the numerical results in Figure 1. The defining advantages are related to losses reduction, counted with less friction and leakage values due to dynamic pressure regulation, higher system efficiency that is improved up to 80 % and improved motor operation control through lower pressure values dynamically adjusted according to real demands.

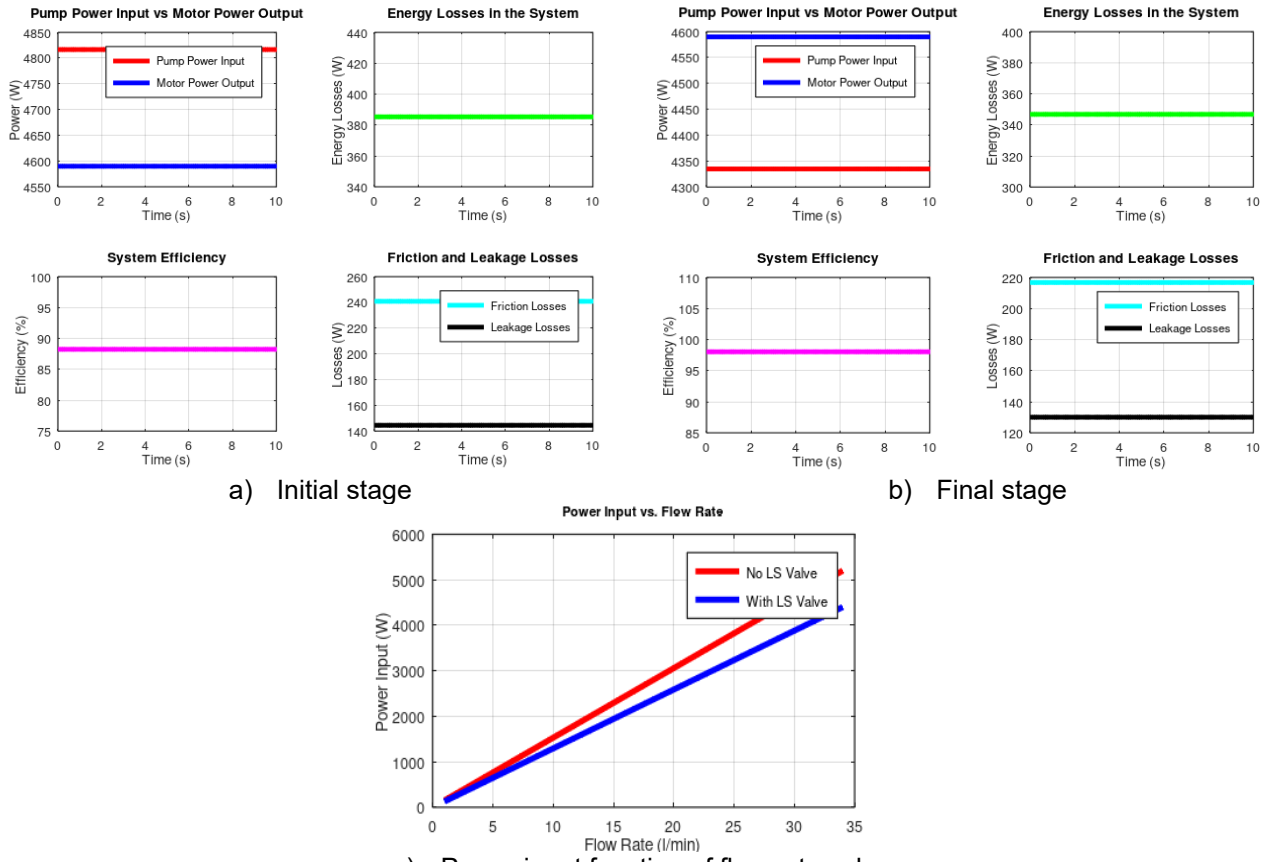

a) Initial stage b) Final stage

c) Power input function of flow rate values

Fig. 1. Analysis efficiency results

The results are presented in comparative terms of input and output power, efficiency over time and losses over time of the system for the two cases considered, as well as power as a function of the working fluid flow rate. The advantages of using the LS system for operation are visible because optimizations of the values of the parameters involved are obtained.

4. Conclusions

Based on the numerical analysis results, it is obvious the high impact of the Load Sensing (LS) operation valve on a hydraulic system. Without the LS, the system operates with a constant high pressure and fixed flow rate values, which results in low system efficiency. This inefficiency stems from excessive power consumption that does not align with real conditions load demands.

With the LS valve, the system dynamically adjusts the pressure and flow rate values based on the load, which results in significantly higher system efficiency. This dynamic operation helps avoid unnecessary power use and optimizes the system to match the exact load requirements, improving overall performance.

While the LS valve allows the system to adjust its power input based on the real load is leading to energy consumption reduction and is evident on the result plots, where the system with the LS valve consumes less power for the same flow rate and further the power input decreases as the flow rate decreases.

Without the LS valve, the pump operates at maximum power even when it's not required, leading to higher energy consumption and wasted energy. Energy losses from friction and leakage are significantly reduced with the LS valve as seen on obtained numerical results. The system with the LS valve operates at lower pressures and adjusts flow rate dynamically, resulting in lower friction and leakage losses compared to the constant high pressure system without the LS valve.

These reduced losses directly contribute to the higher system efficiency in the final state (with LS valve).

The LS valve optimizes both flow rate and pressure, ensuring that the system operates only at the levels needed for the current load. This avoids over-pressurizing the system and provides a much more efficient operation.
Without the LS valve, the system runs at fixed parameters that often exceed the needs of the load, resulting in wasted resources and inefficiencies.
The dynamic adjustments enabled by the LS valve allow the system to maintain optimized performance across a range of load conditions. In contrast, the system without the LS valve struggles with less flexibility and efficiency under variable loads.
The addition of a Load Sensing (LS) valve significantly enhances the hydraulic system's efficiency and performance, by dynamically adjusting the system's pressure and flow rate based on the load requirements, leading to lower energy consumption, maximize energy efficiency, reduce operational costs and extend the lifespan of system components.

References

[1] Axinti, S., and F.D. Ștheaua. *Introduction to industrial hydraulics/Introducere în hidraulica industrială*. Galati, Galati University Press, 2015.
[2] Axinti, G., and A.S. Axinti. *Hydraulic and pneumatic drives – Bases of Calculation, Design, Operation, Reliability and Drive Diagrams/Acţionări hidraulice şi pneumatice – Baze de Calcul, Proiectare, Exploatare, Fiabilitate și Scheme de Acționare*, Vol. 3. Chişinău, Tehnica-Info Publishing House, 2009.
[3] Axinti, G., and A.S. Axinti. *Hydraulic and pneumatic drives – Components and systems, Functions and features/Acţionări hidraulice şi pneumatice – Componente și sisteme, Funcții și caracteristici*. Vol. 1. Chişinău, Tehnica-Info Publishing House, 2008.
[4] Dindorf, Ryszard, Jakub Takosoglu, and Piotr Wos. "Review of hydro-pneumatic accumulator models for the study of the energy efficiency of hydraulic systems." *Energies* 16, no. 18 (2023): 6472.
[5] Li, Ruichuan, Qiyou Sun, Xinkai Ding, Yisheng Zhang, Wentao Yuan, and Tong Wu. "Review of flow-matching technology for hydraulic systems." *Processes* 10, no. 12 (2022): 2482.
[6] Kogler, Helmut, Andreas Plöckinger, and Paul Foschum. "Cybernetic Proportional System for a Hydraulic Cylinder Drive Using Proportional Seat-Type Valves." *Actuators* 12, no. 10 (2023): 370.
[7] Li, Yanchao, Ruichuan Li, Junru Yang, Xiaodong Yu, and Jikang Xu. "Review of recent advances in the drive method of hydraulic control valve." *Processes* 11, no. 9 (2023): 2537.
[8] Tian, Yuan, Jingliang Gao, Jianxun Chen, Junshen Xie, Qidong Que, Rodger Millar Munthali, and Tiantian Zhang. "Optimization of pressure management in water distribution systems based on pressure-reducing valve control: Evaluation and case study." *Sustainability* 15, no. 14 (2023): 11086.
[9] Aiqin, Huang, and Wang Yong. "Pressure model of control valve based on LS-SVM with the fruit fly algorithm." *Algorithms* 7, no. 3 (2014): 363-375.
[10] Lisowski, Edward, Grzegorz Filo, and Janusz Rajda. "Analysis of the energy efficiency improvement in a load-sensing hydraulic system built on the ISO plate." *Energies* 14, no. 20 (2021): 6735.
[11] Chao, Qun, Junhui Zhang, Bing Xu, Yaoxing Shang, Zongxia Jiao, and Zhihui Li. "Load-sensing pump design to reduce heat generation of electro-hydrostatic actuator systems." *Energies* 11, no. 9 (2018): 2266.
[12] Mi, Juncheng, Jin Yu, and Guoqin Huang. "Direct-drive electro-hydraulic servo valve performance characteristics prediction based on big data and neural networks." *Sensors* 23, no. 16 (2023): 7211.
[13] Stroita, Daniel Catalin, Dorin Bordeasu, and Florin Dragan. "System Identification of a Servo-Valve Controlled Hydraulic Cylinder Operating Under Variable Load." *Mathematics* 13, no. 3 (2025): 341.
[14] Hossain, Md Shazzad, Ibrahim Sultan, Truong Phung, and Apurv Kumar. "A Literature Review of the Design, Modeling, Optimization, and Control of Electro-Mechanical Inlet Valves for Gas Expanders." *Energies* 17, no. 18 (2024): 4569.

Performance Analysis of a Solar Fruit Dryer under Controlled Conditions

Ioan PAVEL[1], PhD eng. **Gabriela MATACHE**[1], PhD eng. **Gheorghe ȘOVĂIALĂ**[1], **Ana-Maria POPESCU**[1]

[1] National Institute of Research & Development for Optoelectronics/INOE 2000, Subsidiary Hydraulics and Pneumatics Research Institute/IHP, Romania

* fluidas@fluidas.ro

Abstract: *Solar energy is one of the most accessible and environmentally friendly sources of renewable energy, widely used in the drying of agricultural products. Compared to conventional methods, solar drying offers significant advantages such as improved energy efficiency, low operating costs, minimal environmental impact, and better preservation of the nutritional quality of food products.*
This paper analyzes the performance of a mixed-type solar dryer, consisting of an air collector and a drying chamber, used for the dehydration of fruits (apple, pear, and banana) under controlled theoretical conditions. A detailed calculation was carried out to determine the volumetric airflow required to dry 1 kg of fresh fruit, based on real moisture content data and standardized drying conditions. For instance, drying 1 kg of apple (initial moisture 85%, final moisture 15%) at 50°C required approximately 32.1 m³/h of dry air, under ideal operating conditions.
The results indicate that commonly cited values in the literature – estimating the need for 250 W and 62 m³/h of air to dry 1 kg of fruit – can be significantly optimized through proper system design and precise control of operational parameters. The study highlights the drying behavior differences between fruits and provides a basis for the efficient sizing of solar dryers, especially for small-scale producers and farmers seeking sustainable and low-cost food preservation solutions.

Keywords: *Solar drying, renewable energy, fruit dehydration, agricultural sustainability, controlled drying process*

1. Introduction

The continuous growth of the global population and accelerated urbanization have led to an increasing demand for fresh food, particularly fruits and vegetables. However, the lack of adequate storage and preservation facilities often results in significant post-harvest losses, reducing the availability of food products and contributing to price increases. Preserving these products is essential for extending shelf life, maintaining nutritional value, and reducing food waste. Among various preservation technologies, drying stands out for its simplicity and efficiency, being one of the oldest food processing methods used for millennia [1].
Agro-food products can be dried using several methods, but one of the most sustainable solutions is **solar drying**, which relies on a renewable, eco-friendly, and abundant energy source. The conversion of solar energy into heat is a direct and efficient application in this context, allowing for the reduction of moisture content in fruits and vegetables and consequently lowering their mass, which facilitates packaging, storage, and transport [2]. Removing water from the product inhibits microbiological and chemical processes that lead to food spoilage, thereby extending its shelf life [3].
Although traditional sun drying continues to be widely used, it presents significant limitations: high heat losses, exposure to contaminants, dependency on weather conditions, and lack of control over the drying process. These drawbacks have led to the development of **modern solar dryers**, in which drying takes place in a closed and controlled environment, with regulated temperature and moisture, using solar energy either directly or indirectly. These systems are commonly classified as direct, indirect, mixed, or hybrid dryers, and can operate in passive mode (natural convection) or active mode (forced convection).
It is also important to note that traditional sun drying suffers from substantial thermal energy losses, since only a fraction of the incident solar radiation is effectively used in the drying process. Direct exposure also increases the risk of product degradation due to extreme weather conditions

or contamination by foreign particles. Therefore, drying under controlled conditions is necessary for improved product quality. The evolution of sun drying has led to the development of **solar drying systems**, in which products are dried in enclosed environments, maintaining high internal temperatures [4]. In this context, solar dryers offer practical solutions to the challenges of open sun drying. They use solar energy as the primary heat source for drying, while also increasing thermal efficiency compared to traditional sun drying methods.

These solar-powered drying systems have been developed in various designs, and a significant portion of fossil fuel consumption can be reduced through their use [5]. All of these solar dryer configurations rely on the same fundamental mechanism—**evaporation of water molecules from within the product**. The method of heat transfer to the product depends on the system design and can occur through convection or radiation [6].

According to the literature, general estimates suggest that drying 1 kg of fruit with approximately 80% moisture content requires around **250 W of thermal energy** and an **airflow rate of about 62 m³/h**. However, the simulations conducted in this study, using a simplified solar dryer model composed of a solar collector and a drying chamber, indicate optimized values. For example, drying 1 kg of apples, with an initial moisture content of 85% and a final value of 15%, at a constant temperature of 50°C and air relative moisture of 30%, required only **32.1 m³/h of dry air** and resulted in **0.7 kg of water removed**. This approach demonstrates that, through careful design and rigorous control of operating parameters, the efficiency of the drying process can be significantly improved compared to general theoretical estimates.

Therefore, the present study aims to analyze the drying behavior of fruits such as apples, pears, and bananas, in the context of using a solar dryer under controlled parameters. It also seeks to highlight the differences in drying time and air requirements based on the internal structure and initial moisture content of each fruit. The results obtained may contribute to the optimization of solar dryer design, particularly for small-scale producers or farmers, offering a sustainable, cost-effective, and efficient alternative for agricultural product preservation.

2. Classification and operating principles of solar dryers

Numerous researchers have developed and evaluated various types of solar dryers with the aim of improving operational efficiency and thermal performance. Solar dryers can be classified according to several criteria, such as the movement of heated air, structural configuration, airflow direction, exposure to solar radiation, or the inclusion of energy storage systems [7].

Based on their operating principles, the most common types of solar dryers include:

- direct solar dryers,
- indirect solar dryers,
- mixed-mode dryers (combining direct and indirect heat input),
- dryers with thermal energy storage,
- passive solar dryers (with natural convection) and active ones (with forced convection) [7].

In **direct-type solar dryers**, the product is exposed directly to solar radiation and is covered by a transparent cover that allows the passage of solar energy while protecting the product from weather conditions and contaminants [8]. These systems are structurally simple but limited in terms of temperature control and drying uniformity.

Indirect solar dryers use a solar air collector to heat the air, which is then directed into the drying chamber. In this setup, the product is not exposed to direct sunlight, and heat transfer occurs primarily through convection between the hot air and the product surface. This results in higher thermal efficiency and better product quality [9].

Mixed-mode systems combine the advantages of both direct and indirect types by using both direct solar radiation and heated air. This type of dryer offers superior thermal efficiency due to the combined heat transfer mechanisms—radiation and convection [6,7].

Air circulation within solar dryers can be achieved either:

- **naturally**, via thermal buoyancy (in **passive systems**, also known as greenhouse-type dryers) [10],
- or **mechanically**, using fans or blowers (in **active systems**) [11].

A major challenge associated with solar drying is the **variability of solar radiation**. Cloudy or rainy weather and night-time conditions significantly reduce system performance, increasing the risk of poor product quality or spoilage [12].

To mitigate this issue, **thermal energy storage solutions** are integrated into solar dryers to maintain adequate drying temperatures even in the absence of direct sunlight. Materials such as stone, sand, cast steel, iron, bricks, and salt have been explored for storing excess solar heat, which can then be released during periods of low radiation [13].

More recently, **phase change materials (PCMs)** have been used as latent heat storage units. These materials have been successfully integrated into both direct and indirect solar dryers, providing significant benefits such as reduced drying times, consistent temperature maintenance, and enhanced thermal efficiency, even during unfavorable weather or night-time operation [14-17].

Therefore, the incorporation of **thermal energy storage systems** in solar dryers significantly increases their thermal efficiency and shortens the drying time, improving overall system reliability.

In summary, solar dryers can be classified based on the following criteria:

- method of air movement (natural or forced),
- solar exposure (direct, indirect, or mixed),
- airflow direction,
- internal configuration of the drying system,
- type of solar energy contribution (with or without energy storage).

From a functional perspective, solar drying systems are divided into two major categories:

- **passive solar dryers** (operating without external energy input),
- **active solar dryers** (using external energy sources to assist airflow).

These categories can be combined with the three main heat transfer modes—**direct, indirect, and mixed**—resulting in a wide range of adaptable configurations, suitable for various user needs and local climate conditions.

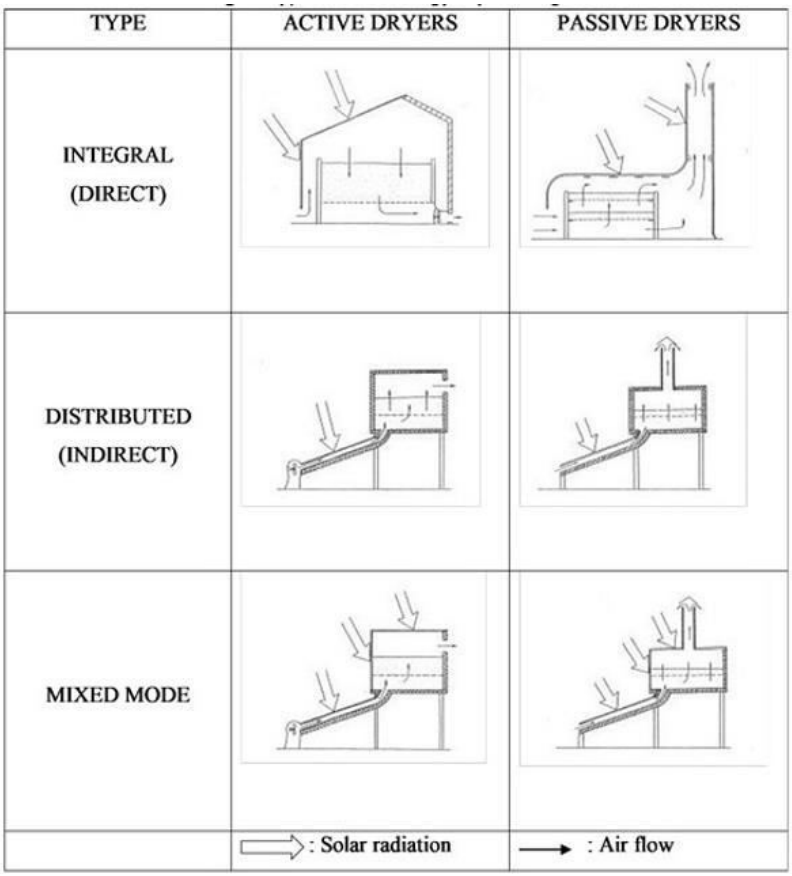

Fig. 1. Classification of solar-powered dryers

Active dryers use external means, such as fans or blowers, to move the heated air from the solar collector to the drying chamber. In contrast, passive dryers rely solely on the natural movement of heated air. Passive dryers are best suited for drying small batches of fruits and vegetables.

Applications of the solar dryer:
• Drying of agricultural crops.
• Food processing industries for dehydrating fruits and vegetables.
• Drying of fish and meat.
• Dairy industry for powdered milk production.
• Treatment of wood and lumber.
• Textile industries for drying fabrics, etc.

3. Methodology

3.1 Construction principles

The double-chamber solar dryer consists of a solar collector, which can also be referred to as an air heater, and a drying chamber that may, for example, contain three layers of trays on which the fruits are placed for drying. The trays in the drying chamber can be loaded with fruits estimated to weigh an average of 50 g per piece, with dimensions of 6 mm in length/width and 5 mm in thickness.
To measure the temperature inside the dryer, a digital thermometer can be used, and moisture loss is determined by weight loss, which is measured using an electronic scale.
For a double-chamber solar dryer, the basic principles are the greenhouse effect and natural convection (draft). The dryer should be placed outdoors with the collector oriented toward the sun. The collector is rigidly fixed to the dryer at an angle of 17.5° from the horizontal so that the beam of solar rays is approximately perpendicular to it.

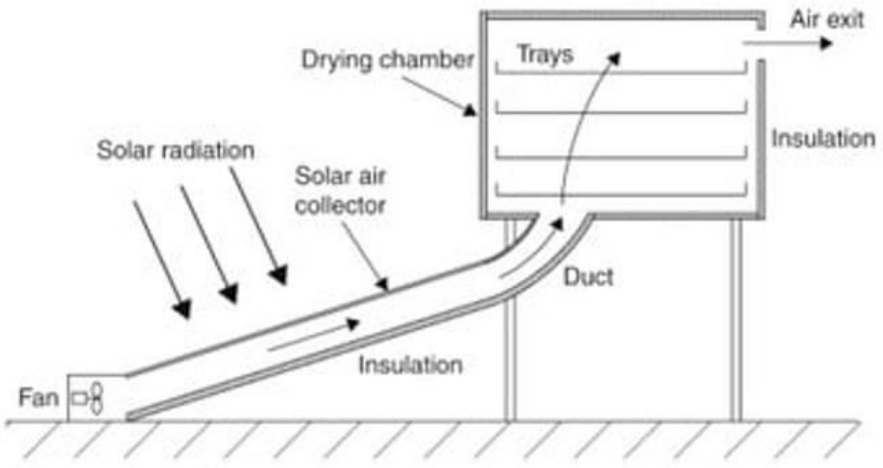

Fig. 2. Two-compartment dryer

3.2 Design principles

For the analysis of solar drying performance in the case of fruits, a simplified theoretical model was proposed, based on a solar dryer consisting of two compartments: a solar air collector and a drying chamber. The objective of the study was to estimate the volumetric airflow rate required to dry 1 kg of fresh product under ideal conditions, without significant thermal energy losses. The fruits analyzed in this study were: apple, pear, and banana.

3.2.1 Initial Data and Calculation Assumptions

A simplified example for calculating the volumetric airflow rate required to dry one kilogram of apples in a two-compartment solar dryer (solar collector + drying chamber) assumes the following data:

- Dried fruit: apple
- Quantity: 1 kg fresh apple
- Initial moisture content (w_1): ~85%
- Final moisture content (w_2): ~15%
- Relative moisture of inlet air: 30%
- Drying air temperature: 50°C
- Air density at 50°C: ~1.09 kg/m³

For each fruit, the following experimental data were used:

- Apple: initial moisture 85%, final moisture 15%
- Pear: initial moisture 86%, final moisture 15%
- Banana: initial moisture 75%, final moisture 15%

It is assumed that the dry air enters the drying chamber (at 50°C) with a moisture content of approximately 0.015 kg water/kg dry air, and at the outlet, the moisture content is ~0.035 kg water/kg dry air. The system efficiency is considered ideal (no heat loss), and the reference duration for complete drying is 1 hour.

3.2.2 Calculation of the amount of water to be removed

The amount of water that needs to be removed is determined by the difference between the initial and final moisture contents, relative to the total mass of the fruit. The formula used is:

$$m_{apa} = m_{fruct} \cdot \frac{w_1 - w_2}{100}$$

Where:
m_{fruct}= 1 kg
w_1 = initial moisture content (%)
w_2 = final moisture content (%)
Example for apple:

$$m_{apa} = 1 \cdot \frac{85 - 15}{100} = 0.7\ kg\ apa$$

3.2.3. Determination of the required dry air mass

Each kg of dry air can take in a quantity of water determined by the difference between the moisture content at the outlet and at the inlet:

$$\Delta x = x_{iesire} - x_{intrare} = 0.035 - 0.015 = 0.02 \frac{kg\ apa}{kg\ aer\ uscat}$$

Therefore, the air mass required for complete drying is:

$$m_{aer} = \frac{0.7}{0.02} = 35\ kg\ aer\ uscat$$

3.2.4. Volumetric airflow calculation

With the air density at the drying temperature (~1.09 kg/m³), the required volumetric airflow is determined by relating the air mass to the density:

$$V = \frac{m_{aer}}{\rho_{aer}} \frac{35}{1.09} \cong 32.1\ \frac{m^3}{h}$$

If this volume is needed for one hour of drying (the duration differs, but we use as an example):
Volumetric air flow = 32.1 m³/h for drying 1 kg of apple in one hour. Observations:

- If you have several layers in the drying room, the air must have sufficient speed and flow rate to penetrate the lower layers as well.
- Depending on the actual drying time, the flow rate adjusts. For example, if drying takes 4 hours, you need a flow rate of:

$$\frac{32.1}{4} = 8.025 \frac{m^3}{h}$$

- These steps can be integrated into a solar dryer sizing, including solar collector sizing (depending on the energy required to heat the air).

3.2.5. Observations on the comparative behaviour of fruits

The differences in internal composition and cell structure between the 3 types of fruits significantly influence the drying time and the efficiency of moisture transfer. We chose for example: apple, pear and banana and we represented a graphic model (fig. 3) that shows how the moisture decreases over time for apples, pears and bananas during drying in a solar dryer.

- The apple starts with a higher moisture (~85%) and reaches 15% in about 10 hours.
- The pear has a slightly slower pace, and
- The banana starts from lower moisture and dries faster.

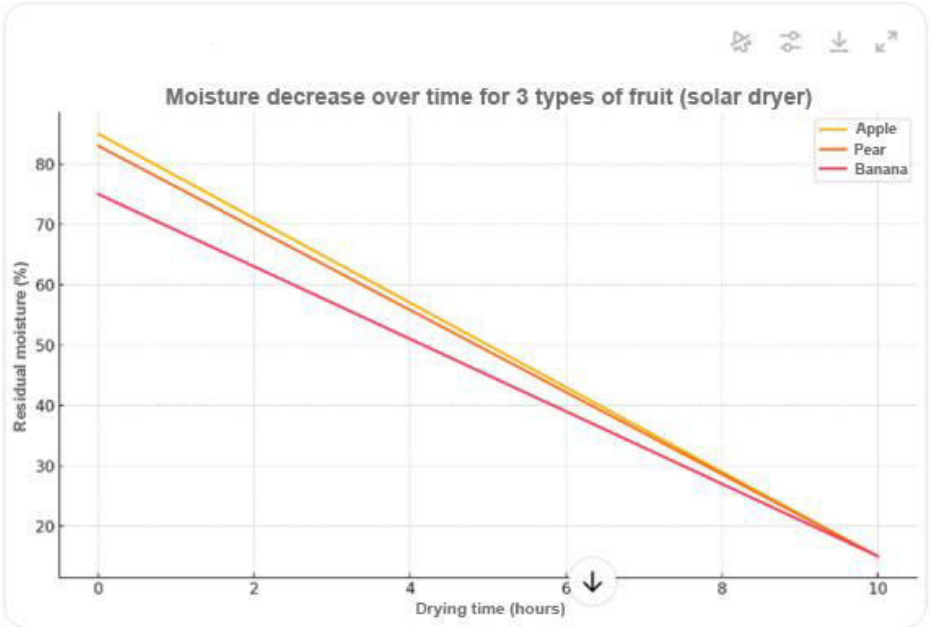

Fig. 3. Moisture decrease

We can extend the model and see how the drying air temperature influences the rate of moisture decrease for the 3 fruits, figure 4. Drying at three different temperatures is simulated: 400 C (slower); 500 C (medium, optimal for many fruits); 600 C (faster, but with a risk of caramelization of sugars).

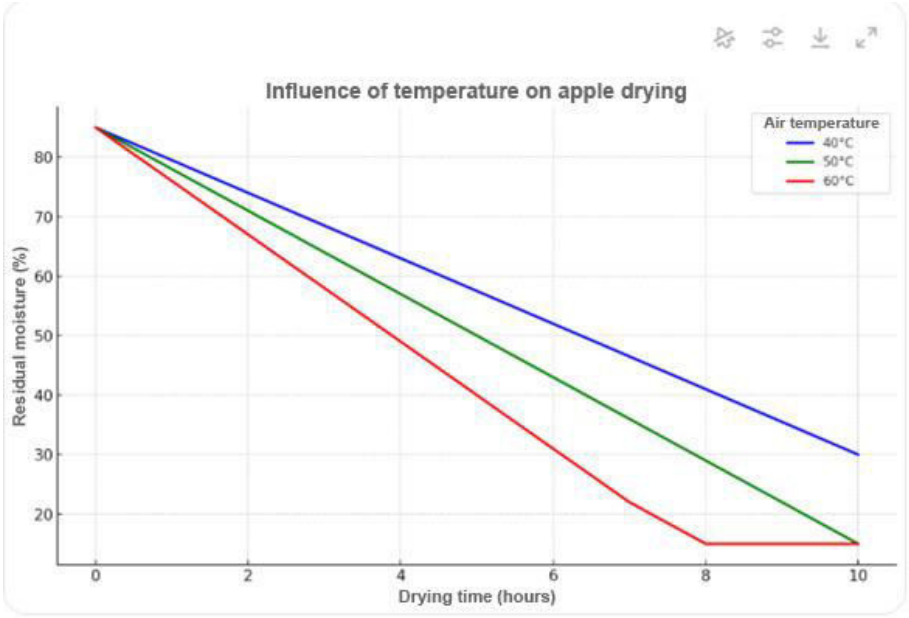

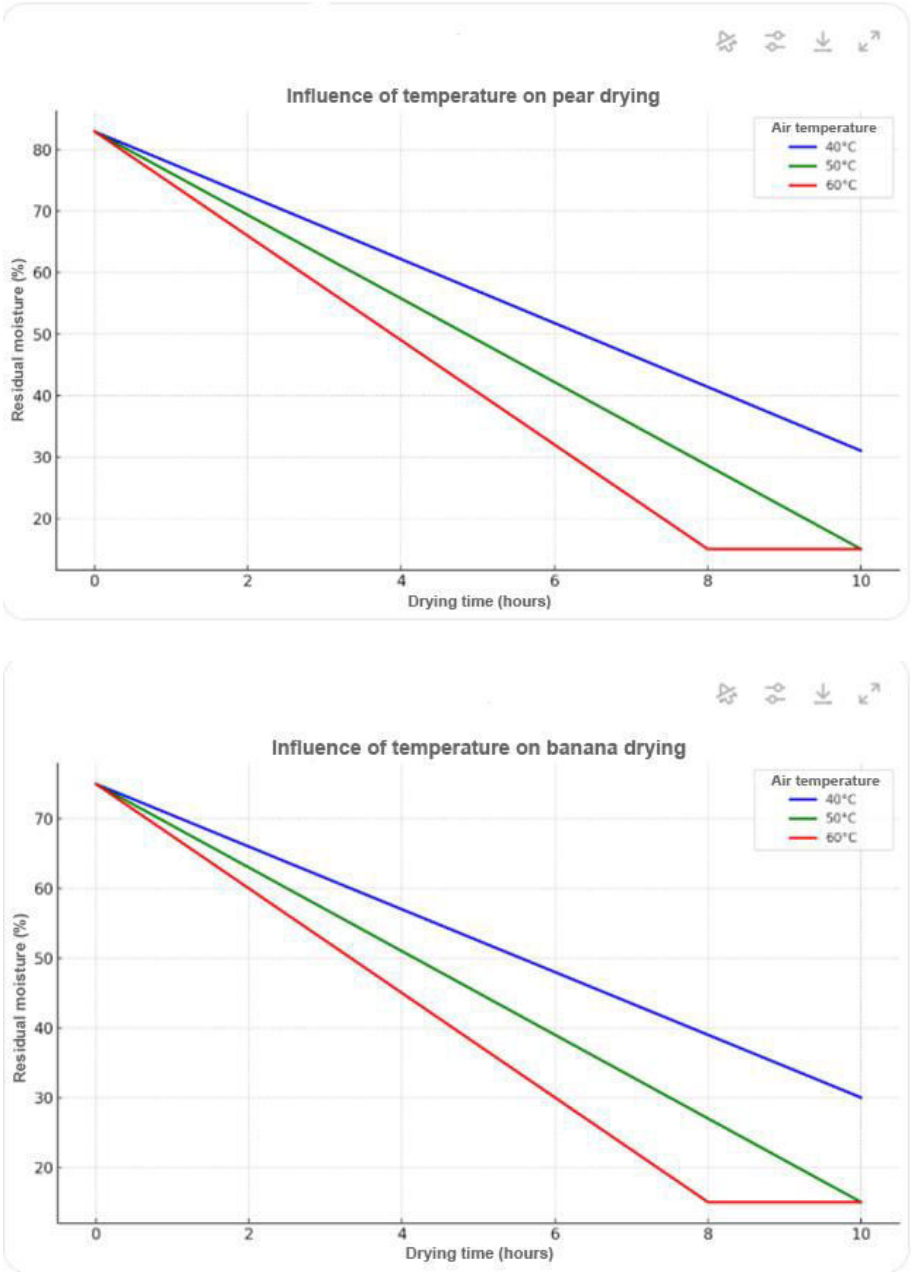

Fig. 4. Influence of temperature on fruit drying

As can be seen, the air temperature influences the drying process of the fruits, so that at 400 C - drying is slower after 10 hours, the moisture has not yet reached 15%; at 500 C – drying is efficient, the target moisture of ~ 15% is reached in about 10 hours; at 600 C – drying is faster, reaching the desired moisture even after 7-8 h, but with the risk of affecting the quality (oxidation, caramelization).

What we can say is that higher temperatures accelerate drying, but a balance must be found between drying speed and preserving fruit quality. Observing this, we must also analyze the influence of air velocity on the drying process.

We will consider a constant temperature—specifically 50°C—since it is regarded as optimal for fruit drying. We will focus only on apples and vary the drying air velocity, starting with 0.5 m/s, 1 m/s, and 1.5 m/s.

From the following graph, Figure 5, we can observe how increasing air velocity influences moisture transfer, accelerating the drying process. However, it should be noted that excessively high air velocities can lead to changes in flavor or texture (especially in soft fruits).

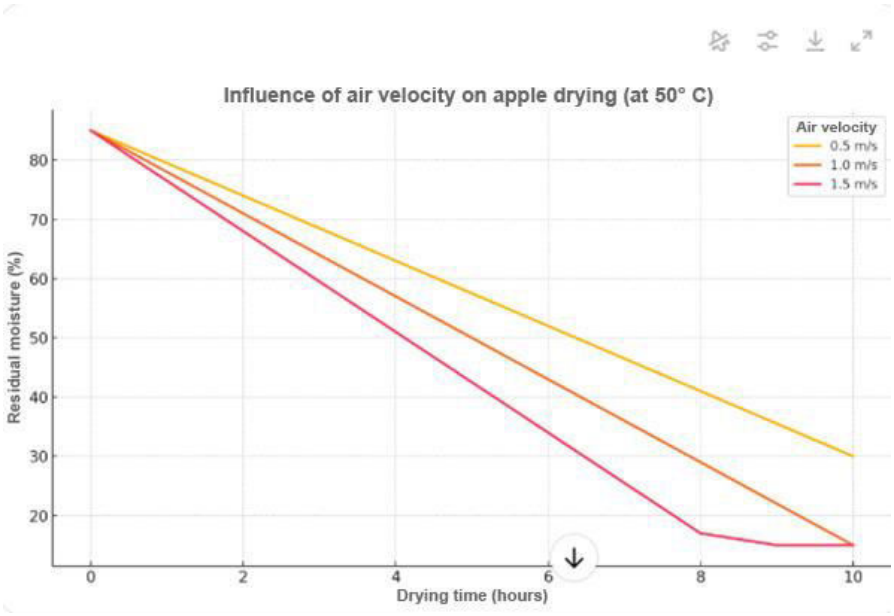

Fig. 5. The influence of air velocity on drying

3.2.6 Calculation of the thermal energy and the average power required for drying a kilogram of fruit (apple, pear, banana)

Let us make some common assumptions:

a. Drying time:

For apple: 10 hours
For pear: 10 hours
For banana: 8 hours

b. Moisture to be removed [18,19]**:**

For apple: 0.7 kg of water (from 85% to 15%)
For pear: 0.68 kg of water (from 83% to 15%)
For banana: 0.6 kg of water (from 75% to 15%)

c. Latent heat of vaporization: LV = 2300 kJ/kg

d. Efficiency of the solar dryer: η = 50% [20]

Based on these common assumptions, we calculate the required energy ($Q = \frac{m_{apa} \cdot L_v}{\eta}$) [21]

For apple $Q = \frac{0.7 \cdot 2300}{0.5} = 3220kJ \approx 0.894kWh$

For pear $Q = \frac{0.68 \cdot 2300}{0.5} = 3128kJ \approx 0.869kWh$

For banana $Q = \frac{0.6 \cdot 2300}{0.5} = 2760kJ \approx 0.767kWh$

After this calculation of the energy we can estimate the average power that is given by the energy divided by the duration of drying, thus we obtain:

For apple (10h): $P = \frac{0.894}{10} = 0.0894kW = 89.4W$

For pear (10h): $P = \frac{0.869}{10} = 0.0869kW = 86.9W$

For banana (8 h): $P = \frac{0.767}{8} = 0.0959kW = 95.9\,W$

As a summary of the estimate we have:

Fruits	Water removed (kg)	Energy (kWh)	Time (h)	Medium power (W)
Apple	0.7	0.894	10	89.4
Pear	0.68	0.869	10	86.9
Banana	0.6	0.767	8	95.9

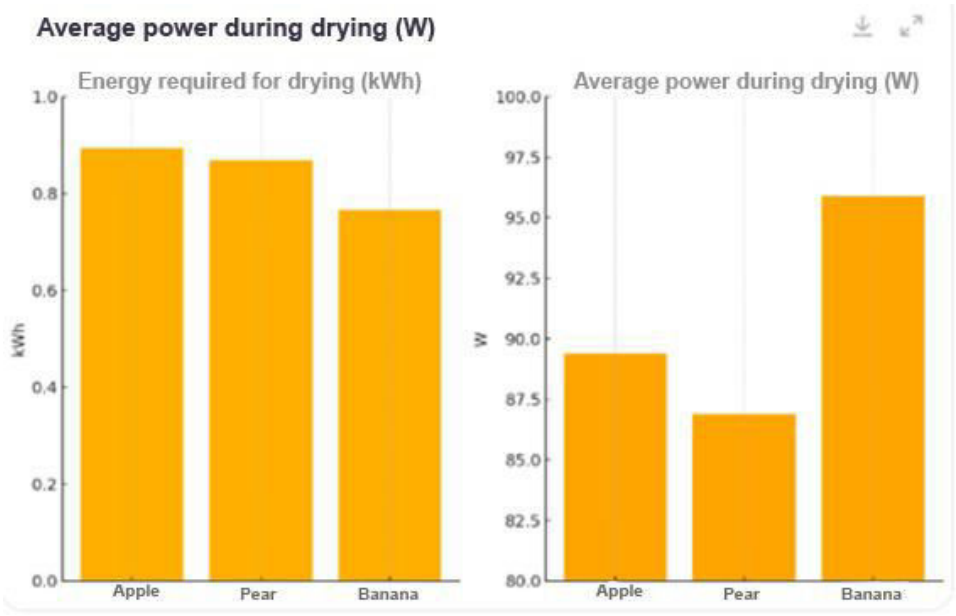

Fig. 6. Average power during drying

An interesting conclusion that results from these calculations and graphs is that bananas, although they require less total energy, having a shorter drying time, need a higher average power during drying

4. Conclusions

The use of solar drying for fruits, vegetables, and other crops holds considerable potential, not only from the perspective of energy savings but also in terms of maintaining product quality. Two main categories of solar dryers can be distinguished: passive dryers (with natural circulation) and those with forced convection. These are further divided into four functional subtypes – direct, indirect, mixed, and hybrid dryers – differentiated by the method of solar energy capture and use, as well as by the architecture of the drying system.

A general estimate from the literature suggests that drying one kilogram of fruit with a moisture content of approximately 80% would require around 250 W of thermal energy and an airflow rate of about 62 m³/h. However, experimental data obtained using a simplified model of a two-compartment solar dryer (collector + drying chamber) shows that these values can be significantly optimized. In an idealized yet realistic scenario, drying 1 kg of apples with an initial moisture content of 85% and a final moisture content of 15%, at a constant temperature of 50°C and an inlet air relative moisture of 30%, required an airflow rate of only ~32.1 m³/h and the removal of 0.7 kg of water. The calculation assumed a hygrometric content of air ranging from 0.015 at the inlet to 0.035 kg water/kg dry air at the outlet. The air density used in the simulation was 1.09 kg/m³, specific to the drying temperature.

These results demonstrate that, in an efficiently designed and well-insulated system, both the energy and airflow requirements can be significantly reduced, contributing to the sustainability of the process. Moreover, the drying behavior of fruits varies depending on their internal structure and water content. In the experiments conducted, it was observed that apples (with a high water content) required approximately 10 hours to reach the desired final moisture level, while bananas, with a lower initial moisture content (~75%), dried more quickly. Pears showed a slower drying rate, indicating higher diffusional resistance in the final stages of the process.

The performance of solar dryers can be significantly improved by reducing heat losses, optimizing air circulation, and precisely controlling operating parameters (temperature, moisture, and airflow). Integrating thermal storage systems and using real-time meteorological data would allow the dryer to dynamically adapt to local climatic conditions. Thus, farmers or small-scale producers can achieve a more efficient, predictable, and regionally adapted drying process, while also reducing conventional energy consumption.

Acknowledgments

This work was supported by a grant of the Ministry of Research, Innovation and Digitization, CCCDI - UEFISCDI, project number PN-IV-P7-7.1-PTE-2024-0039, within PNCDI IV.

Reference

[1] Ahmad, Maqbool, J.C. Hauser, C. Heijnen, and M.A. Chaudry. "Solar drying of fruits and vegetables." *Pakistan Journal of Agriculture Research* 17, no. 3 (2002): 237-244.
[2] Silveira, Semida. "The Solar Economy: Renewable Energy for a Sustainable Global Future: Hermann Scheer, Earthscan Publications Ltd., UK, 2002, 367 pp., £17.99, ISBN I-85383-8357." Book review. *Climate Policy* 3, no. 4 (December 2003): 467-469.
[3] Fortunatus, R., R. Marealle, N. Nenguwo, and T. Stoilova. *Solar Dryers*. *Principles and Basics.* World Vegetable Center. Shanhua, Taiwan. Publication 17-827, 2017.
[4] Rajkumar, P., S. Kulanthaisami, G.S.V. Raghavan, Y. Gariépy, and V. Orsat. "Drying kinetics of tomato slices in vacuum assisted solar and open sun drying methods." *Drying Technology* 25, no. 7-8 (2007): 1349-1357. 10.1080/07373930701438931.
[5] El Hage, H., A. Herez, M. Ramadan, H. Bazzi, and M. Khaled. "An investigation on solar drying: A review with economic and environmental assessment." *Energy* 157 (August 2018): 815-829. 10.1016/j.energy.2018.05.197.
[6] Chavan, U., V. Vitankar, A. Mujumdar, and N. Thorat. "Natural convection and direct type (NCDT) solar dryers: a review." *Drying Technology* 39, no. 13 (2021): 1969-1990. 10.1080/07373937.2020.1753065.
[7] Mohana, Y., R. Mohanapriya, T. Anukiruthika, K.S. Yoha, J.A. Moses, and C. Anandharamakrishnan. "Solar dryers for food applications: Concepts, designs and recent advances." *Solar Energy* 208 (September 2020): 321-344. 10.1016/j.solener.2020.07.098.
[8] Ameri, B., S. Hanini, A. Benhamou, and D. Chibane. "Comparative approach to the performance of direct and indirect solar drying of sludge from sewage plants, experimental and theoretical evaluation." *Solar Energy* 159 (January 2018): 722-732. 10.1016/j.solener.2017.11.032.
[9] Moses, J.A., D.S. Jayas, and K. Alagusundaram. "Resistance to Airflow through Bulk Grains, Oilseeds and Other Agricultural Products – A Review." *Journal of Agricultural Engineering (India)* 50, no. 4 (2013): 1-13. 10.52151/jae2013504.1526.
[10] El Khadraoui, A., I. Hamdi, S. Kooli, and A. Guizani. "Drying of red pepper slices in a greenhouse solar dryer and under open sun: Experimental and mathematical investigations." *Innovative Food Science & Emerging Technologies* 52 (March 2019): 262-270. 10.1016/j.ifset.2019.01.001.
[11] Chaouch, W.B., A. Khellaf, A. Mediani, M.E.A. Slimani, A. Loumani, and A. Hamid. Experimental investigation of an active direct and indirect solar dryer with sensible heat storage for camel meat drying in Saharan environment." *Solar Energy* 174 (November 2018): 328-341. 10.1016/j.solener.2018.09.037.
[12] Sarsavadia, P.N. "Development of a solar-assisted dryer and evaluation of energy requirement for the drying of onion." *Renewable Energy* 32, no. 15 (2007): 2529-2547. 10.1016/j.renene.2006.12.019.
[13] Koçak, B., A.I. Fernandez, and H. Paksoy. "Review on sensible thermal energy storage for industrial solar applications and sustainability aspects." *Solar Energy* 209 (October 2020): 135-169. 10.1016/j.solener.2020.08.081.
[14] Jain, D., and P. Tewari. "Performance of indirect through pass natural convective solar crop dryer with phase change thermal energy storage." *Renewable Energy* 80 (August 2015): 244-250. 10.1016/j.renene.2015.02.012.
[15] Pankaew, P., O. Aumporn, S. Janjai, S. Pattarapanitchai, M. Sangsan, and B.K. Bala. "Performance of a large-scale greenhouse solar dryer integrated with phase change material thermal storage system for drying of chili." *International Journal of Green Energy* 17, no. 11 (2020): 632-643. 10.1080/15435075.2020.1779074.
[16] Singh, D., and P. Mall. "Experimental investigation of thermal performance of indirect mode solar dryer with phase change material for banana slices." *Energy Sources, Part A: Recovery, Utilization, and Environmental Effects* 46, no. 1 (2020): 15268-15285. 10.1080/15567036.2020.1810825.
[17] Swami, V.M., A.T. Autee, A. T R. "Experimental analysis of solar fish dryer using phase change material." *Journal of Energy Storage* 20 (December 2018): 310-315. 10.1016/j.est.2018.09.016.
[18] Ratti, C. "Hot air and freeze-drying of high-value foods: a review." *Journal of Food Engineering* 49, no. 4 (2001): 311-319. 10.1016/S0260-8774(00)00228-4.
[19] Esper, A., and W. Mühlbauer. "Solar drying – an effective means of food preservation." *Renewable Energy* 15, no. 1–4 (1998): 95–100.
[20] Ekechukwu, O. V., and B. Norton. "Review of solar-energy drying systems II: an overview of solar drying technology." *Energy Conversion and Management* 40, no. 6 (April 1999): 615-655.
[21] Heldman, D.R., and D.B. Lund (eds.). *Handbook of Food Engineering*. 2nd edition. Boca Raton, CRC Press, 2006.

Simulation of Hydraulic Motor Controlled by the Control Valve

Dr. eng. **Tiberiu AXINTE**[1,*], Dr. eng. **Mihăiță CAZACU**[2], Dr. math. **Elena Gabriela CURCĂ**[1], Eng. **Lidia CALANCEA**[1], Eng. **Mihai DIACONU**[1], Eng. **Camelia PASCU**[1]

[1] Research and Innovation Center for Navy, Romania

[2] Ovidius University of Constanta, Romania

* tibi_axinte@yahoo.com

Abstract: *The paper presents an overview of the importance of installations with hydraulic motors. In this manuscript, we are studying two hydraulic circuits and one electro-hydraulic circuit, which contains 4/2-way hand-lever valves. Thus, the first hydraulic circuit contains the following devices: fixed displacement pump, three tanks, 4/2-way hand-lever valve, two throttle valves, pressure relief valve, and hydraulic motor (HM 1-1). Next, the second hydraulic circuit contains the following components: a pump unit, two tanks, a 4/2-way hand-lever valve, 3-way pressure regulators, two check valves, two throttle valves and hydraulic motors (HM 2-1 and HM 2-2). Finally, the last circuit, which is actually an electro-hydraulic system, contains the following devices: a fixed displacement pump, three tanks, a 4/2-way solenoid valve, two throttle check valves, a hydraulic motor (HM 3-1), two relays, valve solenoid and a magnetic proximity switch.*

Keywords: *System, hydraulic, energy, motor, valve*

1. Introduction

Hydraulic motors are resistant devices that convert hydraulic energy into mechanical energy in a short time.
One of the first rotary hydraulic motors to be developed was that constructed by William Armstrong in 1850. But since then, the hydraulic motors have developed a lot.
These devices are used in a variety of applications, including conveyors, metalworking machines, mining machinery, construction equipment, transportation, agricultural installations, etc.
In practice, hydraulic motors are usually more efficient than electric motors because they can operate in a wider range of conditions (e.g., temperature, pressure, etc.) [1].

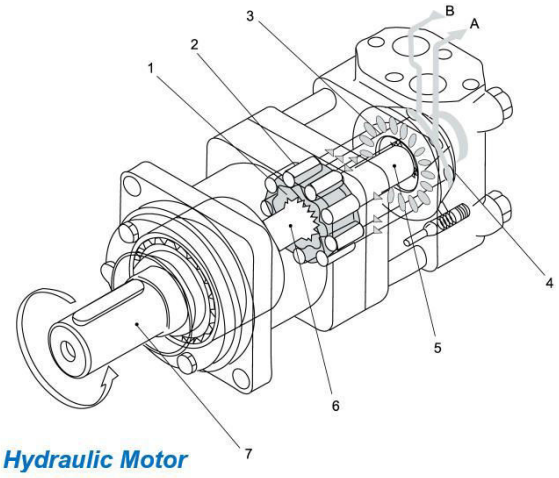

Fig. 1. The main components of the hydraulic motor

Moreover, there are three types of hydraulic motors:
• Vane motor: is used to generate the rotational force.
• Piston motor: pistons are used to generate the rotational force.
• Gear motor: gears are used to transfer hydraulic pressure into rotational force.
Anyway, these components are shown in the figure above, Fig. 1.

The main components of the hydraulic motor are:
1) Orbit cam
2) Roll
3) Distributor
4) Auxiliary plate
5) Distributor shaft
6) Transmission shaft
7) Output shaft.

In the hydraulic systems, the fluid is controlled directly or automatically by a motor and distributed through hoses, tubes or pipes [2].

In any technical documentation, the hydraulic motor has the symbol below, Fig. 1.

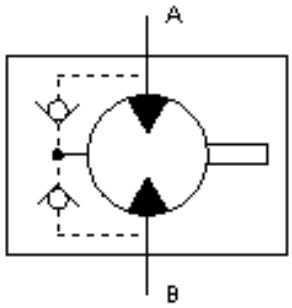

Fig. 2. Symbol of hydraulic motor

MS series hydraulic motors are suitable for hydraulic systems because they operate under difficult operating conditions (high pressures, thin oil, etc.) [3].

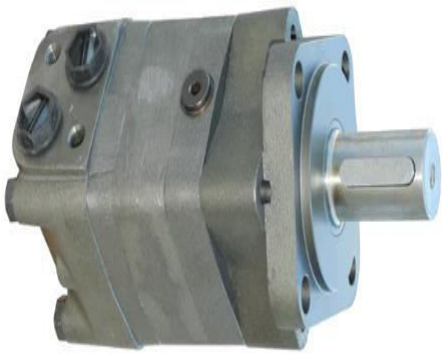

Fig. 3. MS 80 - Hydraulic motor

Technical data for MS 80 hydraulic orbit motor are shown in Table 1.

Table 1: Technical data

Feature	Value
Max. speed	800 rpm
Max. torque	225 Nm
Max. output	16 kW
Max. pressure drop	205 $\cdot 10^5$ Pa
Max oil flow	1083.33 $m^3 \cdot s^{-1}$
Max. inlet pressure	250 $\cdot 10^5$ Pa
Weight	9.8 kg

2. The role of hydraulic motors

The design of hydraulic motor systems has a direct effect on flow rates, friction losses in piping and other plant components.
Hence, the hydraulic devices in the presented installations are selected based on the available dimensions of the components in the product catalogs. In this case, the circuits must be designed to achieve the required flow and pressure in a hydraulic installation [4].
The following equations provide specialists with the basic relations needed for sizing hydraulic motors used in industry:

$$N = \frac{\eta_v \cdot q \cdot 1000}{D} \quad (1)$$

Where:
- N – speed.
- η_v – volumetric efficiency.
- q – hydraulic fluid flow.
- D – displacement.

$$M = \frac{\eta_m \cdot \Delta p \cdot D}{63} \quad (2)$$

Where:
- M – output torque.
- η_m – mechanical efficiency.
- Δp – differential pressure.

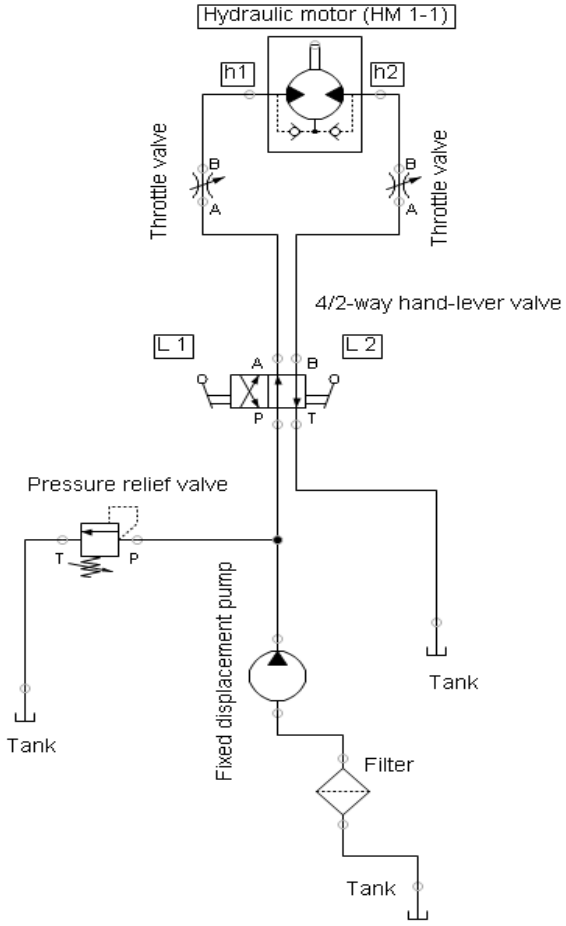

Fig. 4. First hydraulic circuit with HM 1-1

➢ $P = \frac{\eta_t \cdot \Delta p \cdot q}{600}$ (3)

Where:

- P – output power.
- η_t – overall efficiency.
- Δp – differential pressure.

If the operator pushes lever L1, then the output shaft from hydraulic motor (HM 1-1) rotates counterclockwise from point h2 to point h1, Fig. 5.

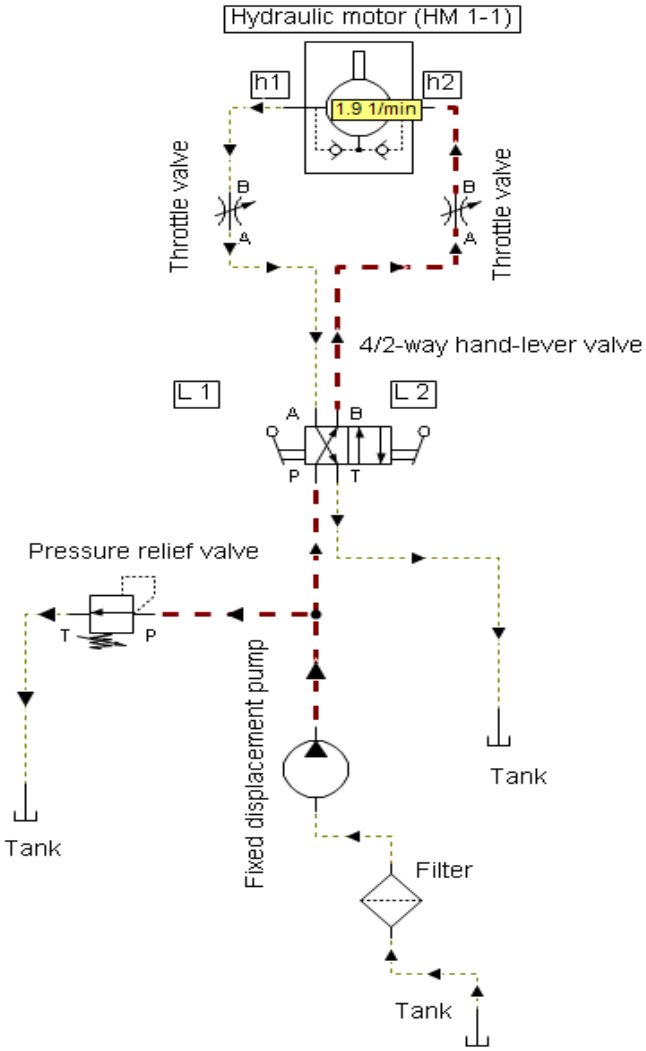

Fig. 5. First hydraulic circuit. Simulation I

But, if the operator pushes the L2 lever to the left, then the output shaft from hydraulic motor (HM 1-1) rotates clockwise from point h1 to point h2, Fig. 6.

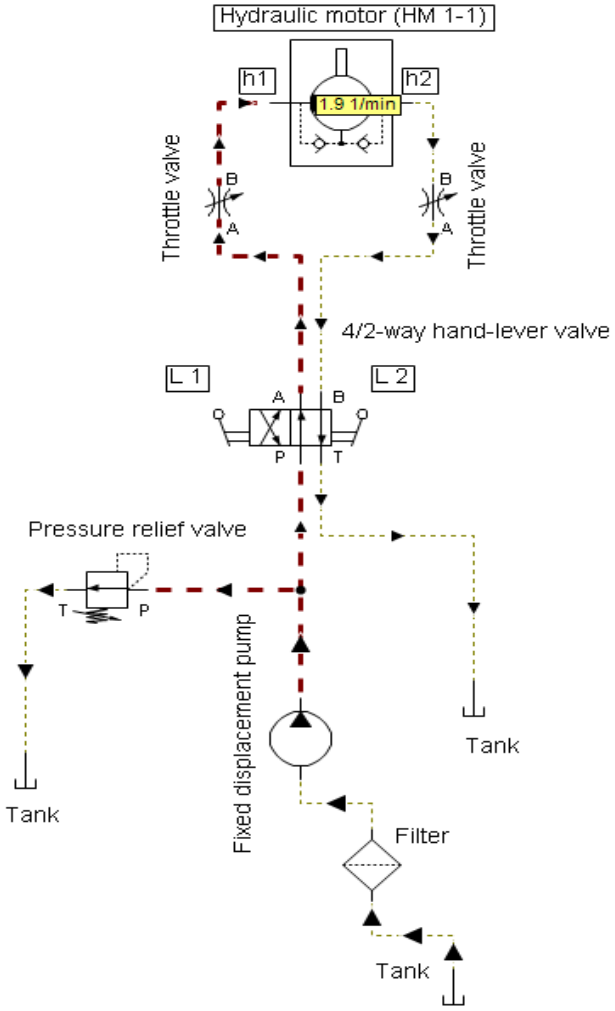

Fig. 6. First hydraulic circuit. Simulation II

Depending on the 4/2-way hand-lever valve, the parameters of the hydraulic motor: revolutions per minute (rpm) and volume flow rate (q), Fig. 7.

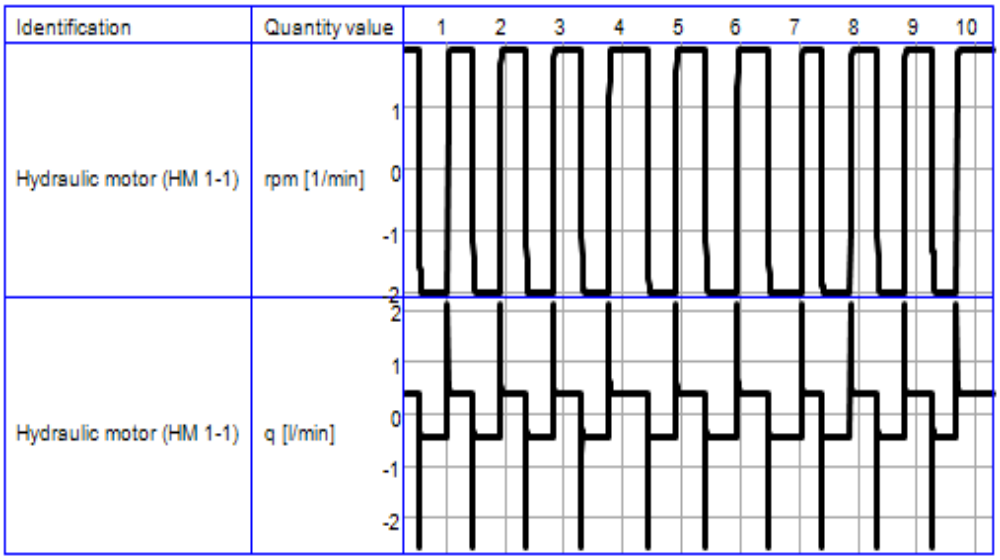

Fig. 7. Diagrams of parameters rpm and q

The second installation has two hydraulic motors (HM 2-1 and HM 2-2), Fig. 8.

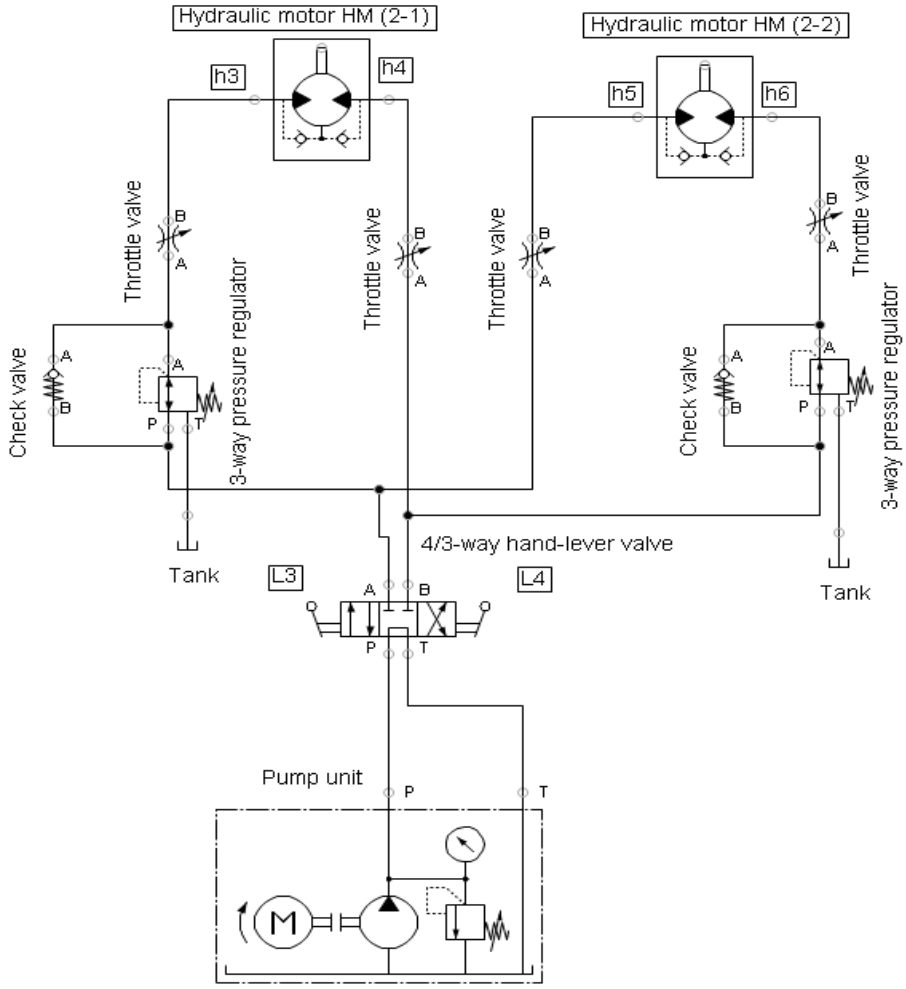

Fig. 8. Second circuit with two hydraulic motors

The second hydraulic system has the following eleven devices, listed in the table below [5].

Table 2: Devices of second electro-pneumatic scheme

Description	Number of components
Hydraulic motor (HM 2-1 and HM 2-2)	1
Throttle valve	2
Check valve	2
3-way pressure regulator	2
4/3-way hand-lever valve	1
Tank	2
Pump unit	1

The second hydraulic circuit with two hydraulic motors opens if the operator pushes L3 to the right. Then, output shafts from hydraulic motors (HM 2-1 and HM 2-2) rotate together clockwise at the same time, Fig. 9.

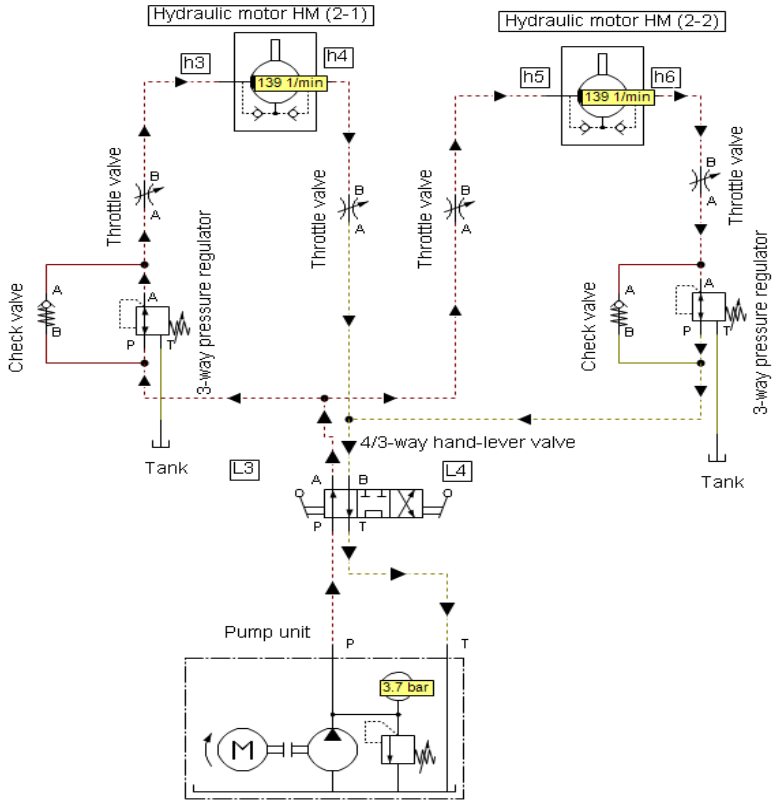

Fig. 9. Second hydraulic with two hydraulic motors. Simulation

Afterwards, in order to close the installation, the manipulator must pull the lever L2 to the left. The third installation is an electro-hydraulic circuit with the hydraulic motor HM 3-1, Fig. 10.

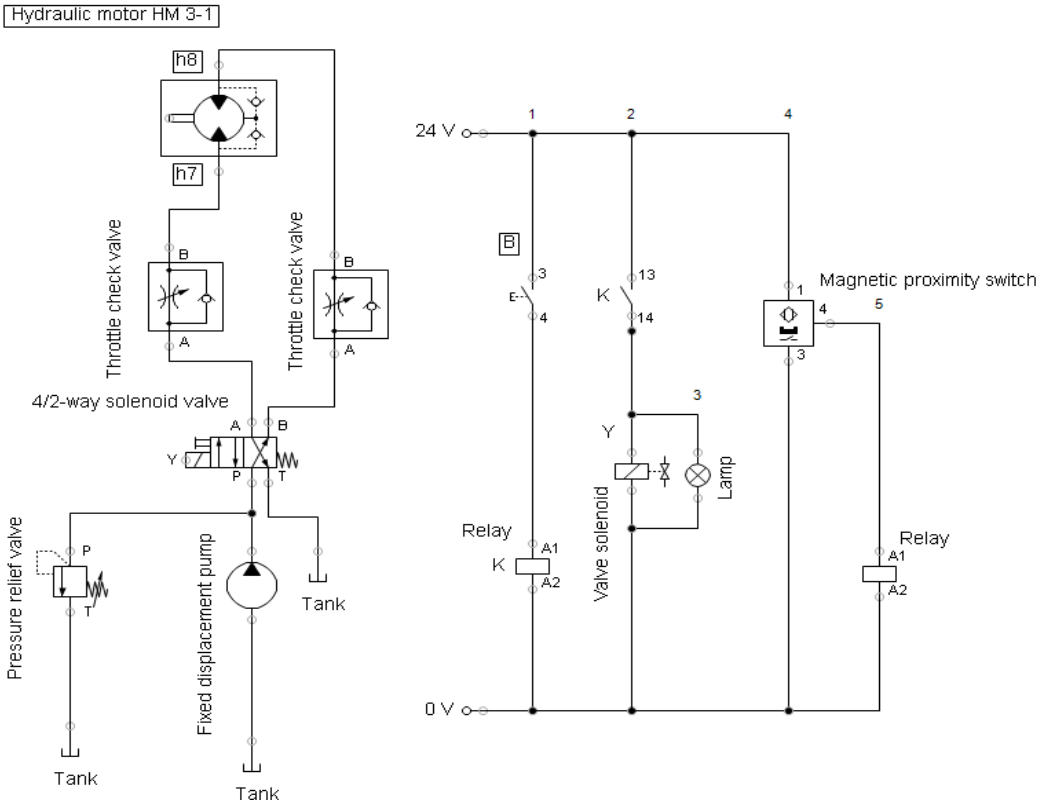

Fig. 10. Electro-hydraulic circuit with one hydraulic motor HM (3-1)

The last of electro-hydraulic system with hydraulic motor HM (3-1) has the following twelve devices, listed in the table below [5].

Table 3: Devices of second electro-pneumatic scheme

Description	Number of components
Fixed displacement pump	1
Tank	3
Throttle check valve	2
4/2-way solenoid valve	1
Hydraulic motor	1
Relay	2
Valve solenoid	1
Magnetic proximity switch	1

In addition, an electro-pneumatic circuit with a 4/2-way solenoid valve has a return spring [6]. When the manipulator presses B button, then output shaft from hydraulic motors (HM 3-1) rotates clockwise from point h7 to point h8 and a lamp shows an orange signal, Fig. 11.

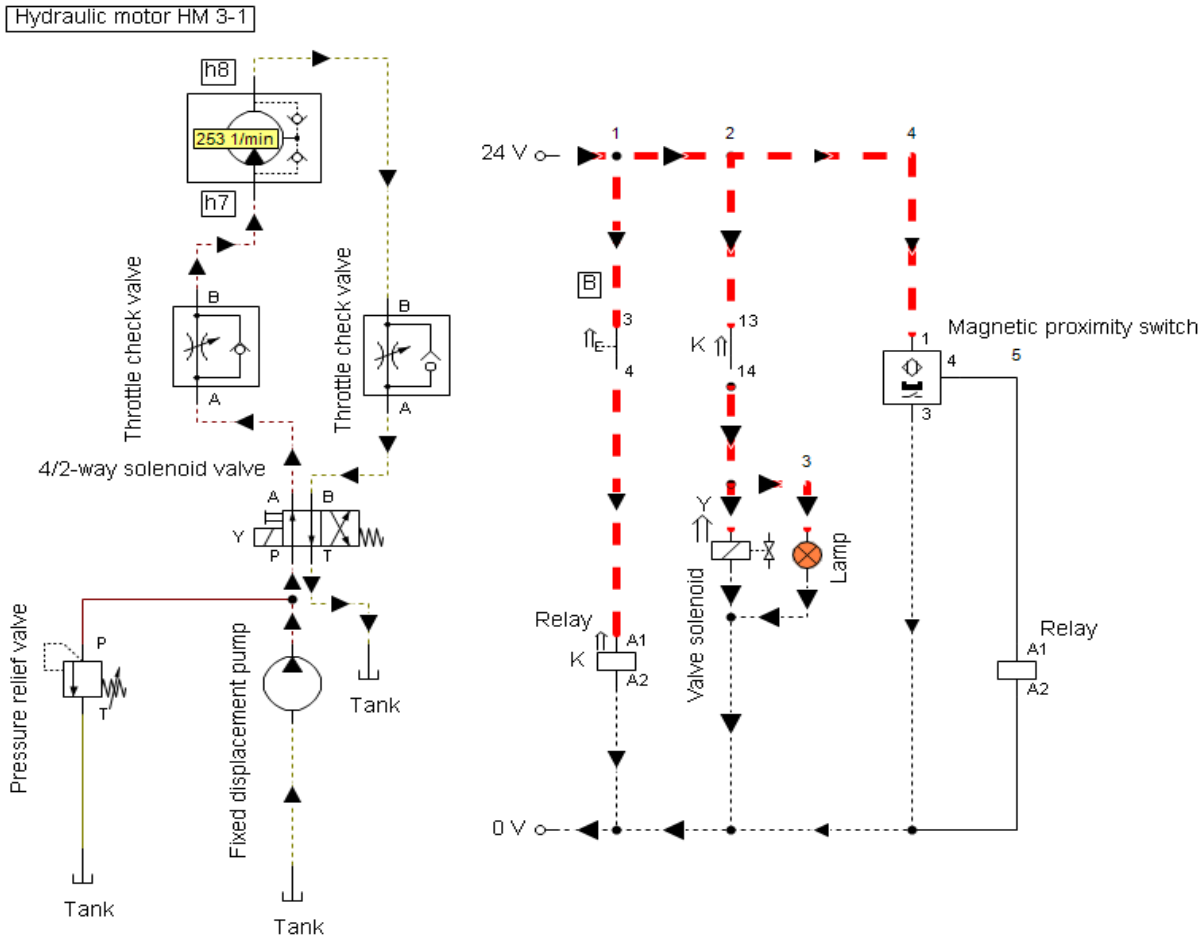

Fig. 11. Electro-hydraulic circuit with hydraulic motor HM (3-1). Simulation

At the end, when the operator stops pressing the button, then the lamp stops lighting up and output shaft rotates counterclockwise from point h8 to point h7.

3. Conclusions

Systems using hydraulic motors are a common choice for various engineering applications.
Nevertheless, the hydraulic motor installations form the basis for many industrial upgrades in the modern era.
The main advantages of hydraulic motors are: high torque, low output speed, simpler than piston engines, more durable than vane motors, do not pollute, low vibrations, easy to maintain, etc.
In stationary industrial applications, the following factors of hydraulic motors are more important: performance, durability and cost, than its size or position in the installation.
In order to choose hydraulic motors according to the objectives they have to fulfill, the specialists must consider the following characteristics: operating temperature, estimated life of the motor, contamination potential and type of control. Consequently, specialists are advised to contact the hydraulic motor manufacturers to discuss the requirements of their application.

References

[1] Matache, G., E. Maican, I. Pavel, R.I. Rădoi, and M.A. Hristea. "Applied research and experimental validation of a TULD industrial solution." *Hidraulica Magazine*, no. 3 (2017): 18-26.
[2] Galea, A., E. Francalanza, P.J. Farugia, and J.C. Borg. "Analysing product development working practices for enhancing innovation through collaboration and simulation." Paper presented at the International Design Conference – Design 2012, Dubrovnik, Croatia, May 21 - 24, 2012.
[3] Rădoi, R., I. Bălan, and I Duțu. "Repairing and testing of the hydraulic servo valves." *Hidraulica Magazine*, no. 3 (2013): 32-37.
[4] Scupi, A. A., M. Panaitescu, and F.V. Panaitescu. "Numerical simulation centrifugal pump." *Journal of Marine Technology and Environment (JMTE)* 1 (2023): 50-53. doi: 10.53464/JMTE.01.2023.08.
[5] Dumitrache, C.L., and D. Deleanu. "Water centrifugal pump, design and fluid flow analysis." *International Journal of Modern Manufacturing Technologies* 14, no. 3 (2022): 56-61.
[6] Predoi, M.V., A. Craifaleanu, M. Duțu (David), G.C. Ion, and C.C. Petre. "New techniques used for structural life time estimation using probabilistic techniques." *Romanian Journal of Acoustics and Vibration* 3, no. 2 (2006): 59-63.

Implications of Dedicated Environmental Information Systems in the Firiza Valley Area (Baia Mare, Romania) Characterization to Establish the Dynamics of Pollutant Transfer from Soil to Crop Plants

PhD stud. eng. **Marcela HRENIUC (SĂLIȘCAN)**[1], PhD eng. IT exp. **Bogdan-Vasile CIORUȚA**[1-3,*], MA stud. **Ioana-Elisabeta SABOU (CIORUȚA)**[2], Eng. IT exp. **Alexandru Leonard POP**[2,3], Assoc. Prof. PhD eng. **Mirela-Ana COMAN**[1,4]

[1] University of Agricultural Sciences and Veterinary Medicine from Cluj-Napoca, 3-5 Calea Mănăștur, 4000372, Cluj-Napoca, Romania

[2] Technical University of Cluj-Napoca - North University Centre of Baia Mare, Faculty of Letters, Department of Specialty with Psychopedagogical Profile, 76 Victoriei Str., 430083, Baia Mare, Romania

[3] Technical University of Cluj-Napoca - North University Centre of Baia Mare, Office of Informatics, 62A Victor Babeș Str., 430083, Baia Mare, Romania

[4] Technical University of Cluj-Napoca - North University Centre of Baia Mare, Faculty of Engineering - Department of Mineral Resources, Materials and Environmental Engineering, Victor Babeș 62A Street, 430083, Baia Mare, Romania

* bogdan.cioruta@staff.utcluj.ro

Abstract: *We start from the idea that environmental information systems (EISs) - developed under the aegis of environmental informatics (EI) - have been within the reach of specialists and practitioners for more than 3-4 decades, favoring the sustainable development of communities, by making and applying the best possible decisions. From the perspective of soil resource protection and sustainable land management, this paper proposes to analyze the implications of using such information systems in preliminary characterizing an area of specific interest. Through this approach, we aim to draw attention to the facilities we currently have at our disposal - through the mediation of technologies - that prove to be of real use, especially in the characterization and analysis at local, zonal, and regional levels of a site, to subsequently establish the dynamics of the transfer of pollutants from soil to plants. What we have noticed are the multiple possibilities of characterizing an area from the EISs perspective - that have emerged in the last 7-10 years - most of which are intended to emphasize and impose the (re)adaptation of research scenarios and the fight against environmental pollution, and to (re)define opportunities for community development based on sustainable principles. Consequently, it matters not only what we propose to do, but also what each of us can do, with the technology we have at hand; or, in this case, promoting EISs in applied research, in the pollution-affected field, we consider to be a niche of interest that deserves much more attention nowadays.*

Keywords: *Zonal characterization, soil resources protection, environmental information systems*

1. Introduction

According to the Sustainable Development Goals (SDGs) - issued under the auspices of the United Nations (UN) [1] - environmental protection, especially the protection of soil resources, regardless of the area of interest, is one of the greatest challenges of contemporary human society [2]. This challenge addresses politics and economics [3], technology [4-6], informatics, as well as advanced research associated with environmental informatics [7,8]. Under these conditions, the various problems related to environmental protection can be solved very easily by having at hand complex databases, which are also flexible and dynamic [9]. Therefore, public access to data is decisive in the substantiation and decision-making regarding the protection of soil resources, the sustainable management of land, and the risk situations associated with existing pollution at the level of contaminated sites.

In this context, figure 1 highlights how information technology relates to community areas of interest, to provide information, and knowledge that are extremely useful in managing the various problems that inevitably arise from human-environment interaction. The state and dynamics of the environment are described by developing and using biological, physical, chemical, geological, meteorological, and/or socio-economic data sets, that are time and space-dependent [3,7,10].

The processing of environmental data (e.g. *soil stress factors*) and its influence mechanisms are fundamental for any kind of environmental planning and preventive measures. Therefore, solving environmental problems is mainly a processing activity for a wide range of data and appropriate solutions [3,4], specific to each environmental factor [12]. However, solutions to environmental problems depend on and are influenced - to the greatest extent - by the quality of information (re)sources, as it is known that information is a critical factor in initiating political actions and changing attitudes towards the environment.

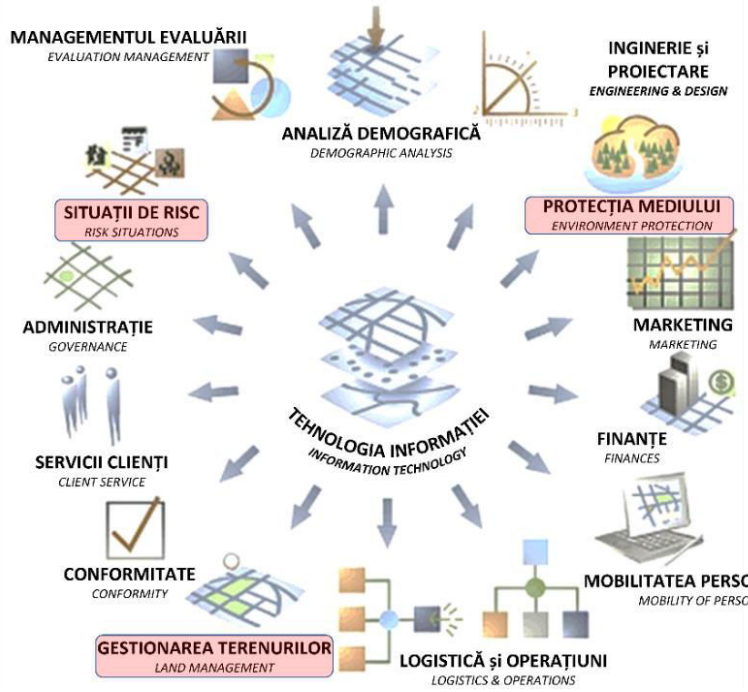

Fig. 1. Current implications of information technology in community activities of interest

Meanwhile, the use of information technology has become essential in the field of environmental protection and engineering, for providing the necessary information at the appropriate level of detail, completeness, accuracy, and speed. This information is equally important as a basis for decisions on actions in the field of environmental protection, as well as for acquiring knowledge in environmental research. Thus, in recent years, environmental information processing systems (EIPSs) have evolved from research and development systems to practical applications.
Currently, many of these systems already support environmental activities at industrial [13], governmental, and global levels [14,15]. At the same time, several trends have been reported regarding the relationship between information technology and the environment, if we refer to aspects such as environmental monitoring through remote sensing and combining global data flows, the policy of sharing and integrating ecological data within political and organizational boundaries, advanced model analysis techniques and industrial applications of environmental information processing [16,17]. However, we cannot fully state that the applications of information technology in the environmental field have often had a solid scientific basis since there has been no significant research oriented toward this topic. This continues to be, certainly, not only a matter related to computer science but also an interdisciplinary task in which several disciplines must be included and involved. On the other hand, regarding the processing of environmental data, this continues to represent a great challenge also for computer science methodologies and their applications, including in the case of dedicated mobile applications, which seem to be coming strongly and more and more visibly behind.
In the sense of the above, it is worth remembering that the application of new information and communication technologies to solve environmental problems began in the 1950s, with the first numerical models used for the management of water and soil resources. Applications followed for atmospheric dispersion models, socio-economic and resource planning models, models for renewable energy production, etc., all require a systematic interdisciplinary methodology [3,4,9].

Environmental data processing systems (EDPSs), including the EISs, play a special role in environmental decision-making, closely related to the demands of society in recent decades. At the same time, EISs constitute a new subfield of applied informatics, which comes up with specific methods and tools for investigating, avoiding, and/or minimizing environmental burdens and damages [2,4]. Later, Page and Rautenstrauch [14] define environmental informatics as a subdiscipline of applied informatics that deals with the development of methods, techniques, and tools for the analysis, support, and establishment of those information processing procedures that contribute to the investigation, avoidance, and minimization of environmental burdens and damages. Thus, for the first time, the emphasis is placed on the mediator role of this discipline, which analyzes real-world problems at length and (re) defines the requirements for environmental data processing, as shown in Figure 2.

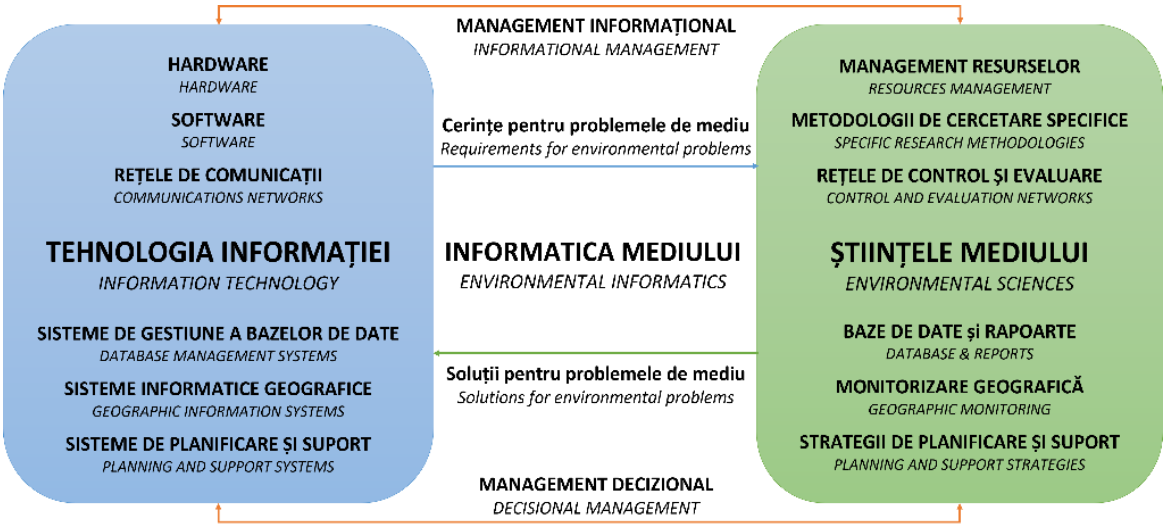

Fig. 2. Environmental Informatics as a bridge between Information Technology and Environmental Sciences

Since the emergence of Environmental Informatics (EI) in the period 1992-1996, EISs have constantly changed; the boundaries of EISs have expanded, so that industrial processes causing significant energy consumption and emissions have increasingly come into the spotlight. The focus has shifted from effects to causes, and implicitly from environmental impact to processes that can be modified to minimize it. For this reason, methods for simulating industrial production processes must be integrated with approaches to the analysis of information flows.

In these circumstances, we conclude, from the current field practice, that the conceptual models that underlie the definition of EI, respectively the integration of EISs in the community development strategy, start from the acquisition, processing, and use of environmental information and end with the support of decision-making. To explain the existing links between the information environment, society, and the environment, the entire process of acquiring and processing environmental data must be done starting from the ecological problem analysis scheme, with an emphasis on pressure-state response. The public has access to environmental information and can thus make the best decisions concerning the activities they carry out, especially by consulting specific learning communities; moreover, it can elegantly ensure the sustainable development of the community.

As for the impacts that may affect the soil, these can be managed in time and space. Through computational reasoning, mathematical modeling and simulation, fine-grained monitoring, etc., data on soil quality status can be understood and interpreted correctly, allowing for correct and efficient decision-making. Following the same work plan, after 2020, substantial progress has been made to achieve a broader appreciation of the soil's key role, according to the ecosystem services it provides. Science is advancing, with an improved understanding of the fundamental mechanisms that control the dynamics of the qualitative state of soil parameters, as well as in the measurement and modeling of changes, in response to environmental and management factors. As a result of this progress, entrepreneurial programs, and methods have been and are being developed that contribute to paving the way for a better inclusion of soil management in the decision-making process of farmers and livestock breeders.

2. Material and methods - the perspective addressed by current research

However, to move towards aggressive implementation of best land use and management practices to promote global soil health, a new soil information system, with global coverage and the capacity to evolve as science advances, is needed. While the data and many of the necessary tools, technologies, and collaborations exist, the information is often fragmented and its availability is limited. Better coordination, transparency, and accessibility of tools and data between specialists and land managers is needed.
In addition, to understand the specifics of the relationship between EISs users and specific learning communities, in Fig. 3 we have chosen to illustrate a virtual platform for quantifying the data model needed to form the core of a new soil information system. Starting from the left side of the diagram, key data sources are presented to inform and validate soil protection estimates. The usefulness of data from experiments, both in the field and over the long term, helps to formulate, parameterize, and validate predictive models of soil changes.

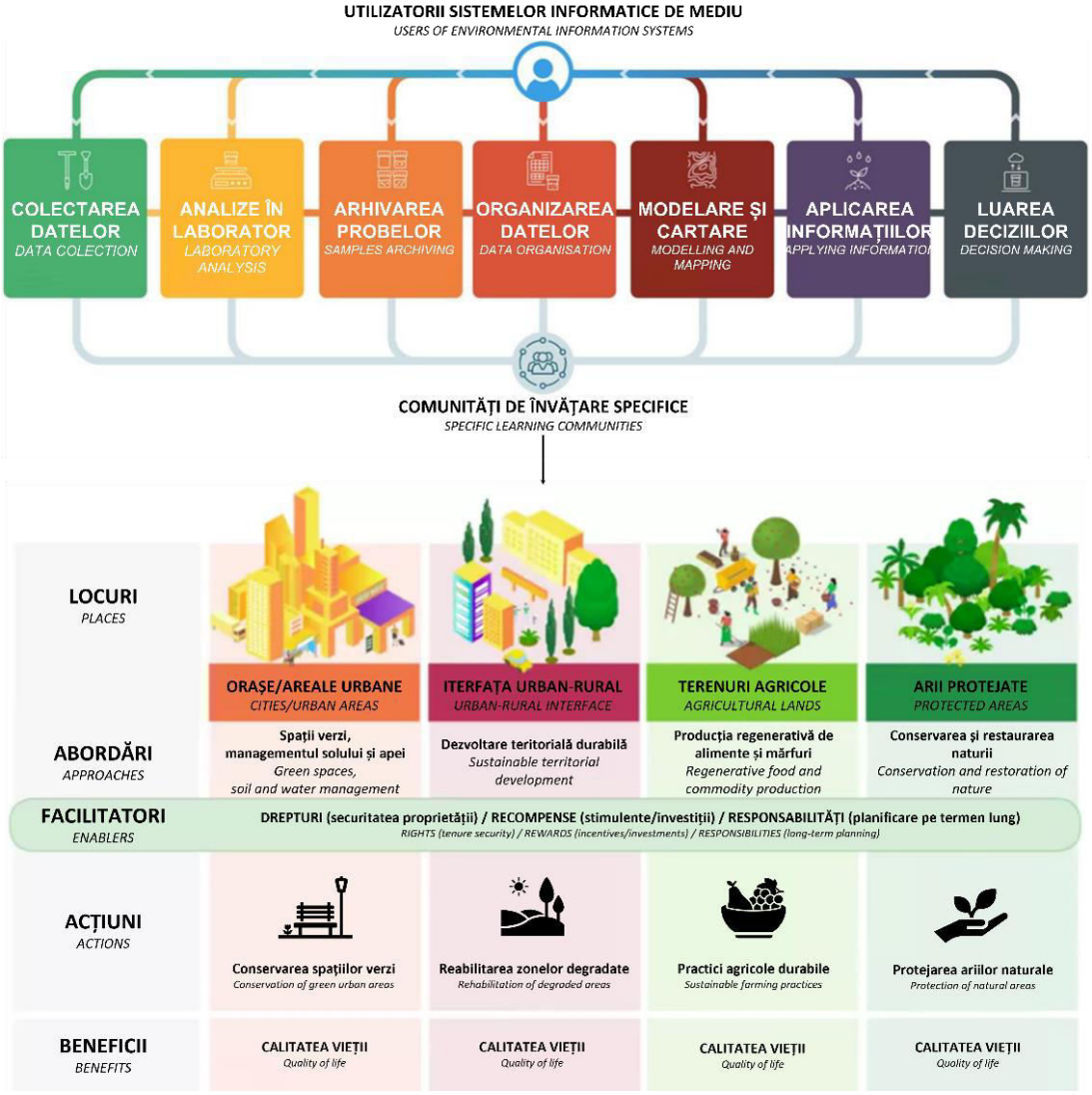

Fig. 3. Information flow from data collection to decision-making and consultation of specific learning communities

Soil monitoring networks can play a vital role in reducing the uncertainty of models provided by mobile applications. However, such monitoring networks are lacking in most countries and, where data exist, they are not easily accessible to the community. Developing data-sharing agreements could pave the way for a consolidated global soil monitoring network, the accessibility and usefulness of which could stimulate other interested entities to join this effort. Such a platform

would support and facilitate the use of innovative approaches, with a focus on the protection of soil resources and sustainable land use, with a focus on reducing CO_2 emissions from the atmosphere and sequestering carbon in the soil.

Model ensembles are driven by spatially generated and modeled datasets (see Fig. 4), including climate variables (e.g., *temperature*, *precipitation*, *solar radiation*), soil conditions (e.g., *soil texture*, *mineralogy*, *soil profile depth*, *topographic features*), and land use, as well as management data (e.g., *crop rotation*, *nutrient management*). Provided that the models used are generalizable over a sufficiently wide range of environmental conditions, the scale of inference for predicted variables is largely determined by the spatial resolution of the input data, which can be obtained both by remote sensing and by mobile applications directly in the field. Remote sensing, as well as mobile applications, offers the potential to provide low-cost, small-scale, and globally available data on land cover and crop species, as well as data on soil cultivation and irrigation practices, which can assist the user in making the right decisions.

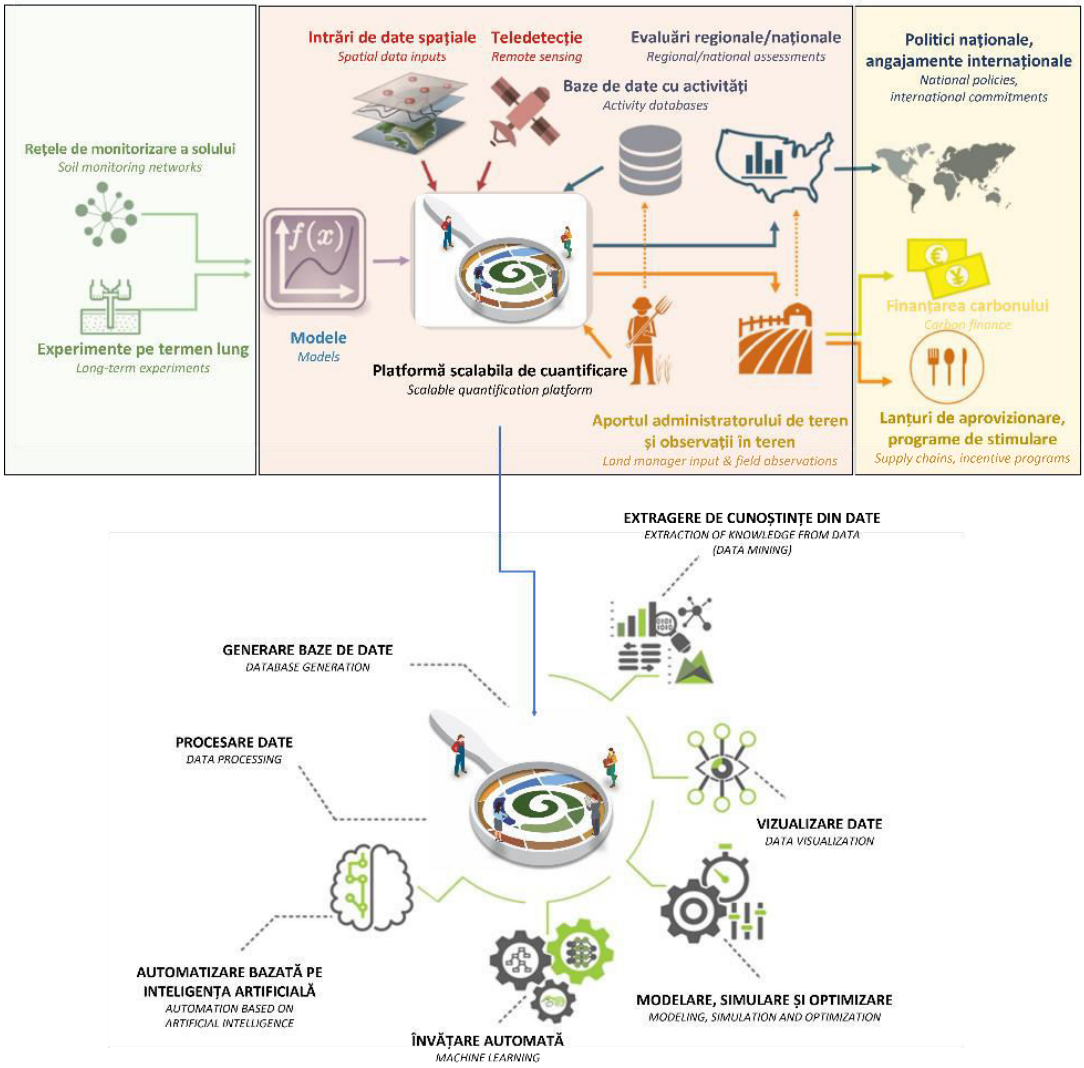

Fig. 4. The range of IT tools used to understand soil protection issues (after PAUSTIAN et. al, 2019)

Therefore, there is a need to test promising methods on a larger scale and then develop capabilities that can rapidly provide data on management practices at high spatial resolution, anywhere in the world. Dynamic models supported by experimental mobile applications based on spatially distributed soil, climate, and management data can support land managers' decisions. A scalable system, capable of country-level analysis, will be needed to support national policies and international agreements, to support sustainable supply chain initiatives and/or financing schemes that can incentivize farmers to adopt sustainable practices for land use and current technology use.

From the perspective of environmental engineering and protection specialists, it is well known that the assessment of the dynamics, specificity, and intensity of pollution in a given contaminated site is usually carried out by comparison with the natural background (reference) in adjacent areas - with values established according to the area and the existing geological formation - and with the alert threshold and intervention threshold values provided for in specific regulations.
A contaminated site, as defined by the European Commission reports, represents a confirmed and well-demarcated area that represents a potential risk to humans, animals, and the environment. The number of contaminated sites at the international and national levels has been high in the past and has continued to grow in many areas [18], where certain specific measures have not been considered and applied. At the international level, numerous studies and research have been carried out to find the best treatment methods, when preventing the contamination of a site has not been possible. Numerous methods, more or less viable from an economic and ecological point of view, have been considered. These methods include *thermal treatment*, *electrochemical treatment*, *bioremediation*, *dechlorination*, *thermal desorption*, *washing*, *solvent extraction*, etc. All these methods were applied according to the needs, taking into account various other factors.
For the present research, we established as the investigation perimeter an area in the Firiza Valley area, taking into account the fact that the geomorphological and climatic particularities of the area are relatively similar to those in the urban area of Baia Mare (Romania). In the reference area (Firiza Valley - Baia Mare, Romania), as well as globally, one of the most polluted resources is soil. This resource has been and is polluted as a result of industrial activities such as mining, but also the storage and use of associated products. Under these conditions, if certain hazardous substances are not used appropriately and subsequently not stored or eliminated as required by law, the soil can become contaminated, and people can be exposed to soil contaminants through various routes, especially from contaminated soil to crop plants.

3. Results and discussions. Firiza Valley - a brief characterization of the area via EISs

The Baia Mare administrative-territorial unit includes the upper basin of the Firiza Valley, on the right slope, from Valea Pistruia-Blidar upstream, and on the left slope, from Valea Jidovoaia upstream. The highest peaks are located on the ridges that delimit the basin to the west, north, and then east: Calamari peak (1141 m), Ogorohii peak - Dealul Miculi (1191 m), Rotunda peak (1240 m), Stânilor peak (1152 m), Pleşca Mare peak (1294 m), Breze peak (1254 m) and Igniş peak (1307 m).

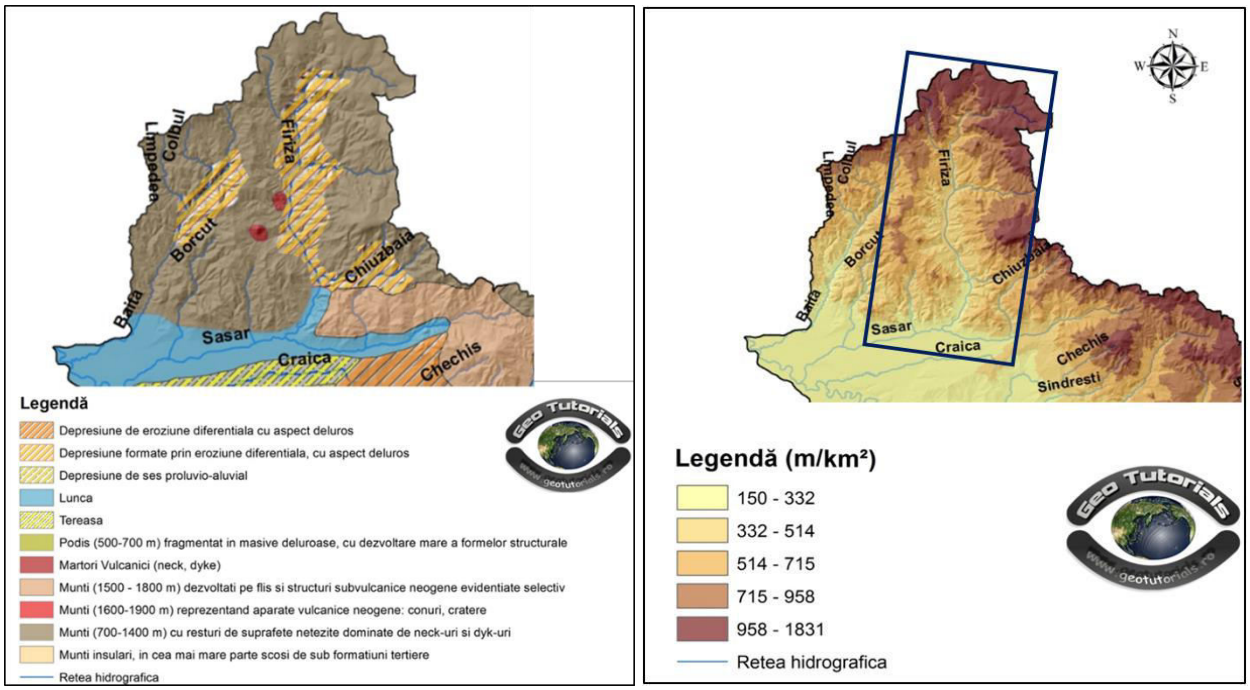

Fig. 5. Geomorphological map of the Firiza Valley (Baia Mare, Romania)

Two depression basins are outlined in the Firiza Valley: Blidar and Firiza (see Fig. 5). The two depression basins have an eruptive geological substrate and were formed by erosion, at the confluence of the Firiza with the most important tributaries Pistruia and Valea Vrivei at Blidari, Valea Neagră, Valea Roşie, Valea Seicina at Firiza. Moreover, in the existing geomorphological complex of the Firiza Valley, slopes with different inclinations and exposures dominate, In small areas other relief forms are also encountered, such as meadows, plateaus, ridges, and glacis, all of which determine changes in the climatic and edaphic regime and the distribution of vegetation.
The numerous streams (the vast majority of them tributaries of the Firiza River) flowing in a north-south direction, small depressions (Chiuzbaia, Firiza, Blidari) as well as marginal depressions that arose through the regressive erosion of rivers with a base level in the Baia Mare Depression such as Ferneziu, strongly fragment the southern flank of these mountains. In terms of altitude, the base level of the Firiza Valley micro-depression is between 150-715 m, with the relief energy gradually decreasing to 150 m within the meadows. Under these conditions, the declivity of the relief represents a morphometric indicator, frequently used in the complex characterization of the relief.

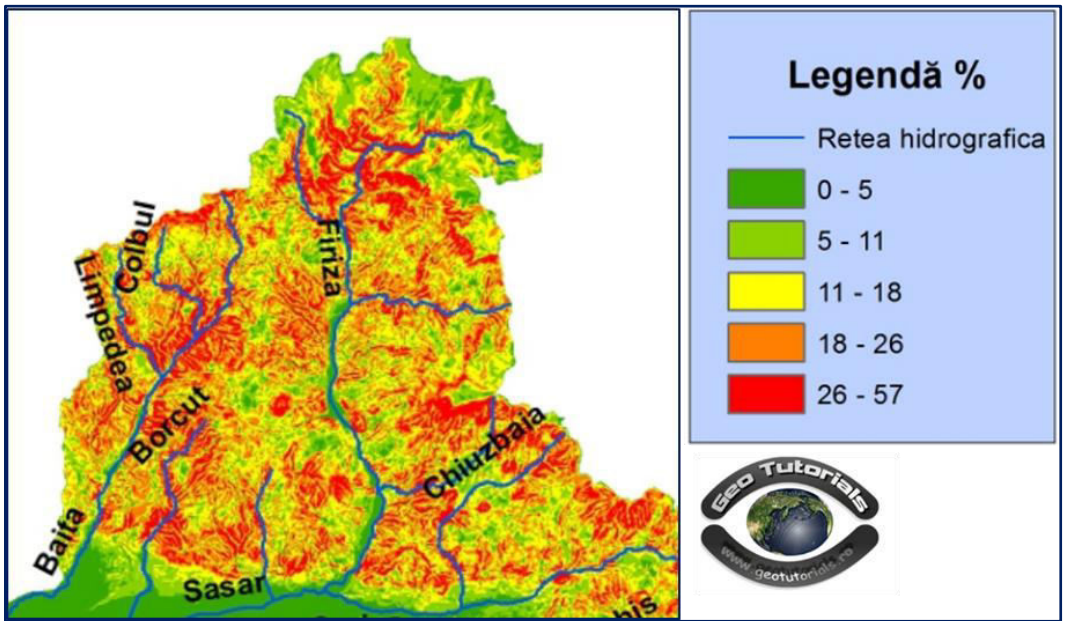

Fig. 6. Slope map of the Firiza Valley (Baia Mare, Romania)

The slope of the relief conditions, together with geological (petrography and structure), climatic, hydrological, biopedogeographic, and anthropogenic factors, the genesis, dynamics, intensity, and type of denudation processes. In the Firiza Valley basin, the high values of slopes between 26% and 57% are given by the slopes of the mountain massifs (see Fig. 6), this fact makes the drainage of the tributaries take place from N to S. The average values between 5% and 26% are found in depressions, hills and peaks and the lowest values are recorded in the river meadow.
The Firiza River basin is the most important tributary of the Săsar, with a river basin that drains a significant part of the mountainous area of the Baia Mare administrative-territorial unit. The Firiza River basin has an area of 168.6 km^2 and a length of 28 km, the springs being located at an altitude of 1050-1070 m. The average altitude (744 m) is almost 100 m higher than that of the Săsar river basin upstream of the confluence with the Firiza, and the average slope is 10 m higher.
On the Firiza river, at approx. 10 km away from the city center, the Strâmtori dam (52 m high) was built, creating a reservoir with an area of 110 ha, which represents the only source of water supply for the Municipality of Baia Mare. Taking into account the characteristics of the Firiza hydrographic basin upstream of the lake, it plays a decisive role in protecting Baia Mare against floods. Construction works took place between 1961 and 1964, and in 1964 the lake was put into operation. Until now, the Firiza Valley has not been the subject of detailed topoclimatic research, with studies focusing on the design and construction of tall dispersion chimneys on the structure's resistance to maximum wind force and on compliance with the maximum permissible concentrations of pollutants in the ambient air.

The climatic characteristics in the Firiza Valley area are approximately the same as those in the Baia Mare area [19], thus we can state that:

- The particularities of the thermal regime in the Firiza Valley micro-depression are also reflected in the distribution of days with different thermal characteristics, which have an obvious altitudinal zonality, with a relatively large number of frost-free days (on average over 183-185 days, maximum 227); rarely, late spring frosts lead to the thawing of seedlings that started vegetation earlier, of newly formed vines (e.g., for beech and maple) or walnut, cherry and ash leaves;
- The relative humidity of the air (by combining water vapor with atmospheric precipitation) gives the climate - through its high values, especially in the spring months (87-88%) - the character of "humid", creating the humidity environment indispensable for life (see Fig. 7);
- cloudiness - a reliable indicator of the thermodynamic processes in their area of existence and of the precipitation - in some places more difficult to notice, is in direct correlation with the heavy (background) precipitation and with the low wind intensities, moreover, the maximum for atmospheric calm and fog is also recorded;
- atmospheric precipitation presents a great variability in time and space (in terms of frequency, intensity, and duration), the highest values are recorded on the southern slopes of the Oaş-Gutâi-Ţibleş mountain range (873.0 mm at Baia Mare);
- data regarding the duration of days of the ground covered with snow show us that the first snowfalls usually fall at the end of November, while the last snowfalls are delayed, being recorded at the end of April, or even in mid-May (18 cm in the Firiza valley, compared to that from the outside of the depression);

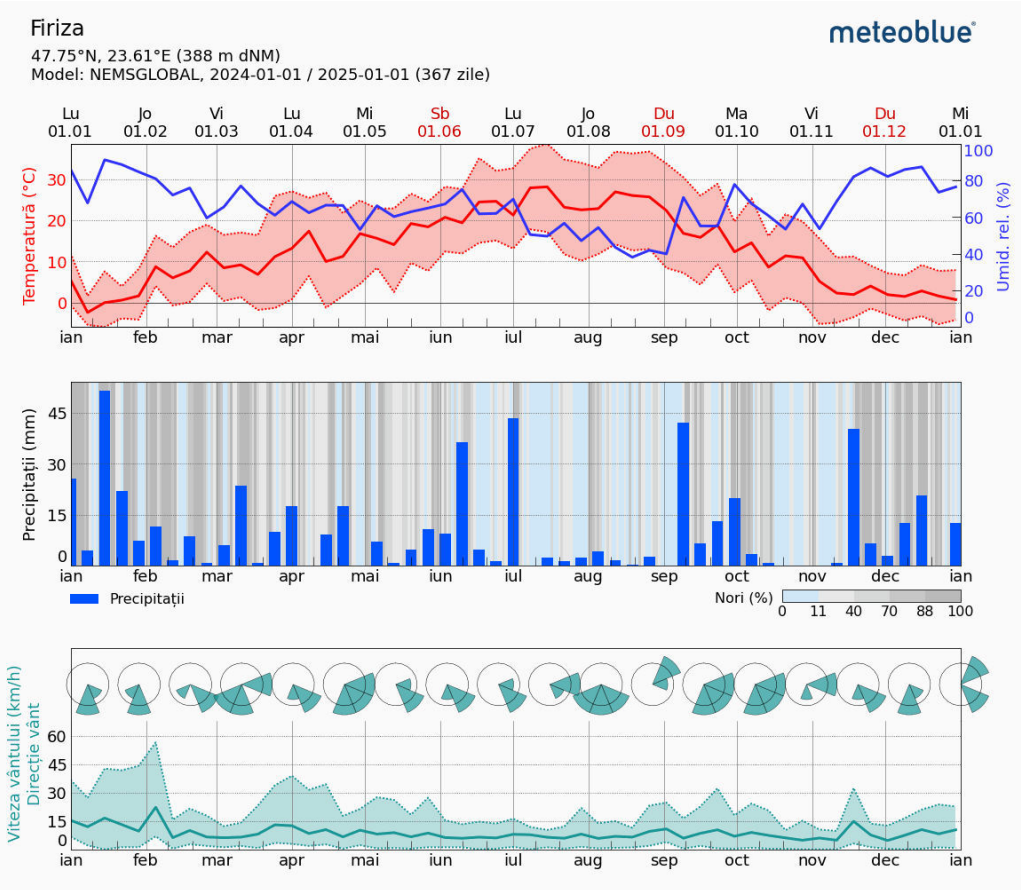

Fig. 7. Meteorological archive containing data on temperature variation, relative humidity, precipitation, cloudiness, wind speed, and direction for Firiza Valley areal, 2024 (www.meteoblue.com) [20]

- The atmospheric calm has an annual average value of 51.2%, so the area is generally weakly windy, while the maximum is recorded in winter (61.9% in January), and the minimum in spring (41.1% in April);

- The annual average wind speeds are low (2.2-3.6 m/s), and the direction in which the wind has minimum values is south (1.8 m/s in January and February), while the directions in which the wind has maximum values are west and northwest (up to 4.5 m/s); these low values associated with the values of atmospheric calm show that in the reference area, the natural dispersal capacity is low.

Regarding the surplus and deficit of soil water, due to the large amounts of precipitation in the Firiza Valley area, there is no deficit of soil water, the soil water regime being alternating percolative in the depressional plain and deep percolative in the hill and pre-mountain areas. In terms of the water regime, the soils are favorable for the development of forest vegetation.

The main types of soils in the researched area are visibly linked and conditioned by the two large relief units, namely the Gutâi Mountains and the Baia Mare Depression. These are presented - under the influence of the main pedoclimatic factors - in two large categories, namely:

- soils of mountain areas - appear on the southern slopes of the Gutâi Mountains and have as their main characteristic the presence of the skeleton and the small thickness of the soil profile; this category includes: undeveloped soils (lithosols) formed on consolidated rocks, andosols in association with brown podzolic soils formed on volcanic rocks, brown-acid soils formed on andesitic volcanic rocks, and eroded brown (eubasic) soils and regosols.
- soils of depression areas - occur in the Baia Mare urban area and on the hills located south of it; the main types of soils in this category are: pseudogleyed and pseudogleyed podzolic soils formed on slightly sloping, poorly drained lands, brown clayey-iluvial soils, the type of brown soils (including podzolites), brown podzolic soils and eroded brown podzolic soils, and amphigleyic podzolic and alluvial soils, along with other soils with a visible and pronounced anthropic character.

Moreover, from a pedological point of view, in the experimental perimeters of the targeted area (Firiza Valley), we encountered representative soils from the luvisols and hydrosols classes, whose use was predominantly agricultural (with and without current crops and/or plowing).

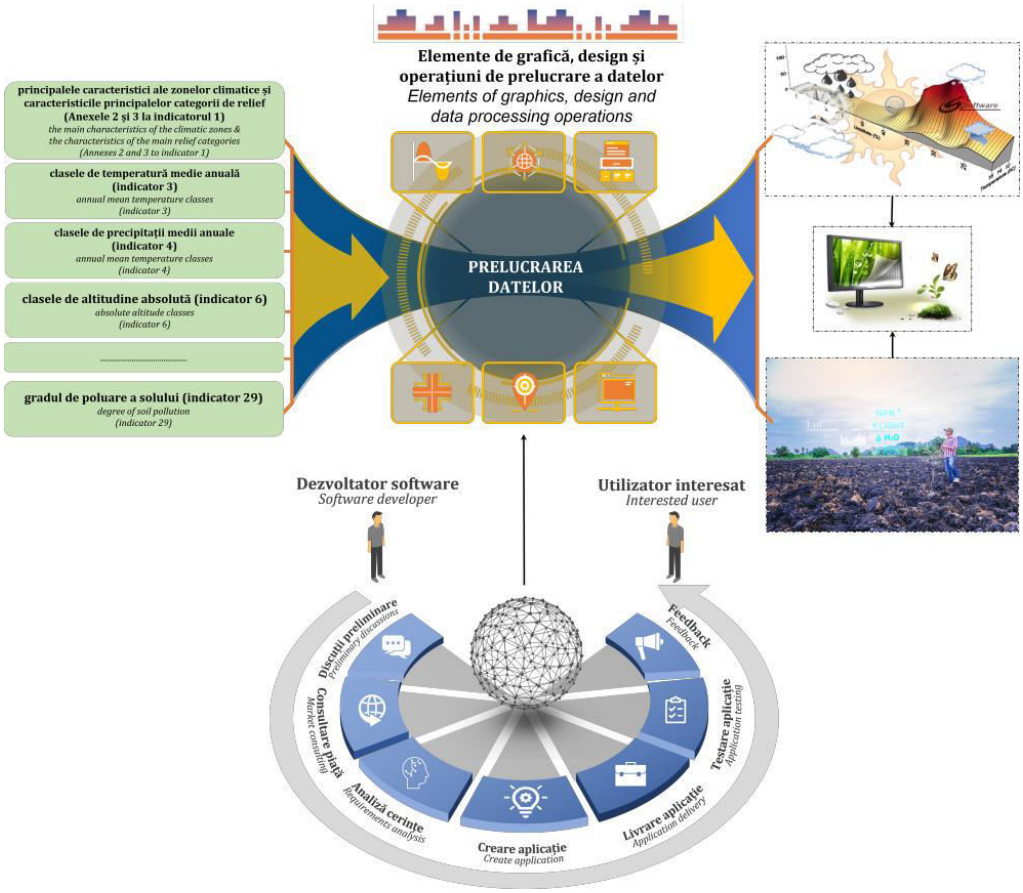

Fig. 8. Selection of eco-pedological indicators as a defining element in the characterization of an area of interest through the facilities offered by the mobile dedicated EISs used

At the same time, it is worth mentioning that in the respective locations, all the characteristics that we found at the level of thematic maps (e.g., relief, climate, spontaneous vegetation, land use) via mobile dedicated EISs (Fig. 8) are fully met, which only confirms that the situation in the reports and maps corresponds to reality. Regarding the current state of knowledge of soil quality and implicitly of current land use, to establish the dynamics of the transfer of pollutants from the soil to crop plants (for inhabited areas), by using mobile applications dedicated to soil protection, it is noteworthy, according to TOOR et al. (2021), an emphasis on the use of technology after 2020, in combination with high-throughput analysis methods (Fig. 9) and new types of analyses based on precision sensors.

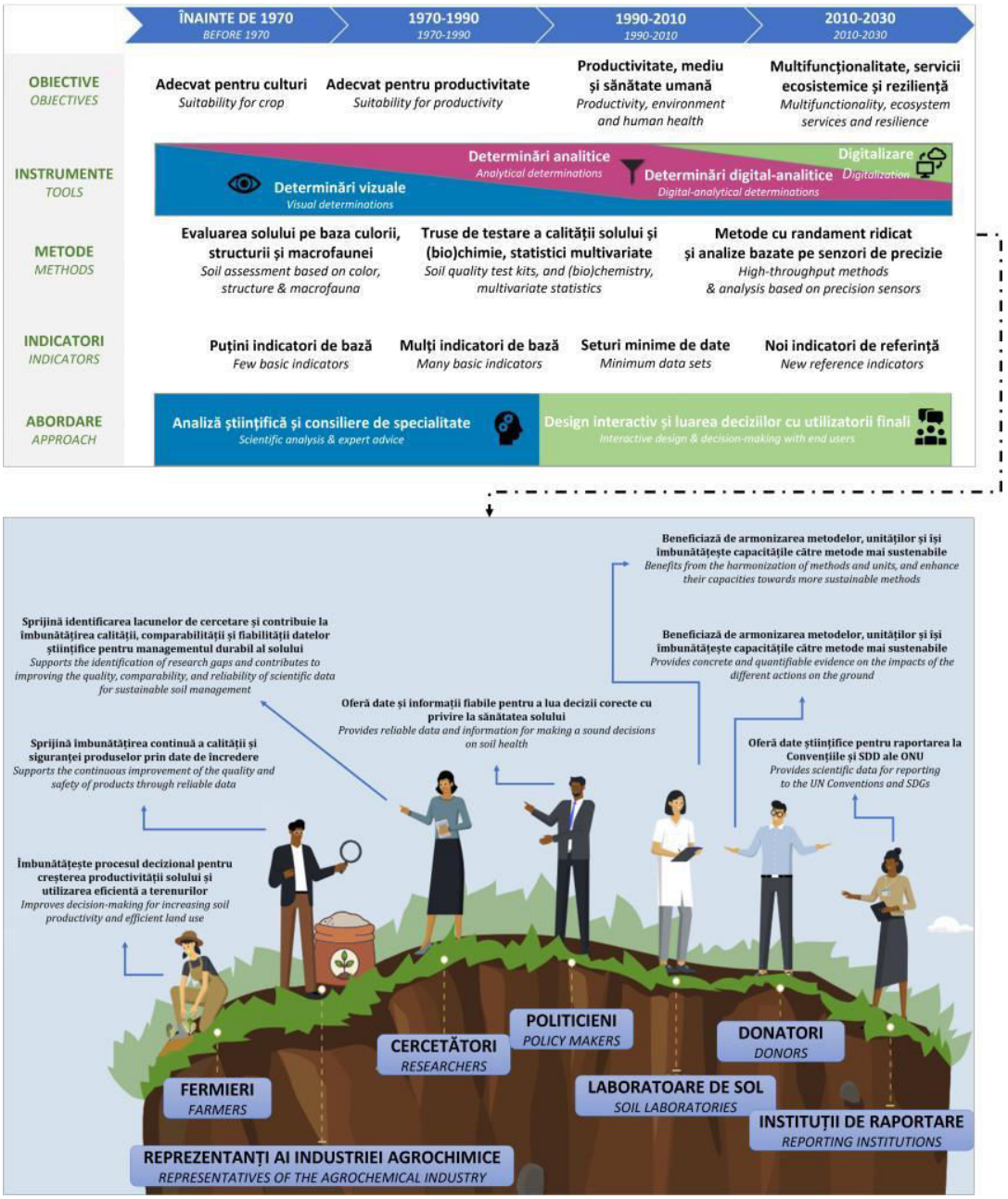

Fig. 9. Current status of the use of modern technologies in soil protection, including for the reference area - Firiza Valley [21]

In the same context, figure 7 shows a gradual shift from objectives that consider soil as suitable for crops (before 1970) and productivity (1970-1990) to those that emphasize soil multifunctionality and ecosystem services. At the same time, it is also noted the need to approach soil protection with new reference indicators that can support the effort made by farmers, researchers,

representatives of various institutions with concerns in the field, etc., who increasingly use digital monitoring and control tools. The use of mobile applications dedicated exclusively to the protection of soil resources has as an extension the generation of empirical models, reports, and maps, the aim is to ensure that authorities, the business environment, and the interested public have access to relevant data and information, approach that is synthetically represented in Fig. 10.

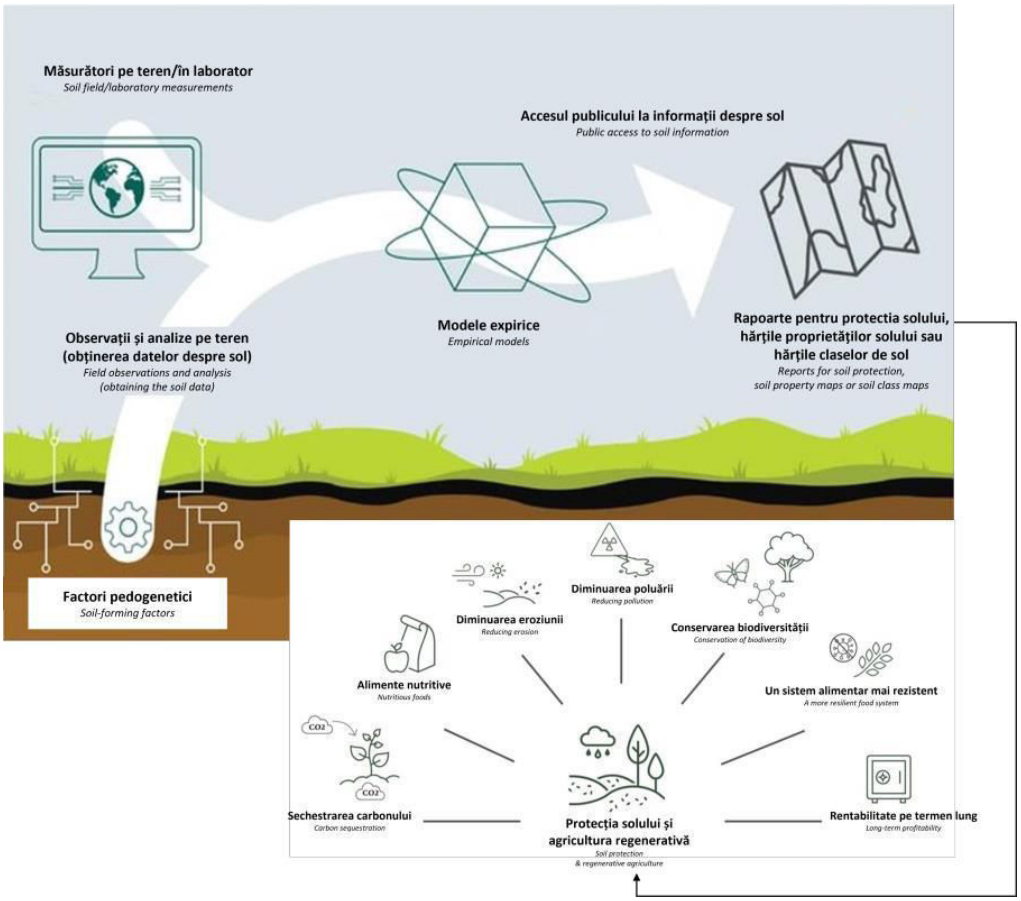

Fig. 10. Soil protection about the 7 benefits of regenerative agriculture

Such an approach also has implications for regenerative and precision agriculture, where we find a significant series of benefits. Starting with carbon sequestration and the provision of nutritious and good quality food, regenerative agriculture as a result of soil protection leads to biodiversity conservation and, implicitly, to long-term economic profitability.

4. Conclusions, perspectives, and proposals

Sustainable development as a concept seeks and tries to find a stable theoretical framework for decision-making in any situation where a human-environment relationship is found, whether it is the environment, the economic environment, or the social environment. Although initially sustainable development was intended to be a solution to the ecological crisis caused by the intense industrial exploitation of resources and the continuous degradation of the environment and sought to preserve the quality of the environment, currently the concept has expanded to the quality of life in its complexity, also from an economic and social perspective.
Soil monitoring and protection - especially in areas where communities have carried out various activities with a pronounced polluting nature over time - as well as field activities carried out by specialists or personnel with concerns in the field, are elements that require an integrated approach, from which the mobile technological component cannot be missing. At the same time, the incursion of these approaches (especially in the preliminary research activity, in the field, for a reference area, such as the one considered) must be carried out with equipment that allows more efficient control in the acquisition, processing, storage/saving, and dissemination of data.

References

[1] ***. "Sustainable Development Goals." European Commission, 2023. Accessed November 10, 2023. https://commission.europa.eu/strategy-and-policy/sustainable-development-goals_ro.
[2] Coman, M.A., and B.V. Cioruța. *From Human-Environment Interaction to Environmental Informatics / De la interacțiunea om-mediu la informatica mediului*. Cluj-Napoca, AcademicPres Publishing House, 2021.
[3] Gunter, O. *Environmental Information Systems*. Springer, 1988.
[4] Avouris, N.M., and B. Page. *Environmental Informatics: Methodology and Applications of Environmental Information Processing*. Dordrecht, Boston, Kluwer Academic Press, 1995.
[5] Hilty, L.M., B. Page, F.J. Radermacher, and W.F. Riekert. *Environmental Informatics as a New Discipline of Applied Computer Science*, 10.1007/978-94-017-1443-3_1. In: Avouris N.M., Page B., *Environmental Informatics: Methodology and Applications of Environmental Information Processing*. 10.1007/978-94-017-1443-3, pg. 1-11, 1995.
[6] Page, B. *Environmental Informatics - towards a new discipline in applied computer science for environmental protection and research*, In: Denzer R., Schimak G., Russell D., *Proceedings of the International Symposium on Environmental Software Systems*, Springer-Science+Business Media Dordrecht, pg. 3-21, 1996.
[7] Haklay, M. *From environmental information systems to environmental informatics: evolution and meaning*. Working paper. CASA Working Papers (7). Centre for Advanced Spatial Analysis (UCL), London, UK, 1999.
[8] Avouris, N.M. "Human interaction with environmental information systems." *Interdisciplinary Environmental Review* 3, no. 1 (2001): 134-144. 10.1504/IER.2001.053871.
[9] Hilty, L.M. *History and Definition of Environmental Informatics*, In: Wohlgemuth V., Voigt K., Pillmann W., Umweltinformatik - Einblick in drei Jahrzehnte der Entwicklung einer Wissenschaftsdisziplin. pg. 13-19. Shaker Verlag, 2014.
[10] Cioruța, B.V., and M.A. Coman. "The evolution, definition and role of Environmental Information Systems in the development of environmental protection strategies / Evoluția, definirea și rolul Sistemelor Informatice de Mediu în dezvoltarea strategiilor pentru protecția mediului." *Journal of Environmental Research and Protection*, no. 27 (2011): 11-14.
[11] Cioruța, B.V., and M.A. Coman. "Foray into modern scientific research of the environment. From Environmental Information Systems to Environmental Informatics / Incursiune în cercetarea științifică modernă a mediului înconjurător. De la Sistemele Informatice de Mediu la Informatica Mediului." *Journal of Environmental Research and Protection*, no. 29 (2011): 17-20.
[12] Hilty, L.M., and B. Page. "Information technology and renewable energy - Modelling, simulation, decision support, and environmental assessment." *Environmental Impact Assessment Review* 52 (2015). 10.1016/j.eiar.2014.10.005.
[13] Radermacher, F., W.F. Riekert, B. Page, and L.M. Hilty. "Trends in Environmental Information Processing." In: *Proceedings of the IFIP Congress 94* – vol. 2, 597-604, 1994.
[14] Page, B., and C. Rautenstrauch. *Environmental Informatics - Methods, Tools, and Applications in Environmental Information Processing*. 10.4018/9781930708020.ch001. In: *Environmental Information Systems in Industry and Public Administration*, 2001.
[15] Page, B., V. Wohlgemuth, and U. Kiekheben. "Review of Environmental Informatics Education in Germany and selected European Universities." Paper presented at EnviroInfo 2009 - 23rd International Conference on Informatics for Environmental Protection, vol. 2, pp. 63-69, 2009.
[16] Page, B., and K. Voigt. "Recent history and development of environmental information systems and databases in Germany." *Online Information Review* 27, no. 1 (2003): 37-50. 10.1108/14684520310462554.
[17] Hilty, L.M., B. Page, and J. Hrebicek. "Environmental Informatics." *Environmental Modelling and Software* 21, no. 11 (2006): 1517-1518. 10.1016/j.envsoft.2006.05.016.
[18] European Environment Agency. "Progress in management of contaminated sites". January 17, 2019. Accessed November 3, 2024. www.eea.europa.eu/data-and-maps/indicators/progress-in-management-of-contaminatedsites-3/assessment.
[19] Coman, M. *Baia Mare Depression - environmental protection from a sustainable development perspective* / *Depresiunea Baia Mare - protecția mediului din perspectiva dezvoltării durabile*. Cluj-Napoca, Risoprint Publishing House, 2006.
[20] Cioruța, B.V., and M.A Coman. "Definition, role, and functions of soil related to the Knowledge Society and the Someș-Tisa hydrographic area (Romania)." *Sustainability* 14, no. 14 (2022): 8688.
[21] Toor, G.S., Y.Y. Yang, S. Das, S. Dorsey, and G. Felton. "Soil health in agricultural ecosystems: Current status and future perspectives." *Advances in Agronomy* 168 (2021): 157-201.

Hydrological and Land Use Changes in the Bajo Balsas River Basin: Impacts on Water Storage at El Infiernillo Dam

M.Eng. **Eduardo JUAN-DIEGO**[1], Dr. **Maritza Liliana ARGANIS-JUÁREZ**[1,2,*], M.Eng. **Margarita PRECIADO-JIMÉNEZ**[3,*], Dr. **Alejandro MENDOZA-RESÉNDIZ**[1], Dr. **Rodrigo ROBLERO-HIDALGO**[3]

[1] Universidad Nacional Autónoma de México, Instituto de Ingeniería

[2] Universidad Nacional Autónoma de México, Facultad de Ingeniería

[3] Instituto Mexicano de Tecnología del Agua

* MArganisJ@iingen.unam.mx, preciado@tlaloc.imta.mx

Abstract: *This paper analyzes trends in water storage at El Infiernillo Dam in Michoacán, Mexico, and its relationship with climate and land use factors. Using historical data from 1994 to 2024, the research identifies a significant decline in the dam's storage volume, particularly after 2002, attributed to increased evaporation and water withdrawals for agricultural and urban use. Land use changes in the Bajo Balsas River basin, including a 17.25% increase in irrigated agriculture and a 9,323% human settlements expansion, have altered hydrological dynamics, it reducing infiltration and increasing surface runoff; natural vegetation loss such as oak and pine forests, further exacerbates water scarcity. Findings highlight urgent need for sustainable water management strategies, including soil conservation, improved water use efficiency, and climate change adaptation measures, to address the growing water crisis at this region.*

Keywords: *Water storage, land use change, climate change, hydrological dynamics, water scarcity*

1. Introduction

Reservoirs' problem in water availability terms is an issue of great relevance worldwide. Dams are critical infrastructures for water storage and management, but they face significant challenges due to factors such as climate change, population growth, and water resources overexploitation [1-2]. In Mexico, this situation is particularly worrying, as many dams operate below their optimal capacity due to prolonged droughts and inadequate water resource management [3-4].

Globally, new dams' construction and existing expansion ones also pose environmental and social challenges. Zarfl et al. (2015) [5] highlight that the boom in the construction of hydroelectric dams can have significant impacts on aquatic ecosystems and local communities. In addition; Grill et al. (2019) [6] point out that rivers fragmentation due to dams can affect the biodiversity and river ecosystems connectivity.

Sustainable dam management is essential to balance human development needs with environmental conservation. Winemiller et al. (2016) [7] suggest that it is possible to find a balance between hydropower generation and biodiversity protection in regions such as the Amazon, Congo, and Mekong. Poff et al. (2016) [8] propose the use of ecological engineering approaches to manage water sustainably under conditions of future uncertainty.

The availability of accurate and up-to-date data on dams and their impacts is crucial for effective management. Lehner et al. (2011) [9] and the International Commission on Large Dams (ICOLD) database [10] provide detailed information on the characteristics of dams and reservoirs globally, which is critical for planning and informed decision-making.

In this study, the behavior of the average daily inflow volumes of the El Infiernillo dam, Mich., was analyzed, with a parallel review of the main variables involved in the operation of the reservoir as well as taking into account the changes in the type of soil that have been reported to have been experienced by analyzed basin; for this purpose, methods were used to analyze independence, homogeneity and variables trend, in addition to quantifying change rates in land use in order to have a basis for making results interpretations.

2. Study site

The Bajo Balsas River Hydrological Basin extends from hydrometric stations La Caimanera, La Pastoría, Los Pinzanes and Los Panches to its mouth into Pacific Ocean, located at Lázaro Cárdenas, Michoacán, situated at coordinates 100° 31' 12" west longitude and 18° 16' 48" north latitude. This basin has a 13,949.96 Km area ² and is delimited by various regions and hydrological basins:

- To north: Cupatitzio and Tacámbaro river basins.
- To south: Hydrological Region 19, Costa Grande de Guerrero.
- To west: Tepalcatepec River Basin.
- To east: Middle Balsas River Basin.

Within this basin is Adolfo López Mateos dam, better known as El Infiernillo (Figure 1). This artificial reservoir is located in the municipalities of Arteaga, La Huacana and Churumuco in Michoacán, as well as in Coahuayutla, Guerrero. It was built by the Hydraulic Resources Ministry between August 1962 and December 1963, entering into operation on June 15, 1964. Its main purpose is electricity generation, in addition to use for irrigation and flooding control.
This dam has a rockfill curtain with a waterproof heart, with a height of 149 m and a length of 350 m at crown. Its powerhouse, located in an underground enclosure, is 21 m wide, 128 m long and 40 m high. On the left bank is the intake work, consisting of three pressure pipes of 8.90 m in diameter, with a capacity to conduct 194 m³/s per pipe. In addition, surplus work has three 13 m diameter spillways, capable of discharging 13,800 m³/s. This hydroelectric plant is located in one of the greatest seismic areas risks in the country, so its structures are continuously evaluated to monitor its dynamic behavior. Reservoir curtain is located 102 Km southeast of Apatzingán de la Constitución and 127.5 Km Uruapan southeast, in Michoacán state [11-14].

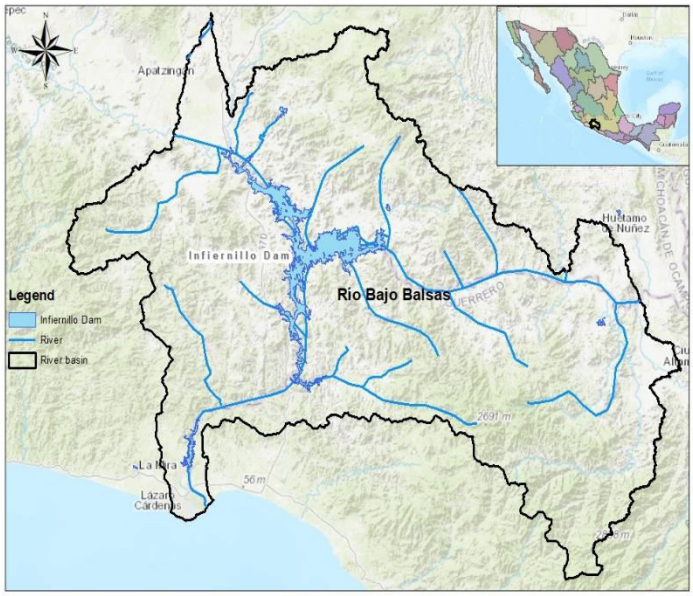

Fig. 1. Infiernillo Dam, Mich. Mexico, Location on Bajo Balsas River Basin

El Infiernillo Dam operation faces several challenges. One of the most important problems is water levels management during rainy seasons. In September 2024, controlled extraction from dam increased due to substantial rainfall, leading to a significant level increase for Balsas River (National Water Commission, 2024). These maneuvers are necessary to ensure dam safety and prevent flooding into surrounding areas [11], [15].
In recent years, Mexico has faced a significant water crisis. Average annual water per capita availability has decreased from 10,000 cubic meters from 1960 to 4,000 in 2012, and is estimated to fall below 3,000 cubic meters by 2030 [3]. In February 2024, the country's main dams were at 50% capacity, reflecting a decrease compared to previous years (Mexican Institute for

Competitiveness, 2024). This situation is due to prolonged droughts and combination water resources overexploitation [4].

3. Methodology

Main concepts and procedures that were considered in this analysis are described below.

Reservoir operation
Fundamental simulation equation for dam operation basin is based on continuity principle, which states that volume stored change in the basin during a time interval is equal to the difference between inputs volume and outputs volume during that same interval. This equation is expressed as follows:

$$\Delta V = I - O \tag{1}$$

Where:

- ΔV is the change in the volume stored at reservoir (hm³).
- I is inputs volume to reservoir (hm³).
- O it is outlets volume from reservoir (hm³) [16].

Variables involved in this equation are following:
Inflow Volume into reservoir (I): Inflows by own basin: surface runoff Volumes generated in the uncontrolled basin that discharges directly to dam. Transfer inflows from other basins: volumes from discharges from dams located upstream or in other basins. Inflows due to direct rain on the basin: volume of rain that falls directly on the free surface of the basin [17].
Outflow Volume (O): volume infiltrated into the reservoir, that is water that infiltrates the soil from the reservoir, spilled volume: water that overflows from the reservoir, volume extracted to meet demand: water used for human consumption, irrigation, power generation, etc.; volume evaporated directly from the reservoir: water that evaporates from the surface of the reservoir [14].
Continuity equation is essential for the design and dams' operation, as it allows modelling and predicting to behavior of water storage based on inputs and outputs, ensuring efficient and sustainable management of water resources [16].

Linear regression to identify trends
Linear regression is a fundamental statistical technique used to model the relationship between a dependent variable and one or more independent variables. In the context of data series analysis, linear regression is used to identify and quantify trends over time. The general equation of simple linear regression is expressed as:

$$y = bo + b1x + e \tag{2}$$

Where:
y is dependent variable (for example, the flow of a river at a given time). X is independent variable (e.g., time), $b0$ is regression intercept, which represents the value of Y when X=0, $b1$ is regression slope of the, which indicates the change in Y per unit change in X.
e is error term, which represents variability in Y not explained by X (Montgomery, Peck, & Vining, 2012) [18].
Linear regression is used to identify trends in data series as follows:

1. Data collection: historical data on interest variable (e.g., water levels, flows, precipitation) are collected over time.
2. Data exploration: data is analyzed to understand its characteristics and relationships, and visualized using scatter plots.
3. Regression model fit: A linear regression model is fitted to data using least squares methods, which minimize squares sum differences between the observed values and predicted values by the model [19].
4. Model evaluation: fit goodness from model is evaluated using determination coefficient (R2R2) and statistical significance tests for the regression coefficients.

5. Results Interpretation: the regression slope ($b1$) is interpreted to determine trend direction and magnitude. Positive slope indicates an increasing trend, while a negative slope indicates a decreasing trend [20].

Linear regression is a powerful tool for trend analysis in data series, allowing engineers and scientists to quantify changes over time and make informed predictions about the future interest variables behavior [18].

Homogeneity and trend tests

Helmert Test

Helmert test is a nonparametric test that is based on sequences and changes from the mean. It is used to detect changes in the homogeneity of a series of data, evaluating the number of sequences and changes in the data [21-22].

Student's t-test

Student's t-test is a parametric test used to compare the means of two samples and determine if they are significantly different from each other. It is useful for assessing the homogeneity of two periods in a series of data [23].

Cramer's test

Cramer test is a nonparametric test that compares the mean of a subperiod with that of the complete record. It is used to detect changes in the mean of a data series, which may indicate a lack of homogeneity [24] [22].

Pettitt Test

Pettitt test is a nonparametric test that detects changes in the median of a data series. It is especially useful for identifying points of change in time series, which may indicate a trend or a change in homogeneity [25].

Standard Normal Test (SNHT)

Standard Normal Homogeneity Test (SNHT) is a parametric test that assesses the homogeneity of a series of data by comparing the means and variances of subperiods. It is widely used in climatological and meteorological studies [26].

Buishand test

Buishand test is a parametric test that uses the graph of cumulative deviations from the mean (residual mass curve) to detect changes in the mean of a data series. It is useful for identifying changes in homogeneity [26].

Von Neumann test

Von Neumann test is a parametric test that detects loss of randomness in a series of data due to unspecified deterministic components. Assesses the independence of data by analyzing variance [24] [26].

Fisher Test

Fisher test is a parametric test that assesses the homogeneity of variances between different groups of data. It is useful for detecting inconsistencies in the dispersion of data [27].

Spearman's Test

Spearman test is a nonparametric test that assesses the correlation of ranges between two variables. It is useful for identifying trends in data series when the relationship is not necessarily linear [28].

Mann-Kendall test

Mann-Kendall test is a nonparametric test that assesses trend in a series of data. It is widely used in hydrological and climatological studies to detect monotonic trends [29-30].

Anderson Independence Test (Correlograme)

Anderson's test, also known as a correlogram, assesses persistence in a data series by analyzing the serial order 1correlation coefficient. It is useful for identifying temporal dependence data patterns [31].

Land Use Layers

In this paper, different Series comparison for two land use and vegetation maps from Bajo River basin Balsas was carried out; these are Serie I and Serie VII. Serie I consist of material digitized by INEGI, 2024, [32] based on printed land use and vegetation maps prepared by INEGI between

1980-1991 years, based on the photointerpretation of aerial photographs taken between 1968-1986 years. Land Use and Vegetation Map Serie VII was obtained from photointerpretation application techniques with geomean images from Landsat satellite constellation selected with base year 2018 [33]; processed in Geographic Data Cube. This interpretation is supported by fieldwork. They are datasets that contain location, distribution, and extent of different plant communities and agricultural uses with their respective variants in vegetation types, crops, and relevant ecological information. Such digital geographic information contains data structured in vector form coded according to the Dictionary of Vector Data on Land Use and Vegetation Series IV for Scale 1:250 000 applicable to different ecological units (plant communities and anthropic uses) contained in the dataset.

Calculation sequence

1. Annual historical average was obtained from daily data on inputs storage volume by own basin, inputs by total basin, evaporation and total outputs by intakes and spillway, as well as from the elevation and area curve.
2. Trend lines were obtained from previously obtained series
3. Methods were applied to identify independence, homogeneity and series trends.
4. Existing land uses were analyzed and land use percentages were obtained to identify their changes.

4. Results

This section highlights main analysis results.

Adjustment to trend lines of the analyzed series

Average annual daily storage volume behavior as well as variables related to its estimation, can be seen at following figures. These figures present trend lines corresponding to entire series and also added trend lines of time periods in which abrupt changes in data were observed behavior. Figure 2 shows an annual average daily storage volume decreasing behavior as a whole; and a sharp decrease in their values from 2002 onwards.

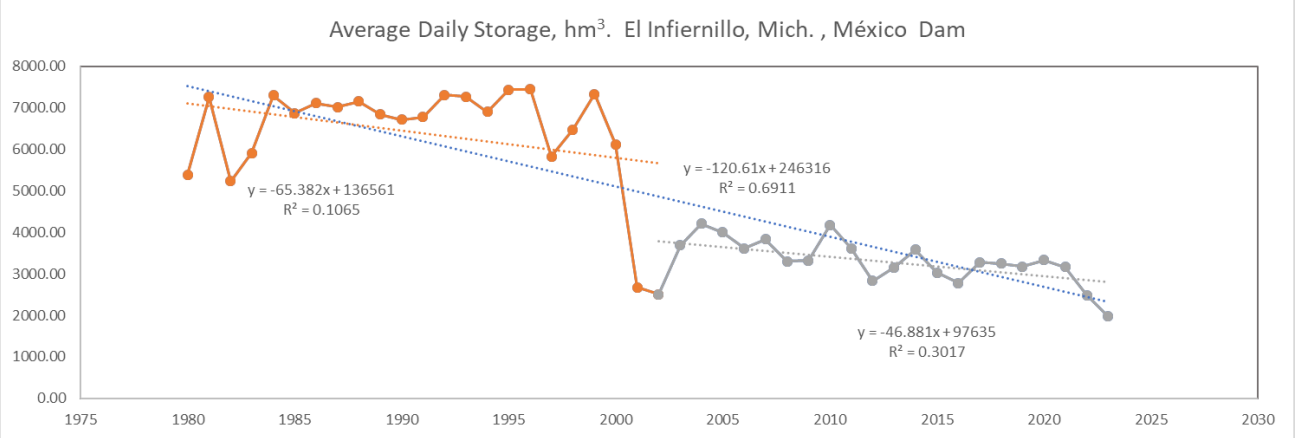

Fig. 2. Annual Average Daily Storage, El Infiernillo Dam, Mich, Mexico

Figures 3 shows a slight increasing trend in entry volumes to dam, both by own basin (OB) and by total basin (TB). Data series analysis for El Infiernillo dam storage volume revealed a downward trend since 1994, with a more pronounced reduction from 2002 (Figure 3).

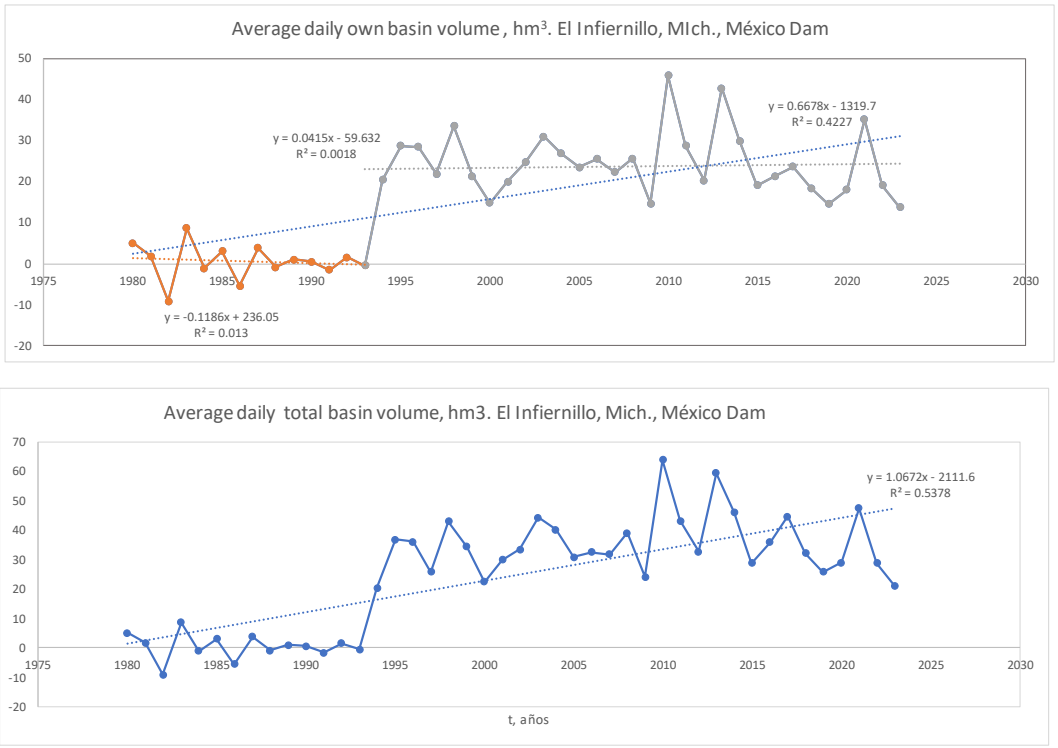

Fig. 3. Annual average daily inflow volume by own basin and by total basin, El Infiernillo dam, Mich, Mexico

This behavior can be attributed to several factors, including increase in evaporation and water withdrawals for agricultural and urban use (Figure 4). Evaporation, in particular, showed an increasing trend, suggesting that climate change could be influencing water stored dam loss. Figure 4 show an increasing behavior in average annual daily evaporation and also in extractions made to this reservoir.

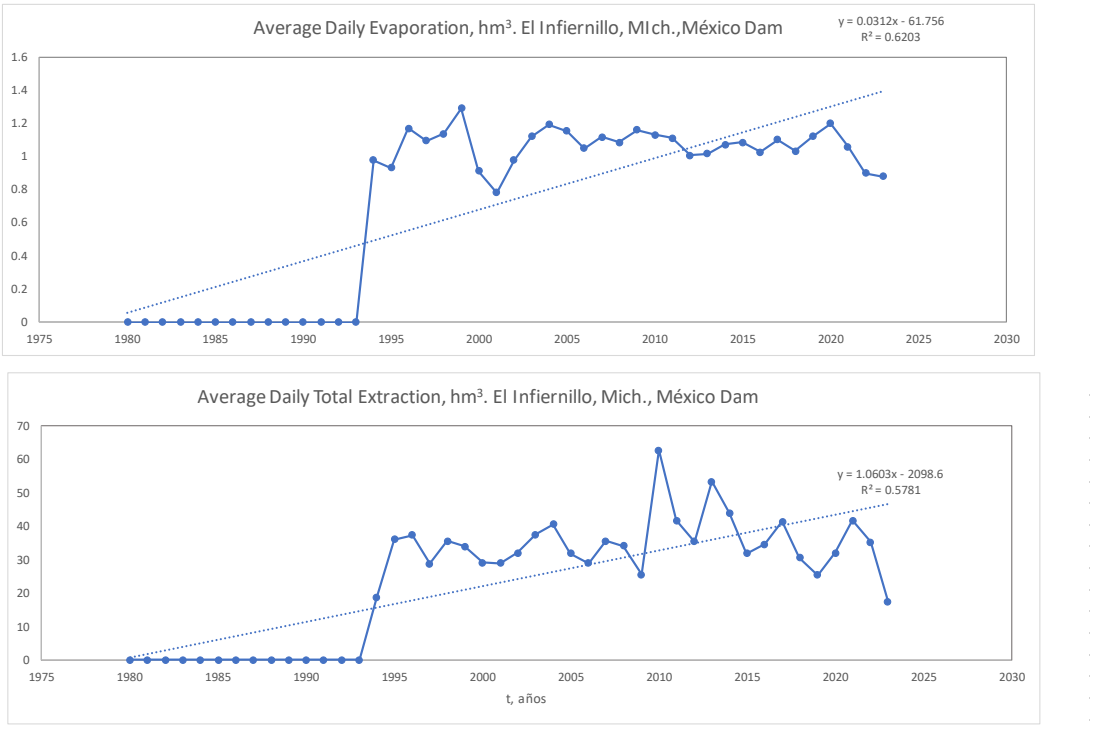

Fig. 4. Evaporated volume and annual average daily withdrawals, El Infiernillo dam, Mich, Mexico

Land use maps analysis

Analyzing land use maps from different years, such as Serie I (1980 year) and Serie VII (2018 year), is crucial for several reasons, comparing maps from different years helps identify deforestation, urban expansion, agricultural development, or industrialization.

It allows for quantifying changes in land cover, such as forest loss, water body reduction, or soil degradation.

Long-term land use changes can reveal ecosystem degradation, biodiversity loss, and increased vulnerability to natural disasters.

It helps assess the impact of human activities on climate change, water cycles, and soil erosion.

Comparing maps can highlight urban sprawl, road expansion, or industrial growth, helping urban planners manage sustainable growth.

It assists in preventing uncontrolled development that could lead to traffic congestion, pollution, or resource depletion.

Useful in environmental forensics, determining illegal land use changes, deforestation, or land encroachments. Evidence in legal disputes regarding land ownership, protected areas, or unauthorized constructions.

Helps in evaluating how land use changes increase flood risks, landslides, and desertification.

Supports the design of mitigation strategies by identifying vulnerable areas.

Detects changes in agricultural patterns, such as shifts from forest to farmland or urbanization of fertile land. Assists in water resource planning by monitoring changes in wetlands, reservoirs, or watershed areas.

Long-term land use analysis provides insights into carbon sequestration, deforestation trends, and changes in green cover, which impact climate models. This kind of analysis can gain a historical perspective on environmental trends and develop strategies for sustainable development, conservation, and policy-making.

Series I and VII Land Use Map Analysis

Series I and VII comparative analysis land use and vegetation maps for Bajo Balsas River basin (Figures 5 and 6 and Table 1) showed significant changes in land cover between 1980 and 2018. Among most notable trends are:

1. Increase in Irrigated Agriculture: An increase of 17.25% was observed in the area allocated to irrigated agriculture, which implies a greater demand for water for this sector. This increase could be putting pressure on the available water resources in the basin, contributing to the decrease in the volume of storage in the dam.
2. Expansion of Human Settlements: The area occupied by human settlements increased by 9,322.97%, reflecting an accelerated urbanization process. This urban growth may be affecting aquifer recharge and increasing surface runoff, which in turn reduces water infiltration into the soil.
3. Reduction of Forests and Jungles: There was a significant decrease in forests, as well as in low deciduous forest (-49.27%) and in Jungles (-44.26%). These natural areas loss affects soil capacity infiltration and contributes to an increase in surface runoff, which may be influencing the reduction in the volume of water stored in the dam.
4. Increase in Secondary Vegetation: A notable increase in secondary shrub vegetation was observed, especially in areas that were previously covered by Forest. This change suggests an original vegetation cover degradation, which may have negative implications on basin hydrological regulation.

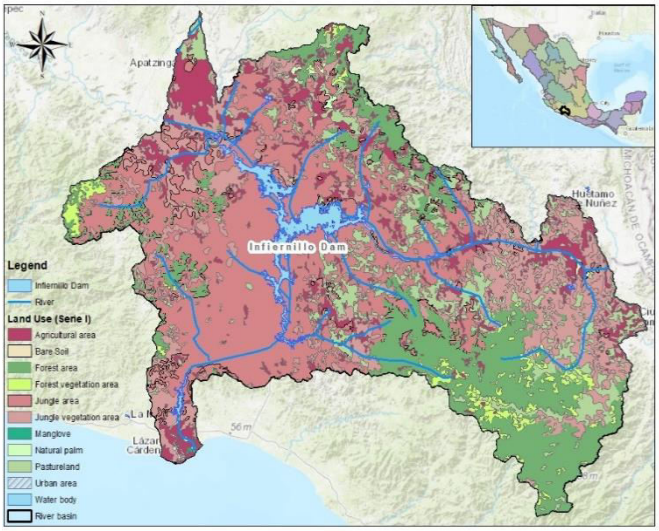

Fig. 5. Land Use Map Series I Lower Balsas River Basin

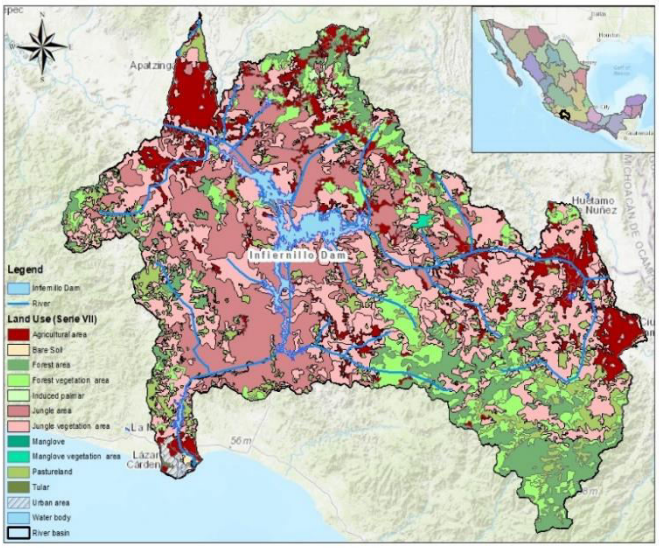

Fig. 6. Land Use Map Serie VII Lower Balsas River Basin

Table 1: Land use maps comparison from series I and VII generated by INEGI

Description	Serie I (Area Km²)	Serie VII (Area Km²)	Exchange rate %
Agricultural area	1,369.08	1,605.25	17.25
Bare Soil	13.45	12.92	-3.91
Forest area	2,439.28	1,237.32	-49.27
Forest vegetation area	373.54	1,459.49	290.72
Jungle area	5,132.93	2,860.97	-44.26
Jungle vegetation area	2,906.28	4,917.51	69.20
Manglove	3.59	4.54	26.63
Natural palm	26.06	29.00	11.29
Pastureland	1,399.39	1,391.15	-0.59
Urban area	1.09	103.02	9,322.97
Water body	280.03	320.39	14.41
Tular		3.15	100.00
Total Km²	13,944.72	13,944.72	-

Land Use Changes Implications

Changes in land use identified in this study have important implications for water management in Bajo Balsas River basin. Natural vegetation cover reduction and the increase in area devoted to irrigated agriculture and human settlements are altering runoff and water recharge patterns. This, in turn, is affecting water availability in El Infiernillo dam, which could aggravate water scarcity situation for this region. In addition, forests and jungles loss may be contributing to rising local temperatures and increased demand for water in agricultural and urban sectors. These factors, combined with the climate change effects, could be exacerbating decrease in storage volume at dam.

5. Discussion

In this section, a detailed discussion of the results obtained from trends analysis in the storage of El Infiernillo dam, as well as changes in land use in the Bajo Balsas River basin, is presented. In addition, the results are contrasted with the conclusions of the study to offer a comprehensive view of the problem and its implications.

When reviewing Figure 7, no appreciable variations are observed in annual average daily area behavior reported in reservoir operation, only small positive slopes reach its trend lines, a change in the rule of areas correspondence from 2001 to 2002 is not clearly distinguished. As for elevations, there is a slightly downward behavior in series as a whole (line slope is negative), in separation by years intervals something similar happens, although it is not such an appreciable reduction that it is considered as a decrease cause in storage volume after the year 2002.

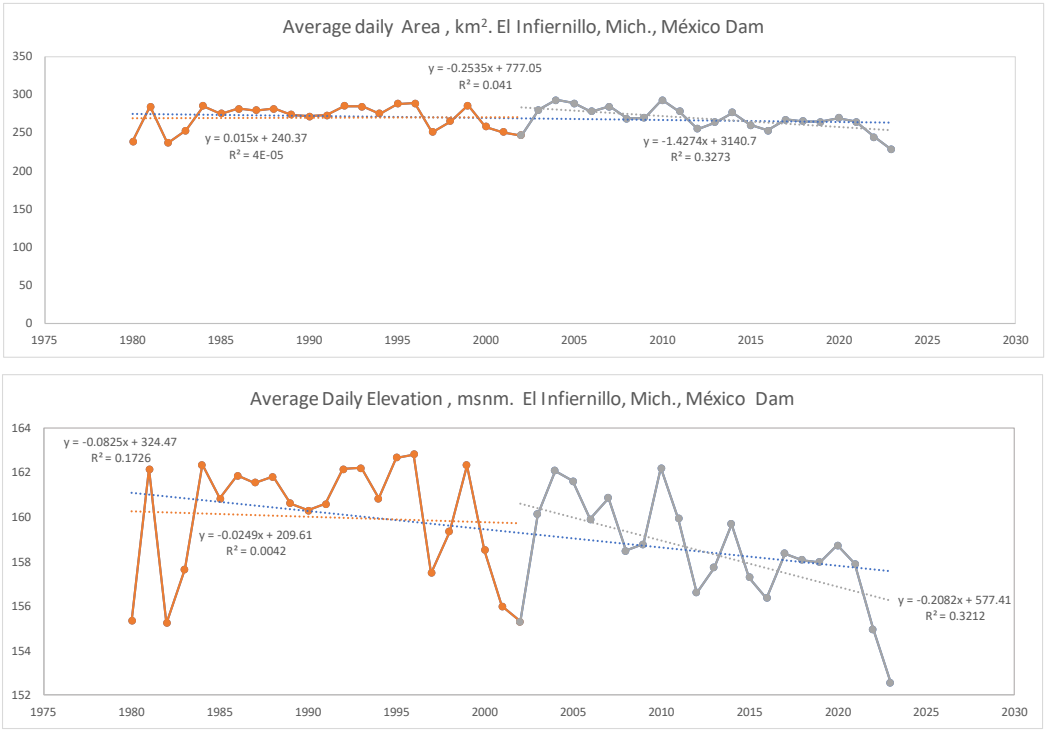

Fig. 7. Areas and Average Annual Daily Elevations, El Infiernillo Dam, Mich, Mexico

In addition, homogeneity and trend tests applied to data series indicated that most variables analyzed (storage volume, inputs by own and total basin) are not homogeneous and are temporally dependent (Table 2). This is due, to a large extent, to runoff exercised regulation by El Caracol dam, located El Infiernillo dam. Upstream. On the other hand, evaporation was the only variable that was homogeneous and independent, which reinforces the hypothesis that this factor is significantly influencing the decrease in storage volume.

Table 2: Results of homogeneity, trend and independence tests for the different variables

Variable	Data number	Homogeneity test								Conclusion
		Helmert	t the Student	Cramer	Pettit	Standard Normal	Buishand	By Neumman	Fisher	
V, Hm^3	30	X	X	X	X	X	X	✓	X	NH
OB, Hm^3	44	X	X	X	X	X	X	✓	X	NH
TB, Hm^3	44	X	X	X	X	X	X	✓	X	NH
Evap, Hm^3	30	✓	✓	✓	✓	✓	✓	✓	✓	H

Table 2: (continuation)

Name	Trend test		Conclusion	Independence
	Spearman	Mann Kendall		Anderson
V, Hm^3	✓	✓	T	D
OB, Hm^3	X	X	NT	D
TB, Hm^3	X	X	NT	D
Evap, Hm^3	✓	✓	T	I

Notes: T Tendency, NT No Tendency, D Dependent, I Independent

From homogeneity tests, only evaporation resulted in a homogeneous and independent series; remaining variables were non-homogeneous and dependent, a result that was expected due to regulation from existing runoff to El Caracol dam located at El Infiernillo dam upstream.
Table 3 presents an analysis of various scenarios, highlighting their results and the conclusions derived from them.

Table 3: Results Comparison

Analyzed Aspect	Results	Conclusions
Storage Trend	This trend has been declining since 1994, with a more pronounced reduction since 2002.	Increased evaporation and withdrawals are influencing the decrease in storage volume.
Land Use Changes	Increase in irrigated agriculture (+17.25%) and human settlements (+9,322.97%).	Agricultural and urban expansion is affecting hydrological basin dynamics.
Forest and Jungle Reduction	Decrease forest (-49.27%) and (-44.26%) jungle.	Vegetation cover loss is increasing surface runoff and reducing infiltration.
Impact on Water Availability	Reduction of storage volume in the dam.	The combination of factors is reducing water availability in the region.

6. Conclusions

This paper identifies a continuous decline in the El Infiernillo Dam storage volume since 1994, with a more pronounced reduction after 2002. The primary drivers of this decline are increased evaporation rates and higher water withdrawals for agricultural and urban use.
Land use changes in the Bajo Balsas River Basin, particularly the 17.25% expansion of irrigated agriculture and the 9,322.97% increase in human settlements, have significantly altered the region's hydrological balance. Natural vegetation loss including a 49.27% decrease in forests and a 44.26% reduction in jungle, has further exacerbated the situation by increasing surface runoff and reducing groundwater infiltration.
These combined factors are leading to a reduction in water availability, which poses a growing challenge for regional water security. To mitigate these impacts, it is essential to implement soil and water conservation strategies, improve water use efficiency, and integrate climate adaptation

measures into future water management policies. Additionally, continuous monitoring of seepage and hydrological trends will be crucial for sustaining water resources in the region.
This research provides a critical foundation for developing sustainable water management strategies that balance human demand with ecological conservation, ensuring long-term water security for the Bajo Balsas River Basin.

Acknowledgment

The authors thank the DGAPA UNAM for the support in carrying out this work. PAPIIT PROJECT IN102625.

References

[1] Liu, Junguo, Hong Yang, Simon N. Gosling, Matti Kummu, Martina Flörke, Stephan Pfister, Naota Hanasaki, Yoshihide Wada, Xinxin Zhang, Chunmiao Zheng, Joseph Alcamo, and Taikan Oki. "Water scarcity assessments in the past, present, and future." *Earth's Future* 5, no. 6 (June 2017): 545-559. https://doi.org/10.1002/2016EF000518.

[2] Mekonnen, M. M., and A. Y. Hoekstra. "Four billion people facing severe water scarcity." *Science Advances* 2, no. 2 (February 2016): e1500323. https://doi.org/10.1126/sciadv.1500323.

[3] Montejo, E. "What is the current situation of water in Mexico and the scarcity?" *National Geographic in Spanish*, 2024. Accessed January 20, 2025. https://www.ngenespanol.com/ecologia/cual-es-la-situacion-actual-del-agua-en-mexico/.

[4] Mexican Institute for Competitiveness (IMCO). "Water situation in Mexico". 2024. Retrieved from https://imco.org.mx/situacion-del-agua-en-mexico/

[5] Zarfl, Christiane, Alexander E. Lumsdon, Jürgen Berlekamp, Laura Tydecks, and Klement Tockner. "A global boom in hydropower dam construction." *Aquatic Sciences* 77, no. 1 (2015): 161-170. https://doi.org/10.1007/s00027-014-0377-0.

[6] Grill, G., B. Lehner, M. Thieme, B. Geenen, D. Tickner, F. Antonelli, S. Babu, P. Borrelli, L. Cheng, H. Crochetiere, H. Ehalt Macedo, R. Filgueiras, M. Goichot, J. Higgins, Z. Hogan, B. Lip, M. E. McClain, J. Meng, M. Mulligan, C. Nilsson, J. D. Olden, J. J. Opperman, P. Petry, C. Reidy Liermann, L. Sáenz, S. Salinas-Rodríguez, P. Schelle, R. J. P. Schmitt, J. Snider, F. Tan, K. Tockner, P. H. Valdujo, A. van Soesbergen, and C. Zarfl. "Mapping the world's free-flowing rivers." *Nature* 569 (2019): 215-221. https://doi.org/10.1038/s41586-019-1111-9.

[7] Winemiller, K. O., et al. "Balancing hydropower and biodiversity in the Amazon, Congo, and Mekong." *Science* 351, no. 6269 (January 2016): 128-129. https://doi.org/10.1126/science.aac7082.

[8] Poff, N. L., C. M. Brown, T. E. Grantham, J. H. Matthews, M. A. Palmer, C. M. Spence, R. L. Wilby, M. Haasnoot, G. F. Mendoza, K. C. Dominique, and A. Baeza. "Sustainable water management under future uncertainty with eco-engineering decision scaling." *Nature Climate Change* 6 (2016): 25-34. https://doi.org/10.1038/nclimate2765.

[9] Lehner, B., C. Reidy Liermann, C. Revenga, C. Vörösmarty, B. Fekete, P. Crouzet, P. Döll, M. Endejan, K. Frenken, J. Magome, C. Nilsson, J. C. Robertson, R. Rödel, N. Sindorf, and D. Wisser. "High-resolution mapping of the world's reservoirs and dams for sustainable river-flow management." *Frontiers in Ecology and the Environment* 9, no. 9 (November 2011): 494-502. https://doi.org/10.1890/100125.

[10] International Commission on Large Dams (ICOLD). World Register of Dams. 2021. Retrieved from https://www.icold-cigb.org/GB/world_register/world_register_of_dams.asp.

[11] National Water Commission. "Controlled extraction is increased in the El Infiernillo and La Villita dams, in Michoacán". 2024. Retrieved from https://www.gob.mx/conagua/prensa/282108.

[12] Secretariat of Hydraulic Resources / Secretaría de Recursos Hidráulicos. *Report on the construction of the Adolfo López Mateos Dam* / *Informe de la construcción de la presa Adolfo López Mateos*. Ciudad de México: Secretaría de Recursos Hidráulicos, 1964.

[13] National Water Commission / Comisión Nacional del Agua (CONAGUA). Water projects in Mexico / Proyectos de agua en México. 2024. Retrieved from https://www.gob.mx/conagua.

[14] Turner, S. W. D., J. C. Steyaert, L. Condon, and N. Voisin. "Water storage and release policies for all large reservoirs of conterminous United States." *Journal of Hydrology* 603-A (December 2021): 126843. https://doi.org/10.1016/j.jhydrol.2021.126843.

[15] Federal Electricity Commission / Comisión Federal de Electricidad (CFE). Monograph: Description of the "El Infiernillo" hydroelectric dam / Monografía: Descripción de la represa hidroeléctrica "El Infiernillo". 2021. Retrieved from https://www.cfe.gob.mx.

[16] López Montes, A. "Hydrology applications in a physical model. XXVII Latin American Congress of Hydraulics". 2016. Retrieved from http://www.investigacionesyproyectoshidraulicos.com/web/Material%20Cientifico/Articulos/Mas%20de%201000%20Articulos/181.pdf.

[17] Jain, S. K. *Introduction to Reservoir Operation*. NIH, Roorkee. 2021. Retrieved from https://nihroorkee.gov.in/sites/default/files/uploadfiles/IntroductiontoReservoir-Operation.pdf.
[18] Montgomery, D. C., E. A. Peck, and G. G. Vining. *Introduction to Linear Regression Analysis* (5th ed.). Wiley, 2012.
[19] Draper, N. R., and H. Smith. *Applied Regression Analysis* (3rd ed.). Wiley, 1998. https://doi.org/10.1002/9781118625590.
[20] Kutner, M. H., C. J. Nachtsheim, and J. Neter. *Applied Linear Regression Models* (4th ed.). New York, McGraw-Hill/Irwin, 2004.
[21] Mather, J. R. *Climatology: Fundamentals and Applications*. New York, McGraw-Hill, 1974.
[22] Campos-Aranda, D. F. *Analysis of hydrological series*. Mexican Institute of Water Technology, 1998.
[23] Ostle, B., and R. W. Mensing. *Statistics in Research: Basic Concepts and Techniques for Research Workers* (3rd ed.). Ames, Iowa State University Press,1975.
[24] World Meteorological Organization (WMO). *Guide to Hydrological Practices*. WMO-No. 168. 1971.
[25] Pettitt, A. N. "A non-parametric approach to the change-point problem." *Applied Statistics* 28, no. 2 (1979): 126-135. https://doi.org/10.2307/2346729.
[26] Buishand, T. A. "Some methods for testing the homogeneity of rainfall records." *Journal of Hydrology* 58, no. 1-2 (August 1982): 11-27. https://doi.org/10.1016/0022-1694(82)90066-X.
[27] Fisher, R. A. *Statistical Methods for Research Workers* (11th ed. rev.). Edinburgh, Oliver and Boyd, 1925.
[28] Spearman, C. "The proof and measurement of association between two things." *The American Journal of Psychology* 15, no. 1 (January 1904): 72-101. https://doi.org/10.2307/1412159.
[29] Mann, H. B. "Nonparametric tests against trend." *Econometrica* 13, no. 3 (July 1945): 245-259. https://doi.org/10.2307/1907187.
[30] Kendall, M. G. *Rank Correlation Methods* (4th ed.). London, Charles Griffin, 1975.
[31] Anderson, T. W. "On the distribution of the two-sample Cramer-von Mises criterion." *The Annals of Mathematical Statistics* 33, no. 3 (September 1962): 1148-1159. https://doi.org/10.1214/aoms/1177704477.
[32] National Institute of Statistics and Geography / Instituto Nacional de Estadística y Geografía (INEGI). *Land Use and Vegetation Charter Series I*. 2024. Retrieved from https://www.inegi.org.mx/temas/usosuelo/.
[33] National Institute of Statistics and Geography / Instituto Nacional de Estadística y Geografía (INEGI). *Land Use and Vegetation Charter Series VII*. 2024. Retrieved from https://www.inegi.org.mx/temas/usosuelo/.

"My Soil Protection App" - A Mobile-Based Dedicated Environmental Information System - from a User Testing and Validation Perspective

PhD eng. IT exp. **Bogdan-Vasile CIORUȚA**[1-3,*], MA stud. **Ioana-Elisabeta SABOU (CIORUȚA)**[2], PhD stud. eng. **Marcela HRENIUC (SĂLIȘCAN)**[1], Eng. IT exp. **Alexandru Leonard POP**[2,3], Assoc. Prof. PhD eng. **Mirela-Ana COMAN**[1,4]

[1] University of Agricultural Sciences and Veterinary Medicine from Cluj-Napoca, 3-5 Calea Mănăștur, 4000372, Cluj-Napoca, Romania

[2] Technical University of Cluj-Napoca - North University Centre of Baia Mare, Faculty of Letters, Department of Specialty with Psychopedagogical Profile, 76 Victoriei Str., 430083, Baia Mare, Romania

[3] Technical University of Cluj-Napoca - North University Centre of Baia Mare, Office of Informatics, 62A Victor Babeș Str., 430083, Baia Mare, Romania

[4] Technical University of Cluj-Napoca - North University Centre of Baia Mare, Faculty of Engineering - Department of Mineral Resources, Materials and Environmental Engineering, Victor Babeș 62A Street, 430083, Baia Mare, Romania

* bogdan.cioruta@staff.utcluj.ro

Abstract: *As part of the mobile application development and improvement process, evaluation and feedback along the way are essential elements for any software developer; they can provide him/her with information about both the value that the application has from the perspective of other users, as well as information that needs to be revised or removed from the interface and the functionalities that the application proposes. In this sense, for the mobile application "My Soil Protection App", created in our regime, we proposed to carry out an analysis of the design, interface, and functionalities; thus, through a form with permissive access, created in the open-source variant of the Survio® application we provided access through a link placed on the KnowledgeBase® platform to users both to the application itself and to a questionnaire.*
The questionnaire is composed of 15 questions, to which are added 3 prompts for the personalization of the respondents, to see to what extent the users can test and validate the elements contained in the application. The 15 questions are grouped into 4 classes of interest, numbered from A to D, each analyzing the design, interface, functionalities, and specialist contents included in the application. As a result of the analysis of the 39 responses received from the users (18-28 years), we concluded that the mobile application "My Soil Protection App" is bold and well-received by the users, who greatly appreciate the design elements and the friendly interface, the clearly explained functionalities and the contents that do not require further additions.

Keywords: *Comparative study, mobile applications, MIT App Inventor®, soil protection*

1. Introduction

Mobile applications dedicated to monitoring and protecting soil resources - as mature fruits of environmental scientific research and Environmental Informatics [1-3] - are increasingly common in the work of farmers, ecologists, pedologists, academics, and users all around the world [4,5]. What makes them popular among regular users is the possibility they offer in acquiring, saving storing, and processing environmental data from the field [6]. To see if such an application meets the requirements of ordinary (non-specialist) users, we set out to analyze the mobile application "My Soil Protection App" developed in-house regime using the MIT App Inventor® platform [7,8].
The quantification of the possibilities of acquiring, processing, saving, and storing data from the field, which the dedicated applications offer for mobile devices with the Android operating system, was carried out starting from the analysis of the design, interface, and functionalities proposed by the application in this regard taken into analysis.
As the tendency to Environmental Information Processing Systems [9-12], the application was subjected to a particularly important stage - through the lens of the feedback provided to the software developer, this stage is equivalent to the validation of the application by users; this involves accessing, analyzing, and auditing the application by users to provide constructive feedback to improve the quality of the application.

2. Material and methods - the perspective addressed by current research

In this endeavor (of the application evaluation) [13], we used the free working version of the Survio® platform [14], which from personal experience provides superior options to other similar platforms - Google Forms®, Microsoft Forms®, HubSpot Forms®, Cognito Forms®, etc. - to create an evaluation and feedback form about the self-developed mobile application "My Soil Protection App" (see Fig. 1, and also Fig. 2 and Fig. 3), which has real implications through MIT App Inventor® in the soil sciences e- and mLearning, and in the protection of soil resources [15,16].

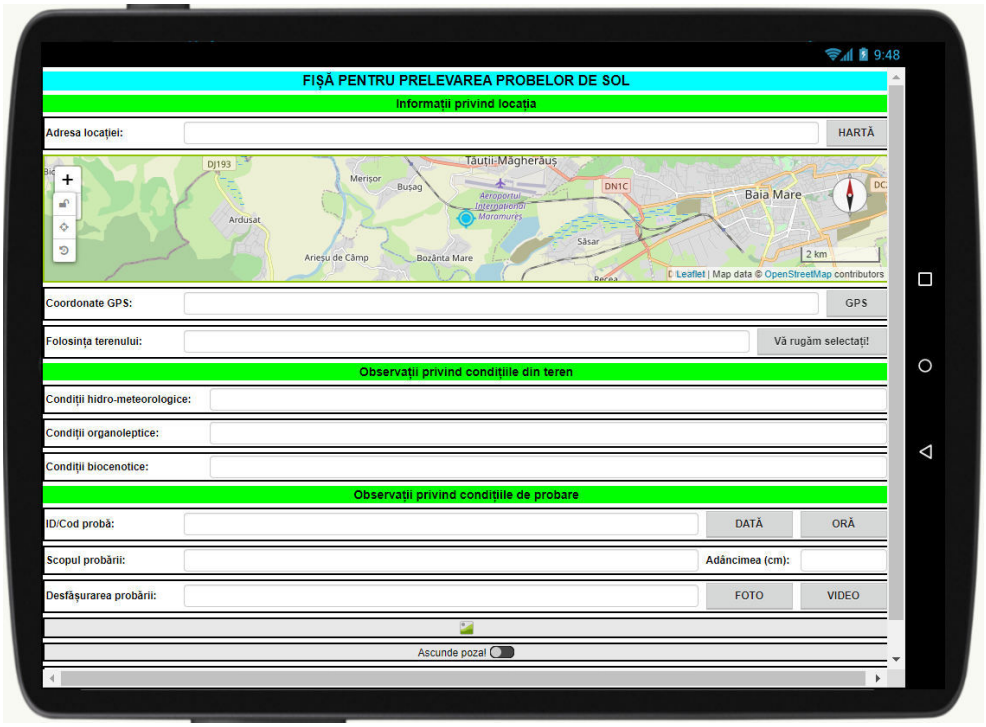

Fig. 1. The "Soil Sampling Sheet" interface where the user manually fills in the data acquisition forms

The questionnaire - associated with the account created through the institutional email address - was made available to the respondents through a permissive link, on the KnowledgeBase® platform [17], where the QR code for downloading and installing the application was also uploaded. The questionnaire in question includes:

- A welcome page that lets users know the purpose of the questionnaire;
  "Dear users,
  We invite you to fill in an evaluation and feedback form about the mobile application "My Soil Protection App", developed in-house. We note that your answers are necessary for me to improve the interface and functionalities of the application so that it is easily accessible and understandable to ordinary (non-specialist) users. Thank you for your time and answers!"
- A page that refers to «A. Evaluation of the general characteristics of the application (design elements and interface)», and contains 5 questions, for which only one answer variant can be chosen ("YES" or "NO");
  - "Does the application icon - represented by a magnifying glass and a soil profile - have an appropriate design about the name of the application (My Soil Protection App)?" [18];
  - "Is data about the version, structure, and purpose of the application presented and expressly provided in the «About the application» section?";
  - "The application contains a mini user guide in the «About the application» section?";
  - "Is data about the creator of the application and its ownership provided clearly?";
  - "Does the application allow identifying the creator and contacting him through social media platforms?" [19,20].

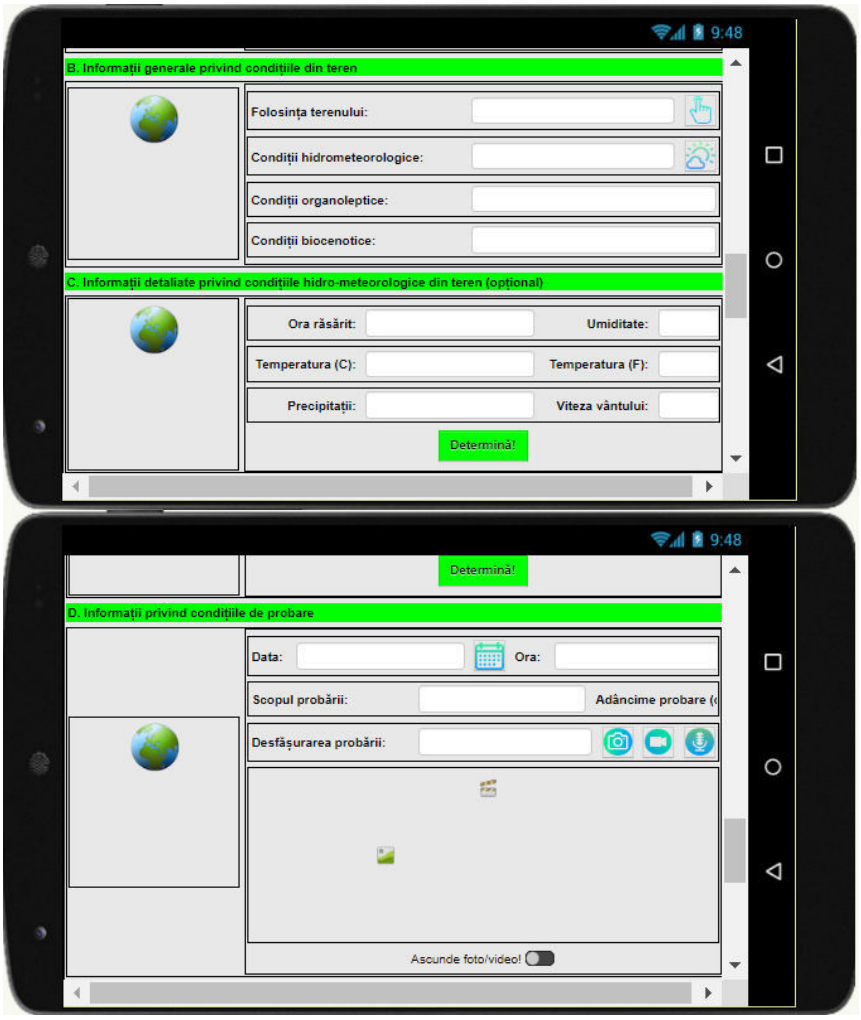

Fig. 2. The screens "B. General information on field conditions", "C. Detailed information on hydrometeorological conditions in the field (optional)" and "D. Information on testing conditions" with the acquisition of field data through the application interface

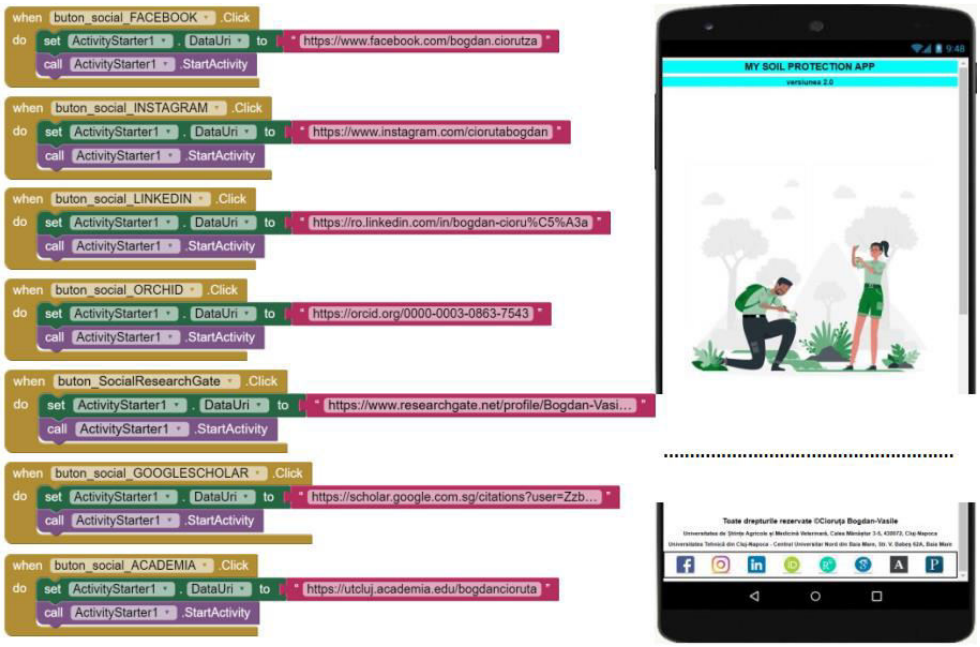

Fig. 3. Configuring and linking the application to various social media platforms (Facebook®, Instagram®, LinkedIn®, OrchID®, ResearchGate®, Google Scholar®, etc)

- a page that refers to «B. Evaluation of the specific characteristics of the application (interface and functionalities)», and contains 5 questions, for which only one answer variant can be chosen ("NO (0%)", "YES (1-25%)", "YES (26-50%)", "YES (51-75%) or "YES (76-100%)";
  - "Does the application propose a sufficient set of elements for characterizing the location of soil resources? (It is checked whether elements such as the name and address of the location, GPS coordinates, display of the location on the map, etc. are included and accessible)" [19];
  - "Does the application have a clearly defined structure (via menus), a friendly and easy-to-understand interface for the average user?" (It is checked whether elements such as labels and explanations, text boxes, checkboxes, and buttons, images, and gif animations, etc. are included and accessible)";
  - "Does the application propose a sufficient set of elements to characterize the soil profile in the field?" (It is checked if elements such as soil type, land use, data on texture, color, and temperature, data on organoleptic, biocenosis and meteo-climatological conditions, etc. are included and accessible, etc.)" [20];
  - "Does the application propose a sufficient set of elements for field data acquisition?" (It is checked whether elements such as text boxes, checkboxes and buttons for data acquisition are included and accessible)";
  - "Does the application propose a sufficient set of elements for saving field data? (Check if elements such as data save buttons, associated file types, and platforms - TinyDB®, File®, Firebase®, CloudDB®, DropBox®, Google Sheets/Drive®, etc) are included and accessible.
- a page that refers to «C. Evaluation of the structural elements of the application (specialized contents)», and contains 2 questions, for which only one answer option can be chosen: "NO (there is no repeated content)", "PARTIALLY YES (the content differs, but there are also common elements)" or "YES (contents different)";
  - "Does the application have specific content for each worksheet? (It is checked if the analyzed elements differ between worksheets)";
  - "Does the application contain explanations of the use of the elements for each worksheet? (It is checked if examples are included and accessible regarding how to operate the elements, especially text boxes and buttons)".
- A page that refers to «D. Proposals and recommendations for improving the application», and contains 6 requests for respondents, of which the first 3 are strictly related to the application:
  - "Choose a percentage where you think the worksheets fall developmentally" (Only one answer option will be selected for each worksheet (0-25%, 26-50%, 51-75%, or 76-100%);
  - "What elements do you think should be included in the application?", (where up to 1000 characters can be inserted), and
  - "Give the app several stars.", while the next 3 refer to "city of residence (county)", "occupation (age)" and "type and model of mobile device" used.

3. Results and discussions

Users of two specializations within the Faculty of Sciences (NUCBM-TUCN), namely Management (18 respondents) and Business Economics (21 respondents), aged between 19 and 28, participated in the questionnaire. Their distribution by age is faithfully reproduced in Fig. 4(a), while the distribution by place of residence and county is reproduced in Fig. 4(b). Also, regarding the type and model of mobile devices used in the analysis and evaluation of the application, the distribution of them is reproduced in Fig. 4(c).
According to the answers provided by the users to the first 5 questions (see Fig. 5), we noticed a reporting trend towards the answer variant "YES" (on average more than 35 favorable answers out of a total of 39), which certifies the fact that the application corresponds, the a little at the design level, the requirements of the average user:

- The application icon - represented by a magnifying glass and a soil profile - has a suitable design for the name of the application (My Soil Protection App);
- data regarding the version, structure, and purpose of the application are presented and expressly provided in the "About the application" section;
- the application contains a mini-guide for use in the "About the application" section;
- data relating to the creator of the application and its affiliation are provided clearly and expressly;
- the application allows identifying the creator and contacting him through social media platforms.

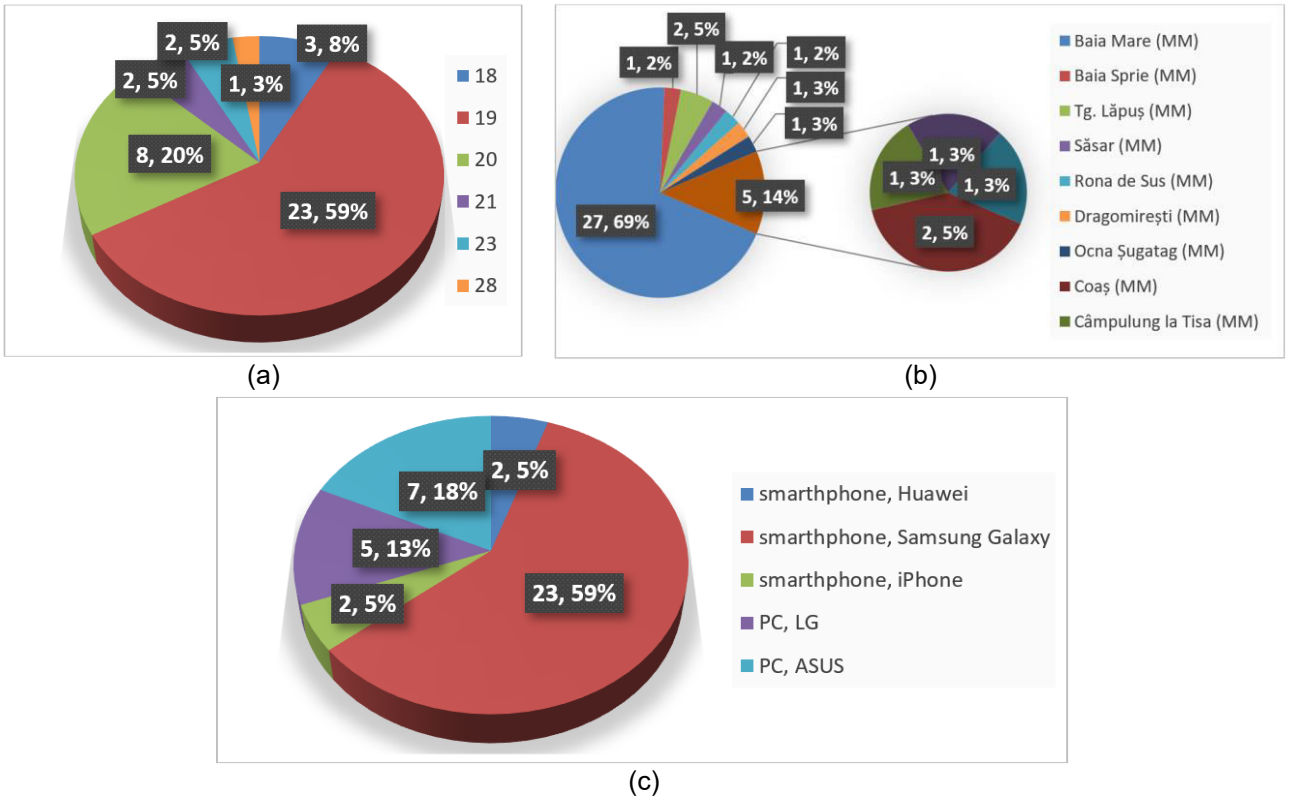

Fig. 4. Distribution of respondents by age (a), by the place of residence and the county (b), and by the type/model of mobile device used (c)

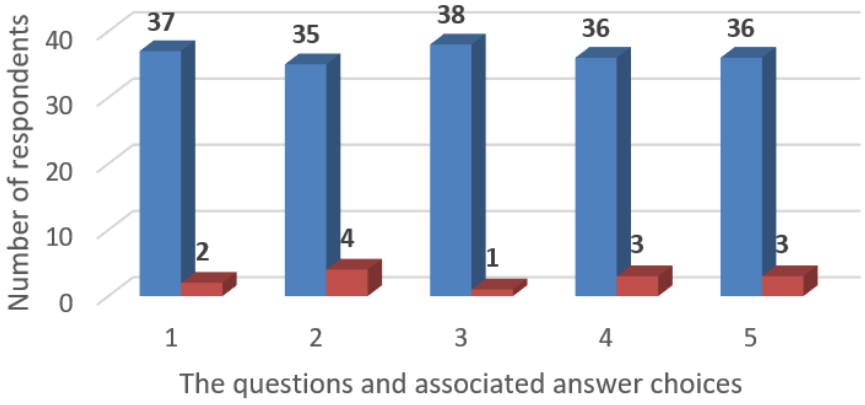

Fig. 5. Users' responses to section/category questions «A. Evaluation of the general features of the application (design and interface)»

Also, according to the answers obtained from the users (see Fig. 6), there is an upward trend towards the answer options "YES (51-75%)" - on average more than 10 answers for each question, respectively "YES (76-100%)" - on average more than 20 answers for each question.

Under these conditions, we can state that more than 50% of the respondents confirmed that the application: has a clearly defined structure (through menus), a friendly and easy-to-understand interface for the average user, proposes a sufficient set of elements to characterize the location of soil resources and their profile and characteristics, and proposes a sufficient set of elements for the acquisition, saving/storage, processing, and distribution of field data.

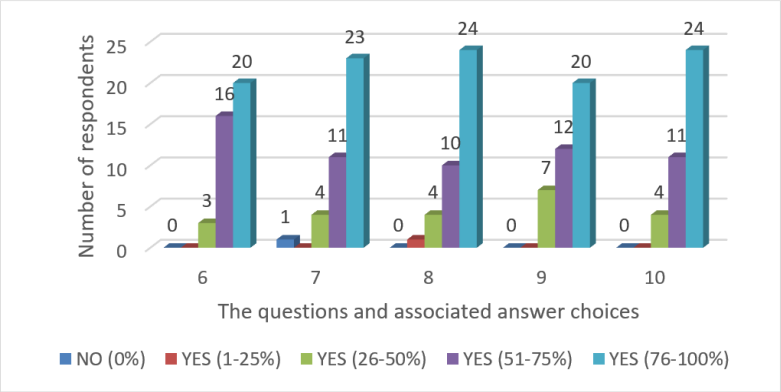

Fig. 6. Users' responses to section/category questions «B. Evaluation of the specific features of the application (interface and functionalities)»

Regarding the level of development of the worksheets proposed through the application menu, the users' answers show us (in Fig. 7, up) that the worksheets have content that differs, although some common elements are also found, which are repeated from sheet to sheet (on average over 15 answers for the option "PARTIALLY YES"/sheet, and over 19 answers for "YES"/sheet).
At the same time, regarding the explanations and indications of how to use the application elements, it can be seen from the users' answers (see Fig. 7, down) that there are on average more than 32 confirmations ("YES") for each worksheet; this aspect shows us that the application developer has made sure that the user has easy access to the documentation for using the text boxes and associated buttons.

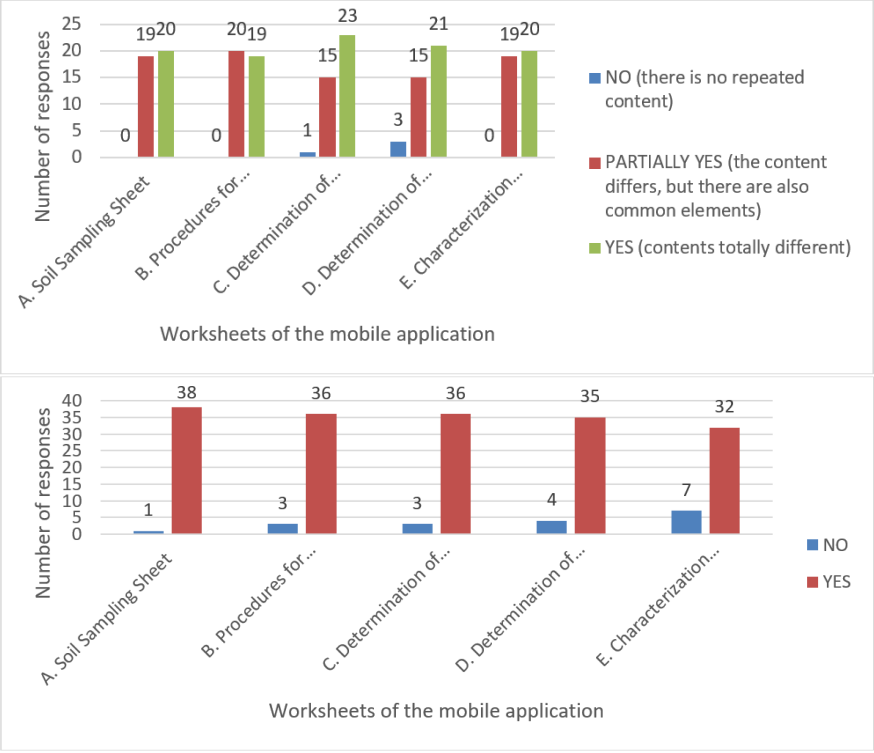

Fig. 7. Users' responses to questions in section/category «C. Evaluation of structural elements of the application (specialized contents)»

In the same context, the users' answers show us that the degree of development of the application is over 51-75% - on average over 10 answers/each worksheet of the application, respectively 76-100% - on average over 17 answers/each application worksheet (see Fig. 8); moreover, in terms of completing the application with other elements or adapting to the general audience, 54% of users' answers show us that "nothing/no element" is needed anymore, while 10% of users say that minor adjustments are needed.

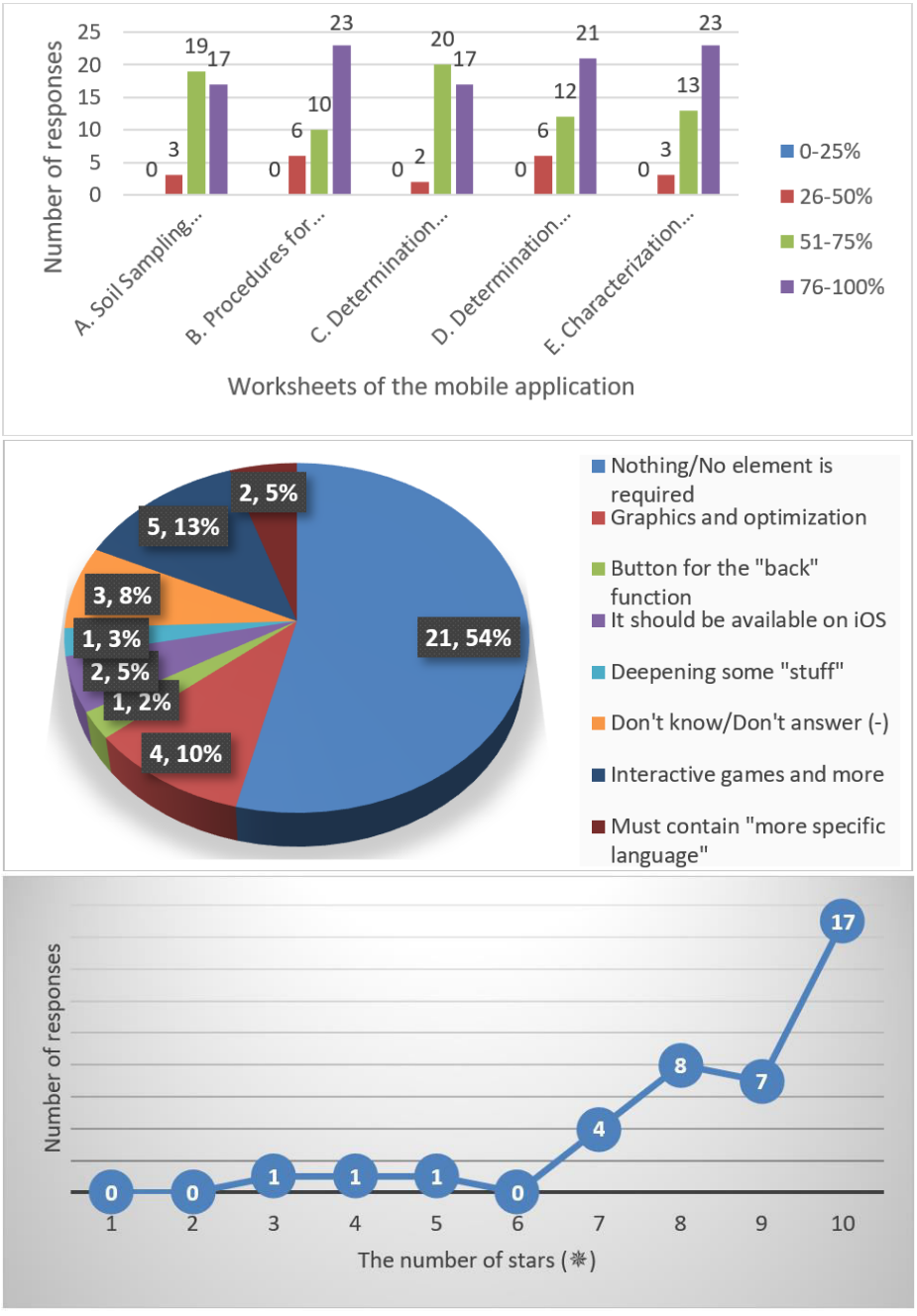

Fig. 8. Users' responses to questions in section/category «D. Proposals and recommendations for improving the application»

As a result of the users' answers, it can be noted that the application has specific content and contains pertinent explanations regarding the use of the elements for each worksheet, the worksheets being developed in the vast majority above 51-75%. In addition, referring to the whole application, in general, it can be noted that only one student each gave 3, 4, and 5 stars, 4 users gave 7 stars, 8 users gave 8 stars, 7 users gave 9 stars and 17 users gave 10 stars, which reveals a weighted average of 8.64 stars.

4. Conclusions, perspectives, and proposals

Third-party access to a mobile app (such as "My Soil Protection App") before the app "goes to market" is a vital process that can add value to the app itself (by changes and removals of design elements, interface, and functionality), but also new elements that can cover new requests from users. At the same time, we are glad that the self-made mobile application "My Soil Protection App" was analyzed and evaluated positively by the users, whose openness to such applications is as significant as possible.

Equally, through the lens of the feedback obtained, we are much more confident in our own decisions about the development scenarios of applications of this kind, testing the application making it possible to understand specific aspects that target not only the average user but also the implications of the application in relative to market requirements. In addition, we consider such an initiative (to analyze and evaluate the application) as opportune and urge all those who develop such dedicated mobile applications (not only for soil resource tracking) to take the time to test and validate the application and through non-specialist users; we believe that any constructive feedback is more than welcome, as the app ultimately manages to establish itself much more easily among the public.

Acknowledgments

We would like to thank all the users from the two specializations (Management and Business Economics) who, in the informatics class, under the auspices of anonymity, actively got involved and responded positively to the request to analyze and evaluate the mobile application entitled "My Soil Protection App", and to record the feedback through the questionnaire.

References

[1] Avouris, N.M., and B. Page. *Environmental Informatics: Methodology and Applications of Environmental Information Processing*. Boston, Kluwer Academic, 1995.

[2] Hilty, L.M., B. Page, F.J. Radermacher, and W.F. Riekert. *Environmental Informatics as a New Discipline of Applied Computer Science*. 978-94-017-1443-3_1. 1995.

[3] Page, B. *Environmental Informatics - towards a new discipline in applied computer science for environmental protection and research*. In: Denzer R., Schimak G., Russell D., *Proceedings of the International Symposium on Environmental Software Systems*, Springer-Science+Business Media Dordrecht, pg. 3-21, 1996.

[4] Haklay, M. *From environmental information systems to environmental informatics: evolution and meaning*. Working paper. CASA Working Papers (7). Centre for Advanced Spatial Analysis (UCL), London, UK, 1999.

[5] Avouris, N.M. "Human interaction with environmental information systems." *Interdisciplinary Environmental Review* 3 (2001): 134-144. 10.1504/IER.2001.053871.

[6] Cioruța, B.V., and M.A. Coman. "Foray into modern scientific research of the environment. From Environmental Information Systems to Environmental Informatics / Incursiune în cercetarea științifică modernă a mediului înconjurător. De la Sistemele Informatice de Mediu la Informatica Mediului." *Journal of Environmental Research and Protection*, no. 29 (2011): 17-20.

[7] Cioruța B.V., and M.A. Coman. "Considerations regarding the implications of mobile-based Environmental Information Systems in contaminated soils characterization." *Journal of Documentation, Research and Professional Training (ProEnvironment®)* 12, no. 38 (2021): 127-131.

[8] Cioruța, B.V., and M.A. Coman. "Implications of Mobile-based Information Systems in Contaminated Soils Characterization." *Natural Resources and Sustainable Development (NRSD®)* 11, no. 2 (2021): 135-142. Accessed December 1, 2021. www.nrsdj.com/issues-year-2021-2/implications-of-mobile-based-information-systems-in-contaminated-soils-characterization.html.

[9] Radermacher, F., W.F. Riekert, B. Page, and L.M. Hilty. "Trends in Environmental Information Processing." In: *Proceedings of the IFIP Congress 94* – vol. 2, 597-604, 1994.

[10] Page, B., and C. Rautenstrauch. *Environmental Informatics - Methods, Tools, and Applications in Environmental Information Processing*. 10.4018/9781930708020.ch001. In: *Environmental Information Systems in Industry and Public Administration*, 2001.

[11] Page, B., and K. Voigt. "Recent history and development of environmental information systems and databases in Germany." *Online Information Review* 27, no. 1 (2003): 37-50. 10.1108/14684520310462554.

[12] Hilty, L.M., B. Page, and J. Hrebicek. "Environmental Informatics." *Environmental Modelling and Software* 21 (2006): 1517-1518. 10.1016/j.envsoft.2006.05.016.
[13] ***. *Mobile application development - start to the golden future of portable technologies* [*Dezvoltarea aplicațiilor mobile - start către viitorul de aur al tehnologiilor portabile*]. Accessed January 17, 2023. https://www.credis.ro/dezvoltare-mobila.
[14] ***. *Survio*® official website https://www.survio.com/en.
[15] Cioruța, B.V., D. Darabă, and M.A. Coman. "Foray into e-education and m-learning for soil protection" / "Incursiune în educația e- și m-learning pentru protecția solurilor." "Education - an essential component of environmental policy" Symposium, 15th edition / Simpozionul „Educația - componentă esențială a policitii de mediu", ediția a XV-a. *AGIR Bulletin* / *Buletinul AGIR*, no. 4 (2022): 22-27.
[16] Cioruța, B.V., M.A. Coman, I.E. Sabou, and D. Darabă. "Implications of the MIT App Inventor® Platform in Soil Resource Monitoring and Protection." / „Implicațiile platformei MIT App Inventor® în monitorizarea și protecția resurselor de sol." "Education - an essential component of environmental policy" Symposium, 15th edition / Simpozionul „Educația - componentă esențială a policitii de mediu", ediția a XV-a. *AGIR Bulletin* / *Buletinul AGIR*, no. 4 (2022): 28-32.
[17] ***. *KnowledgeBase*® official website https://kb.cunbm.utcluj.ro.
[18] Cioruța B.V., and M.A. Coman. "Soil Protection & Mobile Apps created with MIT App Inventor® - a Multidisciplinary Symbiosis?" *Asian Soil Research Journal (ASRJ®)* 6, no. 4 (2022): 33-54.
[19] Cioruța, B.V., and M.A. Coman. "Acquisition of Field Data through Mobile-based Applications dedicated to Soil Protection." *Asian Soil Research Journal (ASRJ®)* 6, no. 4 (2022): 76-83.
[20] Cioruța, B.V., and M.A. Coman. "Saving and Storing Data through Mobile-based Applications Dedicated to Soil Protection." *Asian Soil Research Journal (ASRJ®)* 6, no. 4 (2022): 66-75.

Kinematic Analysis and Geometric Synthesis of Elevator Mechanisms with Non-Articulated X-Bars Mounted on Mobile Robots

Ph'D. stud. **Dana Mirela VĂLEANU[1],*,** Prof.Ph'D.Eng. **Păun ANTONESCU[1]**

[1] School of Doctoral Studies in Industrial Engineering and Robotics, National University of Science and Technology Politehnica Bucharest, 060402, Bucharest, Romania

* valeanu_dana@yahoo.com

Abstract: *X-shaped (scissor) articulated bar lifts take up less space in areas of use, such as warehouses. By folding, when not in use, these scissor lifts lower to their minimum level. The kinematic analysis of the mechanisms of these elevators involves the method of analytical calculation of the displacements of the main characteristic points of the dyadic chains. In the case of elevators with non-articulated bars in X, a problem of geometric synthesis of the quadrilateral deltoid type mechanism is presented and solved.*

Keywords: *Mobile robots, kinematic analysis, elevator mechanisms, kinematic chain*

1. Introduction

The single-level X-joint lifting mechanism (fig. 1) operates in the vertical plane and is actuated by a piston-type actuator (*a*) and an oscillating cylinder (*b*).

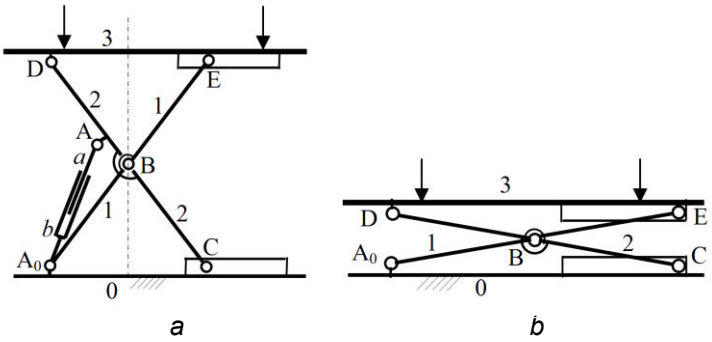

Fig. 1. Kinematic diagram of the X-bar elevator mechanism, upper / open position (*a*) and lower / closed position (*b*)

The technological resistance force acts as the weight of the manipulated object (fig. 1), and the driving force acts in the cylinder b on the piston a, in the direction A0A (fig. 1a).
The construction diagram shown in the color picture (fig. 2) shows an elevator with X-shaped articulated bars, which is placed on a 4-wheel mobile robot cart. This elevator has 2 levels and uses linear guides for translational couplings at the base and at the level of the upper platform.
In other constructive variants of elevators (fig. 3) both bars are articulated at the base (the chassis of the mobile robot), but are not connected to each other, as in the previous variants (fig. 1 and 2).

Fig. 2. Construction diagram (picture) of an X elevator with two levels

As a rule, the actuator of this type of elevator (fig. 3) is mechanical with a screw and nut, being articulated at the upper ends of the two non-articulated X-bars.

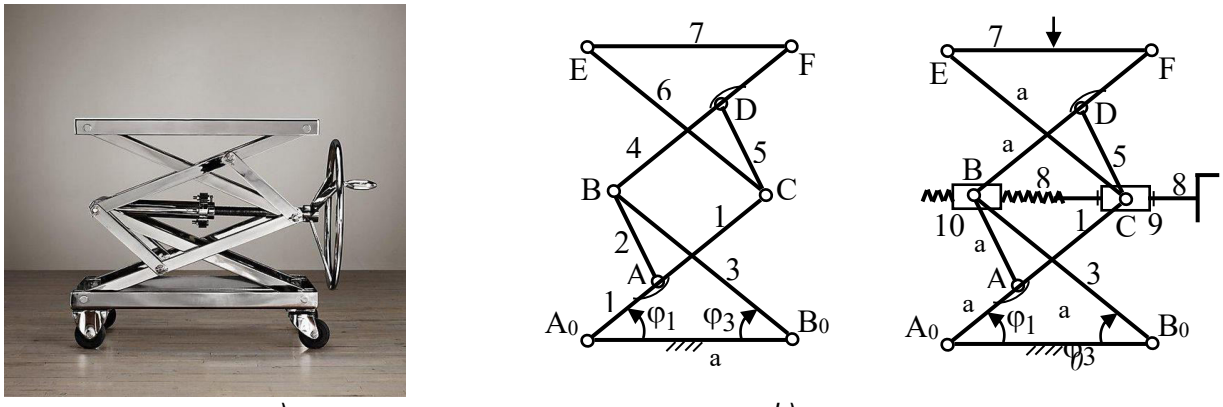

a) *b)*

Fig. 3. Constructive diagram (a) and kinematic diagrams (b) of two-level non-articulated X-bar elevator.

2. Kinematic analysis of X-bar elevator mechanisms

2.1. Lifting mechanisms with articulated bars in X

For comparison, let's first analyze the plane elevator with bars articulated in X (fig. 4), where the first two bars have equal lengths ($A_0B=BC$).. The kinematic diagram (fig. 4a) shows a closed contour in the form of an isosceles triangle A_0BC with a variable base A_0C, which is obtained with the help of a roto-translational kinematic couple C (2,0) [1, 2, 3, 4].

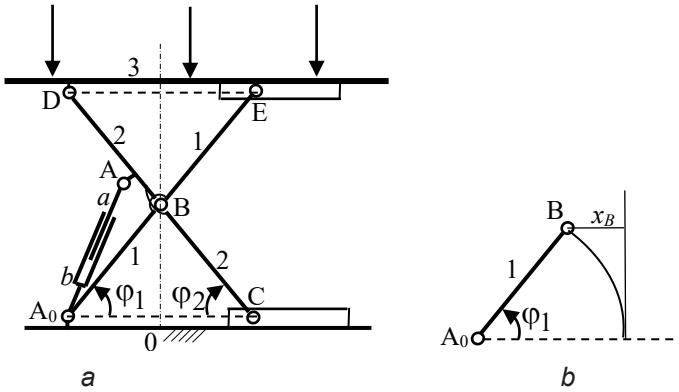

a *b*

Fig. 4. Kinematic diagram of the mechanism with bars 1 and 2 articulated in X

By doubling the length of bars 1 ($A_0B=BE=l_1$) and 2 ($BC=BD=l_2$) the letter X is obtained, thus the points D and E are kept at the same level. Bar 3 represents the horizontal platform, which takes the weight of the materials handled in the warehouse, being articulated at D at bar 2 and resting at point E at bar 1 (fig. 4). With the movement of piston a in cylinder b (fig. 4a), bar 1 rotates in the trigonometric sense, while bar 2 rotates with the angle ϕ_2 (measured clockwise). Thus, the bar 1 rotates with respect to the fixed joint A_0 in the direct direction from ϕ_{1min} (lower position) to ϕ_{1max} (upper position).

For the X-bar elevator with a single level (fig. 4a), the height of the platform 3 is deduced from the formula

$$h_3 = 2l_1 \sin\phi_1 = 2l_2 \sin\phi_2\,; \quad l_1 = l_2 \tag{2.1}$$

where the notations where used (fig. 4): $A_0B = BE = l_1; BC = CD = l_2$.

It is mentioned that the maximum value of the angle ϕ_1 (ϕ_{1max}) is imposed by the limitation of the displacement deviation of point B (x_B) from the vertical (fig. 4*b*).

For $A_0A = s_0$ is obtained $A_0C = x_{Cmax}$, and for $\phi_{1max}$and $A_0A = s_{max}$ results $A_0C = x_{Cmin}$.

It is observed that the maximum displacement of piston *a* in cylinder *b* (fig. 4*a*) is $h=s_{max}-s_0$.

2.2. Kinematic analysis of elevators with non-articulated X bars

In these elevators (fig. 5a) both X bars are articulated at the base, but they are not articulated between them, which structurally distinguishes them from the elevators that were previously analyzed (fig. 4).

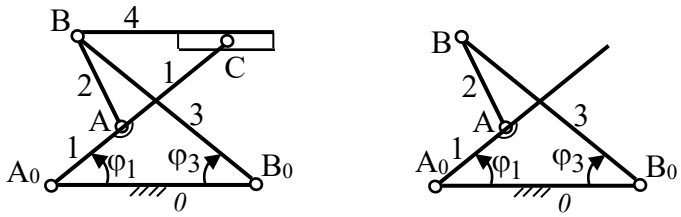

a) *b)*

Fig. 5. Kinematic diagram of the elevator with non-articulated bars in X

As a topological structure, these planar mechanisms of elevators with non-articulated bars in X are composed of an articulated quadrilateral rocker - rocker type (fig. 5) with the two rockers (1 and 3) crossed in X, without being articulated between them.
The planar articulated quadrilateral is the closed kinematic chain $A_0ABB_0A_0$, to whom (fig. 5b): $A_0A=AB$ and $BB_0=A_0B_0$, respectively $l_1=l_2$ and $l_3=l_0$.
In the upper part of the kinematic scheme of the lifting mechanism is the platform 4 which takes the force of the weight of the handled object.
The mobility of the mechanism is verified by the fact that bar 4 is equivalent to a dyadic chain of type (R, R+T), with a joint in B (3,4) and a roto-translational couple in C (1,4).
Kinematic analysis of the quadrilateral mechanism involves writing the closing vector equation of the closed loop (fig. 5*b*):

$$\overrightarrow{A_0A}+\overrightarrow{AB}=\overrightarrow{A_0B_0}+\overrightarrow{B_0B} \tag{2.2}$$

or, using the mentioned notations:

$$\bar{l}_1+\bar{l}_2=\bar{l}_0+\bar{l}_3 \text{ respectively } \bar{l}_3-\bar{l}_2=\bar{l}_1-\bar{l}_0 \tag{2.3}$$

The scalar projection equations are obtained from (2.3) and have the expressions:

$$\begin{aligned} l_3\cos(\pi-\phi_3)-l_2\cos\phi_2&=l_1\cos\phi_1-l_0\\ l_3\sin(\pi-\phi_3)-l_2\sin\phi_2&=l_1\sin\phi_1 \end{aligned} \tag{2.4}$$

Assuming that the angle is known (as an independent parameter), the system (2.4) consists of two nonlinear scalar equations with two unknowns (ϕ_2,ϕ_3).
To solve this system of two trigonometric equations (in *sin* and *cos*) one of the unknowns is isolated (e.g. ϕ_2), obtaining the following expressions:

$$\begin{aligned} l_3\cos(\pi-\phi_3)-l_1\cos\phi_1+l_0&=l_2\cos\phi_2\\ l_3\sin(\pi-\phi_3)-l_1\sin\phi_1&=l_2\sin\phi_2 \end{aligned} \tag{2.5}$$

Squaring the two equations and adding them yields the equation with one unknown ϕ_3

$$[l_3\cos(\pi-\phi_3)-l_1\cos\phi_1+l_0]^2+[l_3\sin(\pi-\phi_3)-l_1\sin\phi_1]^2=l_2^2 \tag{2.6}$$

or, more conveniently:

$$[-l_3\cos\phi_3-l_1\cos\phi_1+l_0]^2+[l_3\sin\phi_3-l_1\sin\phi_1]^2=l_2^2 \tag{2.7}$$

A trigonometric equation of the known form was obtained [1, 2]

$$a_3\sin\phi_3+b_3\cos\phi_3+c_3=0 \tag{2.8}$$

In equation (2.8) the three coefficients have the expressions:

$$a_3 = 2l_1l_3\,sin\,\phi_1\,; \quad b_3 = 2l_3(l_0 - l_1\,cos\,\phi_1);$$
$$c_3 = 2l_0l_1\,cos\,\phi_1 + l_2^2 - l_1^2 - l_3^2 - l_0^2 \tag{2.9a}$$

To solve equation (2.8) the trigonometric functions are replaced *sin* and *cos* with *tg* function:

$$sin\,\phi_3 = \frac{2tg(\phi_3/2)}{1+tg^2(\phi_3/2)}; \quad cos\,\phi_3 = \frac{1-tg^2(\phi_3/2)}{1+tg^2(\phi_3/2)} \tag{2.9b}$$

Using the notation $tg(\phi_3/2) = t$, the equation (2.8) is written

$$a_3\frac{2t}{1+t^2} + b_3\frac{1-t^2}{1+t^2} + c_3 = 0 \tag{2.9c}$$

This is an algebraic equation of degree 2, which results in the form

$$(b_3 - c_3)\cdot t^2 - 2a_3\cdot t - (b_3 + c_3) = 0 \tag{2.9d}$$

The two solutions of equation (2.9d) are expressed by the formula

$$t = \frac{a_3 \pm \sqrt{a_3^2 + b_3^2 - c_3^2}}{b_3 - c_3} \tag{2.9e}$$

Taking into account the notation introduced in equation (2.9c), the expression for the ϕ_3 angle is deduced:

$$\phi_3 = 2arctg(t) = 2arctg\left[\frac{a_3 \pm \sqrt{a_3^2 + b_3^2 - c_3^2}}{b_3 - c_3}\right] \tag{2.9f}$$

It is noted that only one of the two solutions (2.9f) corresponds to reality ($\phi_3 < \pi/2$).
As a numerical example, given the lengths of the quadrilateral (fig. 5*b*) for $\phi_1 = 30°$, is deduced the $\phi_3$angle, first calculating the coefficients a_3, b_3, c_3 defined by equations (2.9a):

$$a_3 = 2l_1l_3\,sin\,\phi_1 = 2\cdot 0.35\cdot 1\cdot sin\,30° = 0.35$$
$$b_3 = 2l_3(l_0 - l_1\,cos\,\phi_1) = 2\cdot 1\cdot (1 - 0.35\cdot cos\,30°) = 2 - 0.35\sqrt{3} = 1.4$$
$$c_3 = 2l_0l_1\,cos\,\phi_1 + l_2^2 - l_1^2 - l_3^2 - l_0^2 = 2\cdot 1\cdot 0.35\cdot 0.5\sqrt{3} + 0.35^2 - 0.35^2 - 1^2 - 1^2 = -1.4$$

With these numerical values of the variable coefficients entered in the formula (1.9f) is obtained:

$$\phi_3 = 2arctg\frac{0.7}{2.8} = 2arctg(0.25) = 2\cdot 14° = 28° \tag{2.9k}$$

The difference between $\phi_1 = 30°$and $\phi_3 = 28°$ is 2°, which is convenient.

3. Structural and kinematic analysis of non-articulated bar multi-storey elevator in X

This overloaded elevator in X (fig. 6*a*) is obtained from the single-level kinematic scheme (fig. 5) by amplifying it with two dyadic chains LD (4,5) and LD (6,7).

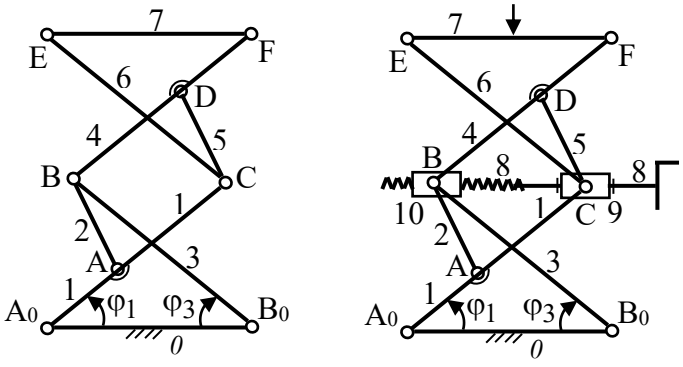

a) *b)*

Fig. 6. The kinematic diagram of the multi-storey elevator with non-articulated bars in X

It should be noted that bar 7 is the platform on which the object manipulated at a certain level is placed to be placed in another area of the warehouse.
The mobility of the articulated plane mechanism with multi-storey structure (fig. 6) is checked immediately with the help of the formula [1, 2]:

$$M_3 = 3n - 2C_5 - C_4 \tag{3.1}$$

where the following parameters are identified (fig. 6):
$n = 7$kinematic elements;
$C_5 = 10$ 5th class kinematic couples (with 5 restrictions);
$C_4 = 0$ 4th class kinematic couples (with 4 restrictions);
By substituting these numerical values in formula (3.1) it is deduced:

$$M_3 = 3 \cdot 7 - 2 \cdot 10 - 0 = 1 \tag{3.2}$$

The obtained result shows that the multi-storey elevator (fig. 6a) can be operated with a single driving element, for example by bar 1 positioned by the angle ϕ_1.
The actuator can be with a pneumatic cylinder (articulated at base 0 and bar 1), but it can also be operated with a mechanical screw actuator that is articulated at points B and C (fig. 6*b*).
In the last variant of the lifting mechanism with mechanical screw actuator (fig. 6*b*), its mobility is deduced with the general formula [2] for complex mechanisms [5, 6]:

$$M_b = \sum_1^5 mC_m - \sum_2^6 rN_r \tag{3.3}$$

The following parameters are identified in the mobility formula (3.3):
$m = 1,2,\ldots,5$ represents the mobility of a kinematic couple;
C_m is the number of mobile kinematic couples m;
$r = 2,3,\ldots,6$ is the rank of an independent closed kinematic contour;
N_r is the number of independent closed kinematic contours.
For the mechanism of the complex multi-story elevator (fig. 6b) the following numerical values are identified: $m = 1$ corresponds to planar joints (0,1), (0,3), (1,2), (2,3), (3,4), (4,5), (1,5), (1,6), (4,7), (6,7), (8,9), (1,9), (8,10), (3,10): accordingly $C_1 = 14$;
$r = 3$ corresponds to independent closed kinematic chains (0,1,2,3,0), (1,2,4,5), (4,5,6,7);
$r = 4$ is the rank of the independent closed kinematic contour (1,2,10,8,9).
Substituting these numerical values in formula (3.3) results $M_b = 1 \cdot 14 - (3 \cdot 3 + 4 \cdot 1) = 1$
Kinematic analysis of the multi-storey elevator mechanism includes the calculation of the height of the ceiling 7 according to the $\phi_1$angle(fig. 15*a*).
In the first stage of the kinematic analysis, the angle is calculated from the trigonometric equation (2.8), its value being close to that of the ϕ_1 angle.
In the second stage, we consider the dyadic chain LD(4,5) represented by the triangle BDC (fig. 7) where the coordinates of points B and C are obtained with the formulas:

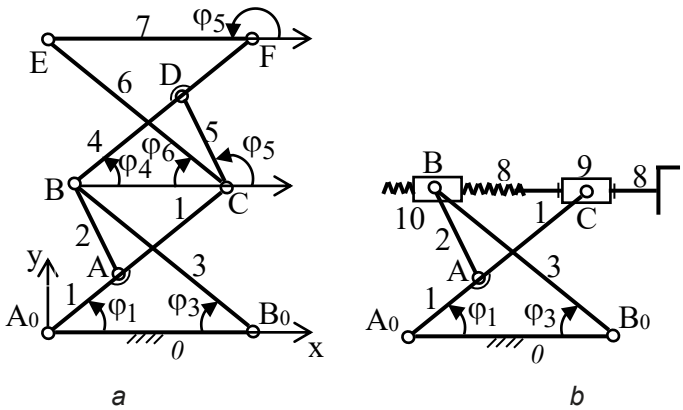

a *b*

Fig. 7. The kinematic diagram of the over-storey elevator

$$x_B = l_0 + l_3\, cos(\pi - \phi_3)$$
$$y_B = l_3\, sin(\pi - \phi_3) \tag{3.4}$$

$$x_C = l_1 \cos\phi_1$$
$$y_C = l_1 \sin\phi_1 \quad (3.5)$$

The closed vector equation of the closed contour DBC (fig. 7*a*) is:

$$\overrightarrow{BD} - \overrightarrow{CD} = \overrightarrow{BC} \quad (3.6)$$

The equations of the projections on the orthogonal coordinate axes are:

$$l_4 \cos\phi_4 - l_5 \cos\phi_5 = x_C - x_B$$
$$l_4 \sin\phi_4 - l_5 \sin\phi_5 = y_C - y_B \quad (3.7)$$

From the system of two scalar equations (3.7) one of the two unknowns is deduced, by the method of elimination ϕ_4 and ϕ_5, from a trigonometric equation of the form (2.8):

$$a_i \sin\phi_i + b_i \cos\phi_i + c_i = 0, \quad i = 4{,}5 \quad (3.8)$$

In the third stage, the kinematics of the dyadic chain LD(6,7) from the triangle CEF is solved, where the coordinates of points C are known, from the expression (3.5) and of F belonging to bar 4 (fig. 7a):

$$x_F = x_B + l_4' \cos\phi_4$$
$$y_F = y_B + l_4' \sin\phi_4 \quad (3.9)$$

The non-linear scalar equations are written from the CEF triangle(fig. 7*a*):

$$l_6 \cos\phi_6 - l_7 \cos\phi_7 = x_F - x_C$$
$$l_6 \sin\phi_6 - l_7 \sin\phi_7 = y_F - y_C \quad (3.10)$$

This system of two equations with two unknowns is solved by eliminating one of the unknowns in turn, obtaining a trigonometric equation of the form (3.8)

$$a_i \sin\phi_i + b_i \cos\phi_i + c_i = 0, \quad i = 6{,}7 \quad (3.11)$$

If bars 4 and 6 have equal lengths the angles and are equal and it follows that bar 7 is horizontal (fig. 7*a*), so $\phi_7 = 180°$. It should be emphasized that the screw actuator kinematic chain (8,9,10), which is articulated at points B and C (fig. 7*b*), it has zero mobility, being a neutral kinematic chain.

4. Geometric synthesis of the quadrilateral mechanism of the elevator with non-articulated bars in X

For this articulated quadrilateral mechanism (fig. 8) it is required to determine the geometric condition for positioning the crank and the rocker at equal angles $(\phi_1 = \phi_3)$.

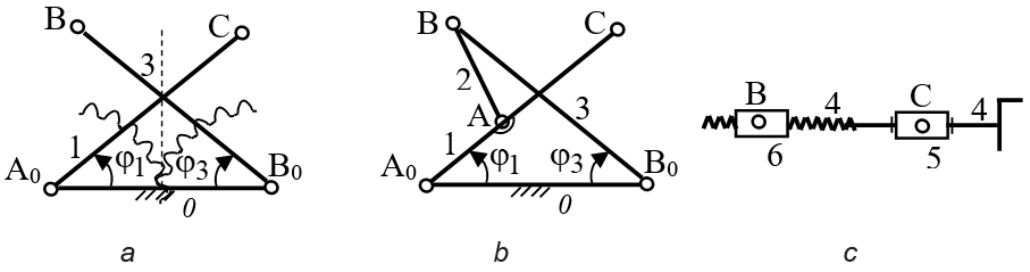

Fig. 8. Kinematic schemes of planar mechanisms with bars and gears

A first solution (fig. 8*a*) consists in the use of two equal toothed sectors, in external gearing, with bar 1 and bar 3 solidarized to each toothed sector.
The gear is external, so the toothed sectors rotate in the opposite direction, so the angles of rotation are equal $(\phi_1 = \phi_3)$. Therefore, points B and C are located at the same height $(y_B = y_C)$.
The screw actuator can be used to actuate this elevator mechanism with non-articulated bars (fig. 8*c*), it being mounted at points B and C through the respective joints (fig. 9*a*).

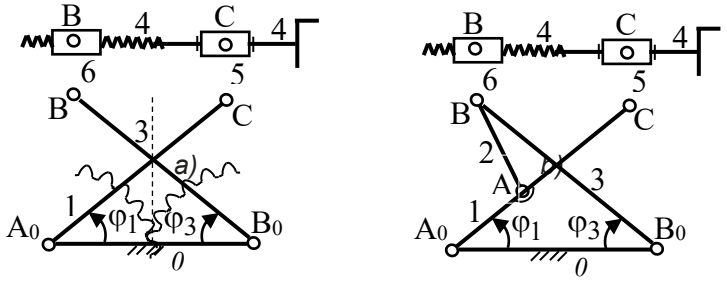

Fig. 9. Kinematic diagrams of screw actuator assembly

Similarly proceed with the assembly of the screw actuator (4,5,6) to the articulated quadrilateral mechanism with crank 1, connecting rod 2 and rocker arm 3 (fig. 9*b*).
After mounting the screw actuator, in both versions (fig. 9), by turning the screw 4, the joints B and C come closer, when the angles $\phi_1,\ \phi_3$ of bars 1 and 3 are increasing.
Similarly, if screw 4 is turned in the opposite direction, the distance between points B and C increases. so that the angles ϕ_1 and ϕ_3 are decreasing.
After assembling the screw actuator (fig. 10), a kinematic chain consisting of two dyads linked in series can be added by overlapping LD(7,8) and LD(9,10).

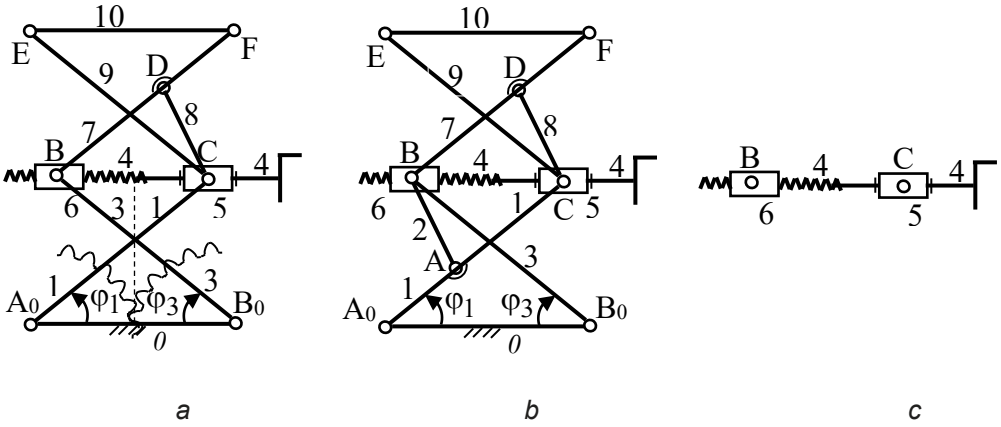

Fig. 10. Kinematic diagram for assembling the variants of overstory mechanisms with screw actuator

5. The geometric synthesis of the quadrilateral mechanism to achieve the condition $\boldsymbol{\phi_1 = \phi_3}$

Consider the kinematic diagram (fig. 11) of an articulated quadrilateral mechanism, deltoid type, where bars 1 and 2 have equal lengths $(l_1 = l_2)$; also, the length of bar 3 (rocker) is equal to the length of fixed bar 0 $(l_3 = l_0)$.

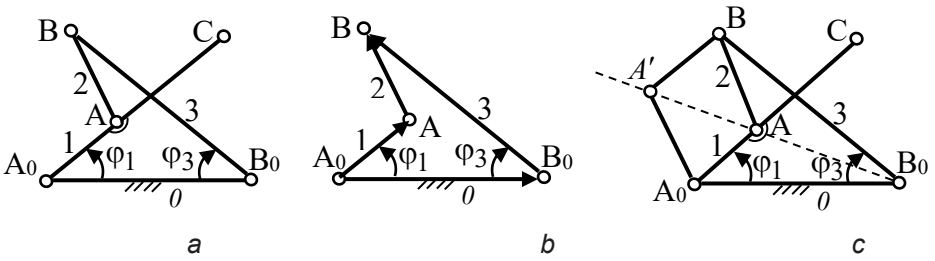

Fig. 11. Kinematic diagram of the quadrilateral deltoid mechanism

For the sides of the articulated quadrilateral (fig. 11*a*) the following notations are used:

$$A_0B_0 = l_0;\ A_0A = l_1;\ AB = l_2;\ BB_0 = l_3 \tag{5.1}$$

The particular case of the analyzed concave deltoid type mechanism is considered:

$$A_0A = AB = l_1; A_0B_0 = BB_0 = l_3 \tag{5.2a}$$

It should be noted that the solution with convex deltoid type quadrilateral $A_0A'BB_0$ (fig. 11a) cannot be accepted because the opposite sides A_0A' and BB_0 do not intersect.
Therefore, only the variant of the concave deltoid quadrilateral will be further analyzed, in order to carry out the synthesis of the concave quadrilateral mechanism that achieves the equality of the angles ϕ_1 and ϕ_3.
The geometric synthesis problem of the concave deltoid quadrilateral (fig. 11*a*) refers to determining the x-ratio between the lengths of bars 1 and 3 ($x=l_1/l_3$) from the condition $\phi_1 = \phi_3$.
The vector contour of the concave articulated quadrilateral is considered (fig. 11*b*), for which the closing vector equation is:

$$\overrightarrow{A_0A} + \overrightarrow{AB} = \overrightarrow{A_0B_0} + \overrightarrow{B_0B} \tag{5.2b}$$

or, using the notations (5.2a), the vector equation is written

$$\vec{l}_1 + \vec{l}_2 = \vec{l}_0 + \vec{l}_3; \quad \vec{l}_3 - \vec{l}_2 = \vec{l}_1 - \vec{l}_0 \tag{5.3}$$

The scalar projection equations are derived as follows:

$$\begin{aligned} l_3\, cos(\pi - \phi_3) - l_2\, cos\, \phi_2 &= l_1\, cos\, \phi_1 - l_0 \\ l_3\, sin(\pi - \phi_3) - l_2\, sin\, \phi_2 &= l_1\, sin\, \phi_1 \end{aligned} \tag{5.4}$$

For the particular case (5.2a) the scalar equations (5.4) are written:

$$\begin{aligned} l_3\, cos(\pi - \phi_3) - l_1\, cos\, \phi_2 &= l_1\, cos\, \phi_1 - l_3 \\ l_3\, sin(\pi - \phi_3) - l_1\, sin\, \phi_2 &= l_1\, sin\, \phi_1 \end{aligned} \tag{5.5}$$

Substituting $l_1 = x \cdot l_3$ the equations (5.5) become:

$$\begin{aligned} -cos\, \phi_3 - x \cdot cos\, \phi_2 &= x \cdot cos\, \phi_1 - 1 \\ sin\, \phi_3 - x \cdot sin\, \phi_2 &= x \cdot sin\, \phi_1 \end{aligned} \tag{5.6}$$

The angle is removed ϕ_2 isolating it on the right side of the equations:

$$\begin{aligned} 1 - cos\, \phi_3 - x \cdot cos\, \phi_1 &= x \cdot cos\, \phi_2 \\ sin\, \phi_3 - x \cdot sin\, \phi_1 &= x \cdot sin\, \phi_2 \end{aligned} \tag{5.7}$$

Squaring these equations, adding and equating $\phi_3 = \phi_1$, results for *x*, the expression

$$x = \frac{1 - cos\, \phi_1}{cos\, \phi_1 - cos\, 2\phi_1} \tag{5.8}$$

It is observed that the ratio value $x= l_1/l_3$ is a non-linear function of the angle ϕ_1, which shows that the equality of the two angles ϕ_1 and ϕ_3 it can only be achieved for one position of the mechanism. Practically, for an elevator with articulated bars (fig. 19), the sharp positioning angles of bars 1 and 3 do not exceed the value of 60°.
For $\phi_1 = 60°$is obtained

$$x = \frac{1 - cos\, 60°}{cos\, 60° - cos\, 120°} = \frac{1 - 1/2}{1/2 - (-1/2)} = 1/2 = 0.5 \tag{5.9}$$

Similarly, for $\phi_1 = 45°,\ 30°,\ 20°, 10°,\ 5°$ the ratio values are deduced *x*:

$$x = 0.41;\ 0.36;\ 0.34;\ 0.337;\ 0.335 \tag{5.10}$$

The obtained result shows that, for ϕ_{1max}, maximum ratio variation *x* is

$$\Delta x = xmin_{max} \tag{5.11}$$

But, for ϕ_{1max}, observing (5.10), the maximum deviation of the ratio x decreases to the value

$$\Delta x = xmin_{max} \tag{5.12}$$

Therefore, for the last case analyzed ϕ_{1max} it can be admitted that the optimal average value of the ratio *x* is: $x = 0.35$.

6. Conclusions

The planar articulated mechanisms of the X-bar elevators are kinematically analyzed by the analytical method, highlighting the vertical movements as in goods warehouses.
For scissor [7, 8, 9] X-bar elevators, the kinematic analysis is simpler than for non-articulated X-bar elevators. For elevators with non-articulated bars in X, the kinematic study includes the identification of independent kinematic contours, the writing of the closing vector equations and the nonlinear scalar equations of projections on the two conveniently chosen axes.
The paper ends with the formulation of a geometric synthesis problem for the optimization of a quadrilateral deltoid type mechanism.

References

[1] Antonescu, Păun. *Mechanisms – Course book*. Bucharest, Printech Publishing House, 2003.
[2] Antonescu, Ovidiu, and Păun Antonescu. *Mechanism and Machine Science - Course book*. Bucharest, Politehnica Press, 2016.
[3] Antonescu, Păun, and Ovidiu Antonescu. "Standardization of terminology of MMS and graphical symbols." Paper presented at The Third National Seminar on Mechanisms SNM'08, Craiova, Romania, September 10-11, 2008.
[4] Antonescu, Ovidiu, and Păun Antonescu. *Mechanisms and manipulators*. Bucharest, Printech Publishing House, 2006.
[5] HESHBON Co., Ltd. "Lift, Instruction manual - HL - 32 F." HBN-H-301-12VER. 1.0. Accessed March 10, 2025. https://centurydistributors.co.nz/wp-content/uploads/HL-32F-MANUAL.pdf.
[6] Safe Work Australia. "Elevating work platforms." Accessed March 10, 2025. https://www.safeworkaustralia.gov.au/duties-tool/construction/hazards-information/plant-and-machinery/elevating-work-platforms.
[7] Adel, Michael. "Understanding Scissors Lift Deflection - autoquip.com". Accessed March 12, 2025. https://anyflip.com/rydp/etnc/basic.
[8] Stanley, Macaulay Oletu. *A project on scissor design for use in the automotive industry*. Bachelor's thesis. Niger Delta University, 2012.
[9] Twin Busch France. "Double scissor lift to be installed / Pont double ciseaux a poser", Art. no. TW S3-19. Accessed March 12, 2025. www.twinbusch.fr.

Experimental Evaluation of the Dynamic Response of Pneumatic Actuators Depending on Constructive and Operational Parameters

PhD. Eng. **Gabriela MATACHE**[1,*], PhD. Eng. **Gheorghe ȘOVĂIALĂ**[1],
PhD. Eng. **Radu-Iulian RĂDOI**[1], **Ana-Maria Carla POPESCU**[1]

[1] National Institute of Research & Development for Optoelectronics/INOE 2000, Subsidiary Hydraulics and Pneumatics Research Institute/IHP, Romania

* fluidas@fluidas.ro

Abstract: *The paper presents the experimental tests conducted in the Pneumatics Laboratory of the Research Institute for Hydraulics and Pneumatics INOE 2000-IHP on the factors influencing the dynamic behavior of medium and high-pressure pneumatic actuators. The tests were performed on two actuator size types from FESTO (DNCKE-100-200-PPV-A and DNCKE-40-130-PPV-A).*
The tests were carried out under no-load conditions and aimed to evaluate: the step response at three points of the stroke at a constant pressure of 8 bar; the response to a sinusoidal signal with an initial amplitude, ranging from the minimum to the maximum value, for three stroke values; and a test to highlight the dynamic performance of the actuators depending on the type of seals and the materials used, as well as the level of machining (quality of the cylinder sleeves and rod surfaces).

Keywords: *Pneumatic actuators, dynamic behavior; influencing factors*

1. Introduction

When developing procedures and protocols for testing pneumatic systems with pneumatic actuators, it is essential to consider their functional characteristics in both static and dynamic conditions, as well as the parameters that define these behaviors. Recent studies highlight the importance of standardized methodologies adapted to the current requirements of modern pneumatic systems, which incorporate advanced control algorithms, innovative materials, and solutions for compensating nonlinearities caused by air compressibility [1],[2].
The actuator systems analyzed in this paper are not merely "classic" pneumatic actuation systems but rather advanced servo systems integrated into automated control architectures. In this context, the development of experimental protocols must take into account current industry trends, such as the integration of advanced sensor technology (high-resolution pressure, position, and force sensors), the use of predictive models based on artificial intelligence to optimize performance, and the implementation of adaptive control strategies to mitigate hysteresis and compressibility effects [3],[4]. Consequently, experimental procedures require a complex approach that enables an accurate evaluation of dynamic performance under variable operating conditions.
The factors influencing their behavior, as well as the methods used to improve their accuracy [5]:

1.1 Main factors influencing the dynamic behavior of medium and high-pressure pneumatic actuators:

- Piston diameter and actuator stroke
- Type of sealing
- Machining quality of the rods and cylinder sleeves
- Difference between piston diameter and rod diameter
- Compressed air quality (level of pollutants in the compressed air and methods used for their removal, compressibility of gas and liquid phases, humidity and condensation, pressure, and flow rate)

1.2 Methods and means of increasing the precision and dynamic performance of medium pressure pneumatic actuators [5]:

To enhance the accuracy and dynamic performance of medium-pressure pneumatic actuators, various methods and means are employed, including design optimization, the use of advanced

materials, and the implementation of modern control techniques. Some of the most effective methods include:

- **Optimization of actuator design**

• Reducing internal friction by using low-friction seals and materials with a low coefficient of friction.
• Improving the guidance of the piston and rod to minimize positioning deviations and premature wear.
• Using progressive damping chambers to prevent mechanical shocks at the stroke ends.

- Increasing rigidity and reducing hysteresis

- Using lightweight yet durable materials (aluminum alloys, composites).
- Minimizing internal clearances and elastic deformations of mechanical components.
- Reducing the stick-slip phenomenon through precision finishing of contact surfaces.

- Utilization of sensors and feedback systems

- Position sensors (LVDT, optical encoder, magnetostrictive sensor) for precise stroke measurement.
- Pressure and flow sensors for real-time monitoring and adjustment of operating parameters.
- Closed-loop feedback to correct position and speed deviations.

- Advanced control of air pressure and flow

- Proportional pressure regulators for fine-tuned force variation.
- Proportional control valves and servo valves for fast and precise response.
- Advanced control algorithms (adaptive PID, fuzzy logic, model predictive control - MPC) for dynamic actuator motion adjustment.

- Reducing the effects of air compressibility

- Using air pre-filling to reduce response delay.
- Regulating the temperature of compressed air to minimize density variations.
- Implementing compensatory algorithms to model thermodynamic effects.

- New technologies and innovative solutions

- Integrating hybrid pneumatic actuators (pneumo-electric or pneumo-hydraulic) to improve precision.
- Using smart materials (e.g., electroactive elastomers, flexible structures with shape memory) to optimize dynamic response.
- AI-based control systems for automatic adaptation to operating conditions.

These methods significantly contribute to improving the accuracy and dynamic performance of pneumatic actuators, making them more efficient for industrial and automation applications.

2. Experimental stand

The tests, conducted on two size types of medium-pressure pneumatic actuators (DNCKE-100-200-PPV-A and DNCKE-40-130-PPV-A), highlight the main influencing factors and methods regarding their dynamic behavior.
The tests will be performed under no-load conditions and will consist of:
a. **Step response** at three points of the stroke, at a constant pressure of 8 bar;
b. **Response to a sinusoidal signal** with an initial amplitude, ranging from the minimum to the maximum value, for three stroke values;
c. **Test to highlight the dynamic performance of the actuators** based on the type of seals and materials used, as well as the level of machining (quality of the cylinder sleeves and rod surfaces). It was previously mentioned that as the size of the actuators decreases, the quality of the component surfaces, as ensured by the manufacturers, increases. The test will consist of comparing the response diagrams for step and sinusoidal signals for both analyzed actuators, under the same testing parameter values.

2.1. Testing Conditions

Based on the pneumatic schematic shown in Fig. 1, two testing stands were built in the Pneumatics Laboratory of IHP Bucharest (Fig. 2). These stands differ in terms of the mounting fixtures for the DNCKE-100-200-PPV-A and DNCKE-40-130-PPV-A actuators on the workbench, as well as the pneumatic connections compatible with the two actuator size types.

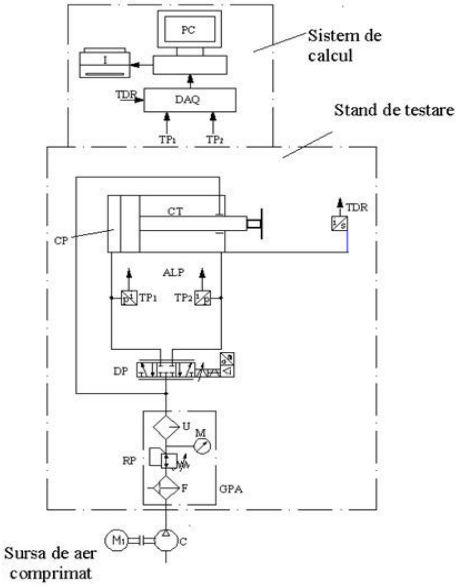

Fig. 1. The pneumatic schematic of the test stand

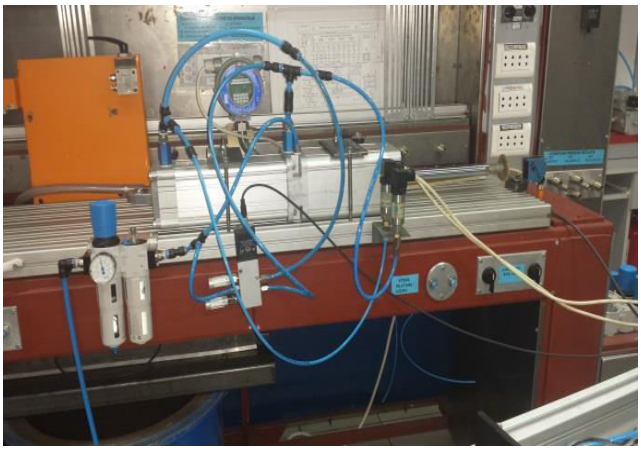

Fig. 2. The test stand for the medium-pressure actuator DNCKE-100-200-PPV-A

The test stand for the medium-pressure actuator DNCKE-100-200-PPV-A is designed to evaluate its dynamic performance under controlled conditions. The setup includes mechanical, pneumatic, and electronic components that allow for precise monitoring and control of the actuator's response.

Key Elements of the Test Stand:

1. Mechanical Setup:

- **Mounting structure** – A rigid frame to secure the actuator in place.
- **Guides and fixtures** – Ensure stability and alignment during testing.

2. Pneumatic System:

- **Compressed air supply** – Delivers air at 8 bar via an air preparation unit.
- **Air preparation unit** – Consists of a filter, regulator, and lubricator to ensure clean and stable airflow.
- **Proportional control valve** – Modulates the airflow to the actuator.
- **Pressure sensors (p1, p2)** – Measure the pressure in the actuator's chambers.

3. Sensor and Data Acquisition System:

- **Position sensor (LVDT or optical encoder)** – Tracks actuator displacement.
- **Flow sensors** – Measure air consumption and flow rate.
- **USB-6218 Data Acquisition Board (DAQ)** – Captures real-time signals from sensors.

4. Control System (LabVIEW-Based):

- **PID controller** – Adjusts actuator performance based on feedback.
- **Step and sinusoidal signal generator** – Simulates different operational scenarios.
- **Graphical interface** – Displays test parameters and real-time graphs.

The test stand configuration (Fig. 2) ensures accurate evaluation of response time, positioning accuracy, damping characteristics, and the impact of control parameters on the actuator's performance.

The testing program, developed in the LabVIEW environment, consists of block diagrams that automate the testing process. The results, including diagrams and databases, are automatically saved.

At the input of the USB-6218 data acquisition board, voltage signals from the pressure transducers (corresponding to the two chambers of the tested actuator) and the displacement transducer (reflex) are fed. One of the two analog signal outputs of the acquisition board is used to control the proportional valve in the testing setup [6].

The power supply for the proportional equipment solenoids, sensors, and data acquisition board is provided by a dual-channel power source, as shown in Fig. 3.

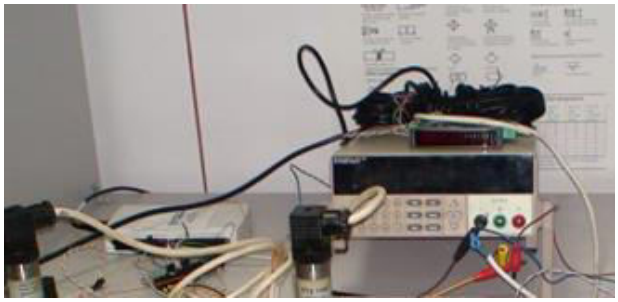

Fig. 3. Two-channel supply source

In the automatic control system used for operating pneumatic actuators, the automatic controller (RA) processes the error signal ε, which is obtained from the linear-additive comparison of the input variable xi and the feedback variable x_r within the comparison element. The controller then outputs a control signal x_c for the actuator.
Current information about the automated process is obtained using the feedback transducer (TR) and is processed by the automatic controller (RA) according to a specific control law, which defines the automatic regulation algorithm (control law) [7], [8].

2.2 Step response at three stroke points at constant pressure

The program schematic for determining the step signal response, developed in the LabVIEW environment, illustrates the control logic and data processing flow used to analyze the dynamic behavior of the pneumatic actuator under step input conditions.

Key Components of the LabVIEW Schematic:

- **Step signal generation module** – creates a sudden change in the input position.
- **Data acquisition system** – collects real-time signals from position, pressure, and velocity sensors.
- **PID control block** – applies proportional control adjustments based on feedback.
- **Graphical display and logging module** – visualizes and records the actuator's response.
- **Processing unit** – analyzes response parameters such as rise time, settling time, overshoot, and damping.

The schematic, as shown in Fig. 4, provides a structured representation of how the LabVIEW-based automation is implemented for evaluating the step response characteristics of the pneumatic actuator.

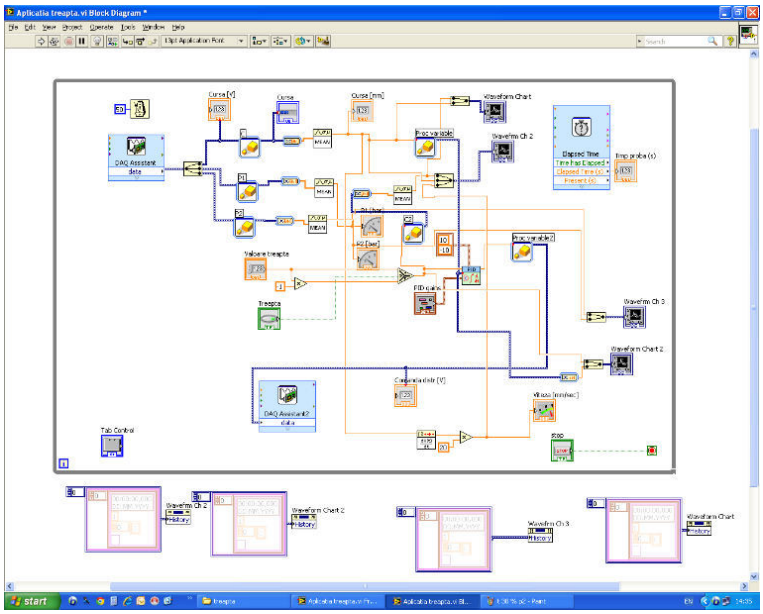

Fig. 4. The program schematic for determining the step signal response, developed in the LabVIEW environment

The tests are conducted at an operating pressure of 8 bar, at three stroke length points—30%, 60%, and 100% of the stroke value specified by the actuator manufacturer—for different values of the proportionality factor kc of the PID automatic controller.
In Window 1 (screenshot), Fig. 5, the following elements are displayed: prescribed position, actual position, velocity, amplitude variation over time, PID parameter values of the automatic controller, and step value.

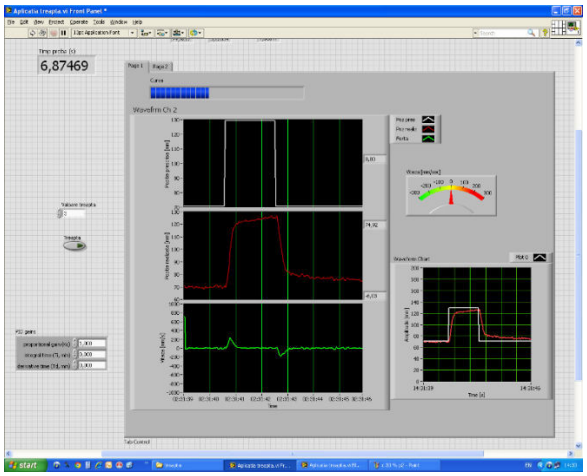

Fig. 5.

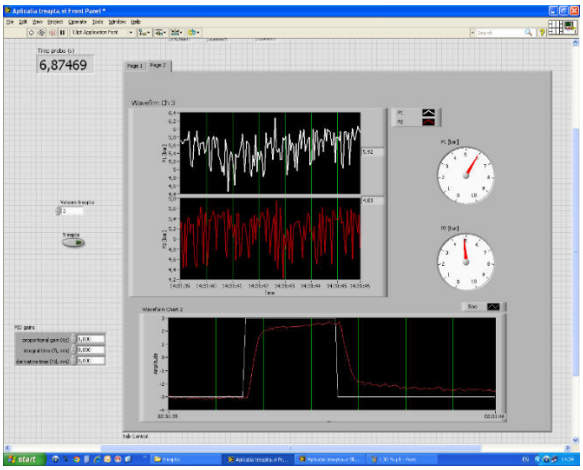

Fig. 6.

The application for a stroke length of 30% of the total stroke, at an operating pressure of 8 bar, with a proportionality factor kc = 1.000 of the PID automatic controller, for the medium-pressure pneumatic actuator DNCKE-100-200-PPV-A

In Window 2, Fig. 6, the following elements are displayed: pressures in the piston chamber (p1) and rod chamber (p2), amplitude, PID parameter values of the automatic controller, step value, and test duration.
The graphs obtained from running the program, corresponding to the two application windows, are shown in Fig. 7.

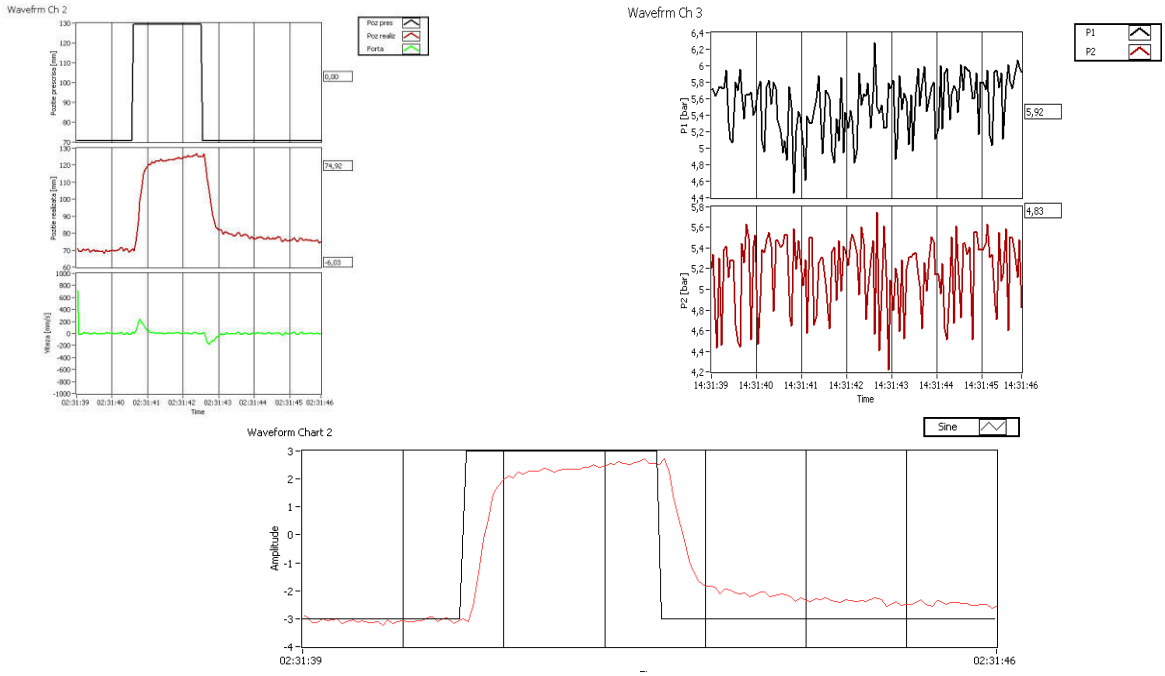

Fig. 7. The appearance of the graphs obtained during the tests regarding the step signal response of the medium-pressure pneumatic actuator DNCKE-100-200-PPV-A

The appearance of the graphs obtained during the tests regarding the step signal response of the medium-pressure pneumatic actuator DNCKE-100-200-PPV-A provides insights into its dynamic behavior under sudden input changes. These graphs typically illustrate:

- Step response curve – showing the actuator's reaction to abrupt position changes.
- Rise time and settling time – indicating how quickly the actuator reaches and stabilizes at the desired position.
- Overshoot and damping characteristics – assessing response stability and precision.
- Velocity profile – visualizing acceleration and deceleration phases.
- Pressure variations in the actuator chambers (p1 and p2) – analyzing air compression effects.

These graphical representations are essential for evaluating the actuator's control accuracy, response time, and overall performance under step input conditions.

2.3 Response to a sinusoidal signal with initial amplitude, from minimum to maximum value, for three stroke value

The program schematic for determining the sinusoidal signal response, developed in the LabVIEW environment, illustrates the control logic, data acquisition, and processing flow used to analyze the dynamic behavior of the pneumatic actuator.
This schematic includes:

- Signal generation module for applying a sinusoidal input to the actuator.
- Data acquisition block to capture position, pressure, and velocity signals from sensors.
- PID control algorithm to adjust the actuator's response.
- Real-time graphing and data storage for further analysis of system performance.

The schematic, as shown in Fig. 8, provides a structured visualization of the LabVIEW-based automation used for testing and evaluating the actuator's sinusoidal response characteristics.

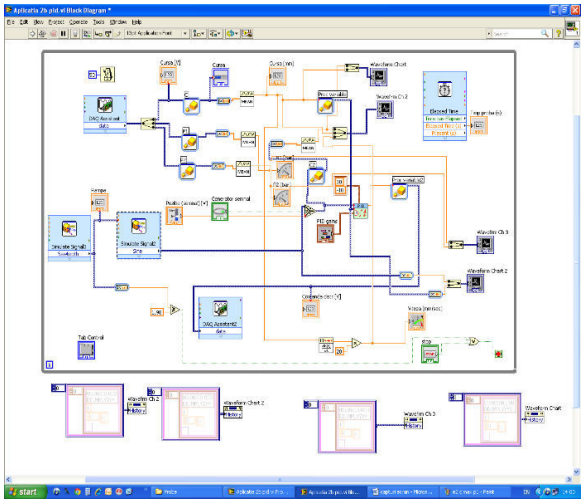

Fig. 8. The program schematic for determining the sinusoidal signal response, developed in the LabVIEW environment

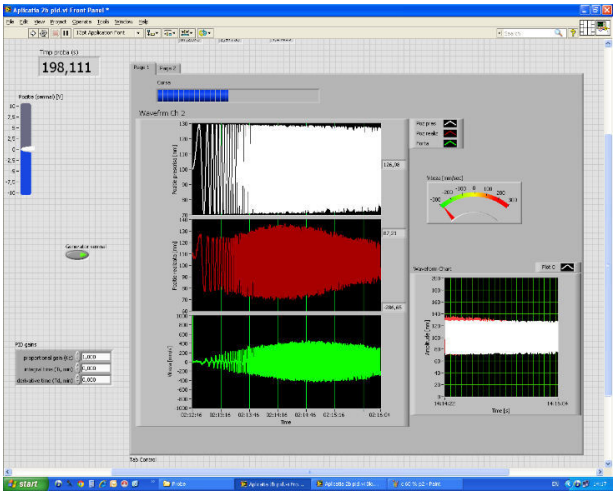

Fig. 9. Window 1 of the application for a stroke length of 30% of the total stroke, at an operating pressure of 8 bar, with a proportionality factor Kc = 1.000 of the PID automatic controller, for the medium-pressure pneumatic actuator DNCKE-100-200-PPV-A

The tests are conducted at an operating pressure of 8 bar, at three stroke length points—30%, 60%, and 100% of the stroke value specified by the actuator manufacturer—for different values of the proportionality factor kc of the PID automatic controller.
In Window 1, Fig. 9, the following elements are displayed: prescribed position, actual position, velocity, amplitude variation over time, PID parameter values of the automatic controller, and signal generator status. These graphical representations help in understanding the actuator's dynamic response, stability, and precision under the given operating conditions.

In Window 2, Fig. 10, the following elements are displayed: pressures in the piston chamber (p1) and rod chamber (p2), amplitude, PID parameter values of the automatic controller, signal generator status, and test duration.
The graphs obtained from running the program, corresponding to the two application windows, are shown in Fig. 11.

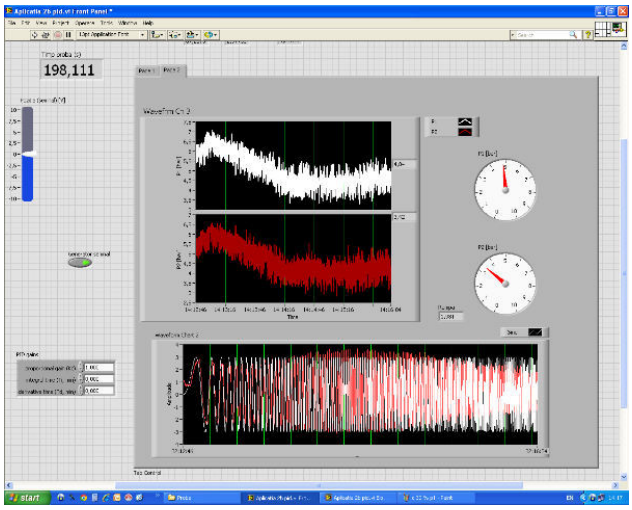

Fig. 10. Window 2 of the application for a stroke length of 30% of the total stroke, at an operating pressure of 8 bar, with a proportionality factor Kc = 1.000 of the PID automatic controller, for the medium-pressure pneumatic actuator DNCKE-100-200-PPV-A

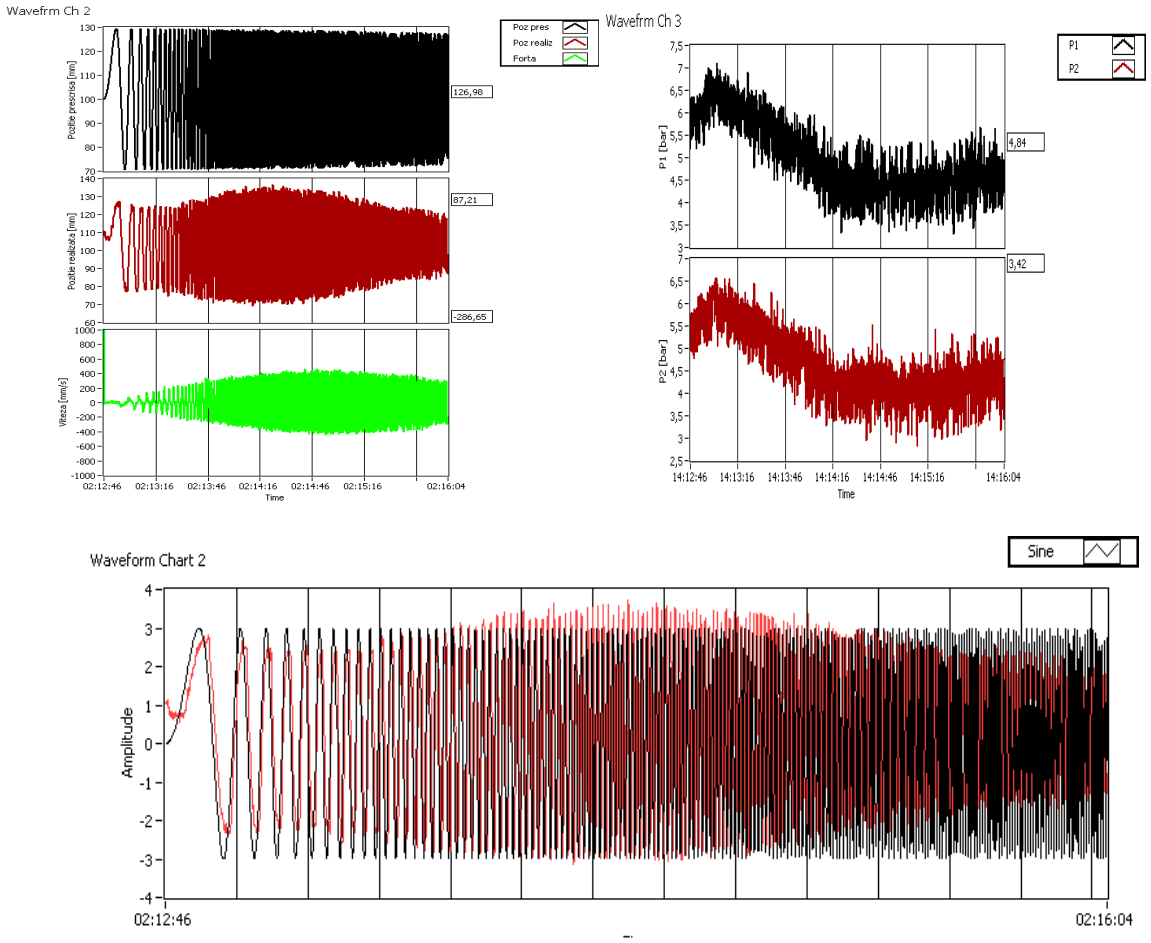

Fig. 11. The appearance of the graphs obtained during the tests regarding the sinusoidal signal response of the medium-pressure pneumatic actuator DNCKE-100-200-PPV-A

2.4. Dynamic Performance of Actuators Depending on the Type of Seals, Materials Used, and Machining Level (Surface Quality of Cylinder Sleeves and Rods)

The main factors and methods influencing the dynamic performance of medium and high-pressure pneumatic actuators—such as the type of seals, materials used, and machining level (surface quality of cylinder sleeves and rods)—have been theoretically analyzed by consulting specialized literature:

2.4.1 Effect of Size (Dimensions) on Forces

Reducing the size of execution elements affects the magnitude of force (or torque) developed**.** Example: In electrostatic actuators, the mechanical work per unit volume (Fl/l^3) is inversely proportional to the square of the length, meaning that the mechanical work developed by electrostatic force increases as the size decreases [5]. Example: For certain actuators, reducing dimensions below a specific limit results in forces (or torques) smaller than the resistive forces (friction, gravity).

2.4.2 Increasing the Strength of Materials Used

Materials with exceptional mechanical properties**:** Monocrystals and amorphous whisker-type materials (very short fibers) have up to 1000 time higher strength than polycrystalline materials of the same chemical composition. This is due to the absence of grain boundaries, leading to lower wear and fewer error sources.

The relationship between size reduction ($\lambda = l1/l2$) and material strength is given by: $c\sigma = \sigma1/\sigma2 = 1/\lambda$, meaning that components reduced by a factor of λ must be made of materials λ times stronger.

2.4.3 Significant Surface Effects

At the micron level**,** $L_2 > L_3$, meaning that surface-related effects dominate over volume-related effects.

Examples:

- Chemical corrosion becomes significant when associated with electrical phenomena.
- Microtribology effects: In flat surfaces and sliding bearings, the friction coefficient (μ) increases significantly as size decreases.
- Adhesion, friction, capillarity, surface tension, etc.**,** become more dominant than mass effects (inertia).

To address these issues, the following approaches are necessary:

- Minimizing contact surfaces in mechanical couplings and applying special coatings**.**
- Replacing sliding friction with rolling friction**.**
- Elastic support of moving elements**.**
- Using low-viscosity lubricants**.**
- Implementing advanced lubrication methods, such as gas (hydro) static or dynamic lubrication**,** magnetic levitation, or electrostatic levitation.

2.4.4 Decreasing Machining Precision

- Tolerance reduction is not proportional to size reduction.
- If $\lambda = l_1/l_2$ (nominal size ratio), at the same machining precision, the tolerance ratio is $T_1/T_2 = 3\lambda$.
- As the nominal size decreases, machining precision must increase.

2.4.5 Speed-Dimension Dependency

- The relationship between speed v [mm/s] and size L [mm] varies significantly compared to conventional actuators.
- According to similarity theory**,** reducing dimensions by a ratio of $\lambda = l_1/l_2$ leads to:

- Mass reduction by $cG = \lambda^3$
- Acceleration increase by $ca = \lambda^{-1}$ **(**a component reduced by λ can be accelerated λ times more)
- Moment reduction by $cM = \lambda^3$

Advantages of Actuation Elements Compatible with Mechatronic Technology

Compared to conventional actuators, mechatronic-compatible execution elements offer:

- Higher power-to-weight ratio
- Lower environmental impact
- Longer operational lifespan

- Adjustable motion parameters
- Higher operational safety
- Compactness
- Simplified construction (fewer moving parts)
- Submicron positioning accuracy [5]

Application Domains:

These advancements apply to various fields, including: Robotics and micro-robotics: Machine tool actuation; Structural components in various equipment; Automotive industry; Aerospace industry; Defense industry; Consumer goods industry; Medical engineering

3. Conclusions

1. The experimental studies on the main factors and methods influencing the dynamic behavior of medium and high-pressure pneumatic actuators were carried out on two size types of medium-pressure pneumatic actuators (DNCKE-100-200-PPV-A and DNCKE-40-130-PPV-A).
2. The tests regarding the step and sinusoidal signal responses, the determination of the starting pressure, and the influence of the automatic controller parameters within the automatic control system (PID) were performed in the LabVIEW environment.
3. The influence of dimensions, the type of seals and materials used, the machining level (quality of the cylinder sleeves and rod surfaces), and the quality of the working fluid on the dynamic performance of the actuators was analyzed based on research in the field presented in the specialized literature.
4. The temperature of the working fluid was strictly maintained at the standard value of 25°C.
5. The operating pressure (at the inlet to the actuator chambers), regulated by the pressure regulator of the air preparation unit, was set at 8 bar.
6. The automatic controller used was of the P (proportional) type, with the proportionality factor (amplification) kc being the only variable parameter in the automatic control system.

Test conclusions

Actuator DNCKE-100-200-PPV-A

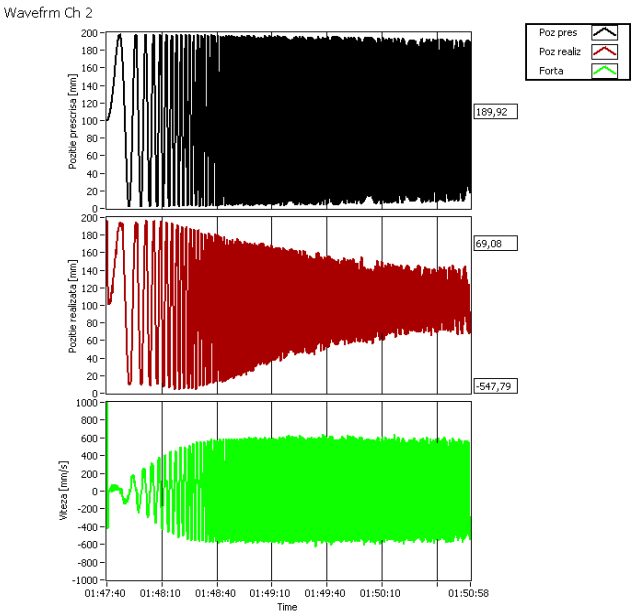

Stroke 100 %

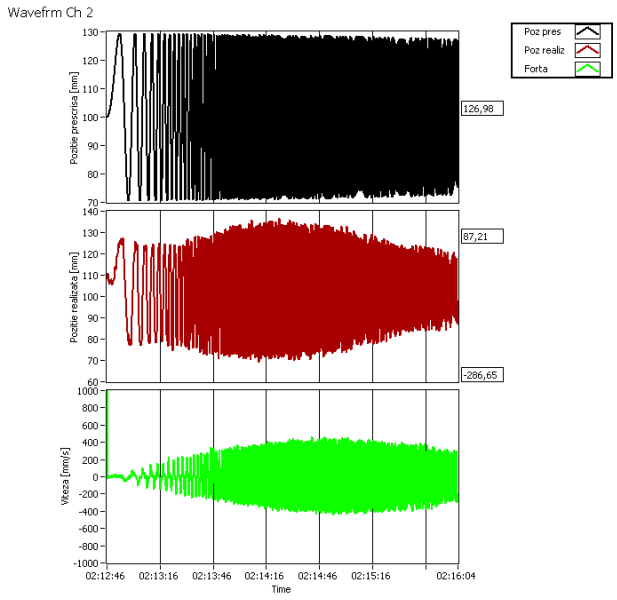

Stroke 30 %

At the same values of the PID controller parameters, it is observed that amplitude attenuation begins within the first third of the frequency range (0…2 Hz).

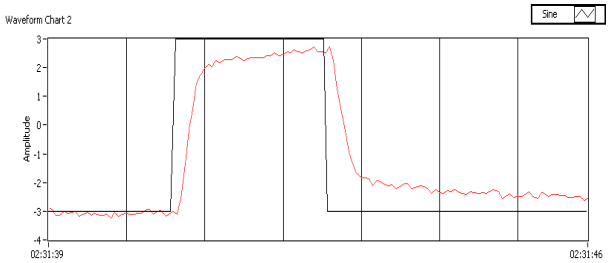

Stroke 30 % Kc = 1

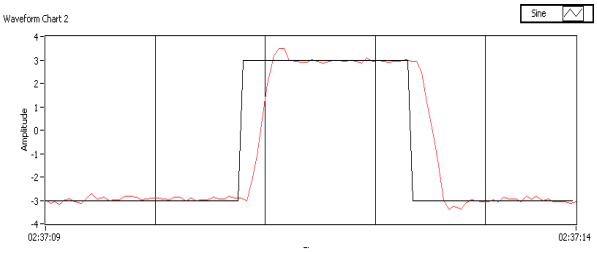

Stroke 30 % Kc = 4

With an **increase in Kp**, an **improvement in response time and positioning accuracy of the cylinder rod** is observed rod is observed.

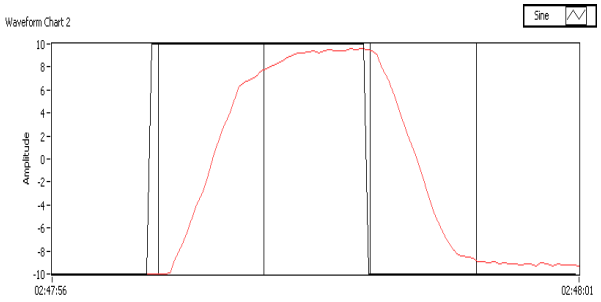

Stroke 100 % Kc = 1

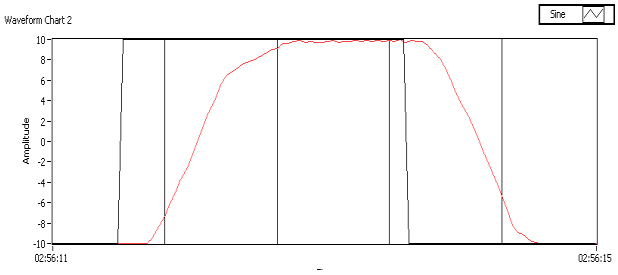

Stroke 100 % Kc = 50

At the maximum stroke of the large-size pneumatic actuator, the response is delayed and cannot be improved by increasing the Kc parameter.
Given the large volume of the cylinder chambers, the response could be enhanced by increasing the available airflow rate.

Acknowledgments

This work was carried out through the Core Program within the National Research Development and Innovation Plan 2022-2027, carried out with the support of MCID, project no. PN 23 05.

References

[1] Zhao, Wenchuan, Yu Zhang, and Ning Wang. "Development and Performance Analysis of Pneumatic Soft-Bodied Bionic Actuator." *Applied Bionics and Biomechanics*, no. 1 (2021): 6623059. DOI: 10.1155/2021/6623059.

[2] Kim, Sungjun, Seung Ryeol Lee, Sinyoung Lee, Dongun Lee, and Dongjun Shin. "Power-Efficient Soft Pneumatic Actuator Using Spring-Frame Collateral Compression." *Actuators* 11, no. 3 (2021): 76. DOI: 10.3390/act11030076

[3] Gariya N., P. Kumar, and T. Singh. "Experimental study on a bending type soft pneumatic actuator for minimizing the ballooning using chamber-reinforcement." *Heliyon* 9, no. 4 (March 2023): e14898. DOI: 10.1016/j.heliyon.2023.e14898.

[4] Xavier, Matheus S., Charbel D. Tawk, Ali Zolfagharian, Joshua Pinskier, David Howard, Taylor Young, Jiewen Lai, Simon M. Harrison, Yuen K. Yong, Mahdi Bodaghi, and Andrew J. Fleming. "Soft Pneumatic Actuators: A Review of Design, Fabrication, Modeling, Sensing, Control, and Applications." *IEEE Access* 10 (2022): 59442-59485.

[5] Avram, M. *Hydraulic and pneumatic drives - Classical and mechatronic equipment and systems / Acţionări hidraulice şi pneumatice - Echipamente şi sisteme clasice şi mecatronice*. Bucharest, University Publishing House, 2005.

[6] Radoi, R., M. Blejan, I. Dutu, Gh. Sovaiala, and I. Pavel. "Determining the step response for a pneumatic cylinder positioning system." *Hidraulica Magazine*, no. 2 (June 2014): 25-31.

[7] Matache, G., R. Radoi, Gh. Sovaiala, and I. Pavel. "Experimental determinations on improving dynamic and energy performance of pneumatic systems." *Hidraulica Magazine*, no. 2 (June 2015): 40-47.

[8] Matache, G., Gh. Sovaiala, and R.I. Radoi. "Experimental research on the factors influencing the dynamics of pneumatic actuators." *Romanian Review Precision Mechanics, Optics & Mechatronics*, no. 48 (2015): 123-127. DOI: 10.17683/rrpmom.issue.48.

FLUIDAS

NATIONAL PROFESSIONAL ASSOCIATION OF HYDRAULICS AND PNEUMATICS IN ROMANIA

fluidas@fluidas.ro